# LOW DOSE EFFECTS OF RADIATION ON BLOOD LYMPHOCYTES

# LOW DOSE EFFECTS OF GAMMA AND NEUTRON RADIATION ON PERIPHERAL BLOOD LYMPHOCYTES

By LAURA PATERSON, B.Sc., B.Ed.

A Thesis Submitted to the School of Graduate Studies in Partial Fulfilment of the Requirements for the Degree
Master of Science
in Radiation Sciences (Radiation Biology)

McMaster University

MASTER OF SCIENCE (2016) McMaster University
(Medical Physics) Hamilton, Ontario

| | |
|---|---|
| TITLE: | Low Dose Effects of Gamma and Neutron Radiation on Peripheral Blood Lymphocytes |
| AUTHOR: | Laura Paterson, B.Sc. (McMaster University), B.Ed. (University of Ontario Institute of Technology) |
| SUPERVISOR: | Dr. Douglas Boreham & Dr. Colin Seymour |
| NO. OF PAGES: | xxi, 168 |

## ABSTRACT

This thesis examines the effects of radiation on human peripheral blood lymphocytes, with the goal of elucidating a biomarker of radiation quality. The issues studied were (1) the effect of thermal and fast neutron exposure on chromosome aberrations, and (2) the effect of thermal neutron and gamma radiation on apoptosis and necrosis induction. As a starting point, a literature review was performed to examine how neutron RBE values vary with neutron energy, reference radiation, anticoagulant status, irradiation container, and RBE calculation method. The dicentric chromosome assay (DCA) was utilized for the microscope-based analysis of chromosome aberrations, whereas imaging flow cytometry was used to examine cell death.

Chromosome aberrations were induced following both low dose $^{252}$Cf and thermal neutron irradiations (doses ranged between 10 mGy – 108 mGy and 1.2 mGy – 13.4 mGy, respectively), with both radiations demonstrating a linear relationship between dose and aberration induction. The results produced were compared to a pre-existing $^{137}$Cs dose response curve and indicated a RBE of 20.1 ± 2.9 for chromosome damage by $^{252}$Cf fast neutron radiation, and 26.1 ± 7.0 following low-dose thermal neutron exposure. When damage is assessed in lymphocytes via the dicentric chromosome assay, these results indicate that $^{252}$Cf is approximately 20 times more damaging than $^{137}$Cs gamma radiation, and thermal neutron radiation is approximately 26 times more damaging than $^{137}$Cs gamma radiation. In contrast, a RBE value could not be assigned to either apoptotic or

necrotic induction following thermal neutron radiation, as no cell death dose-response was observed at doses between 0.2 mGy and 18.9 mGy. However, $^{60}$Co gamma doses between 0.03 Gy and 2.5 Gy demonstrated a quadratic dose-dependent increase for both types of cell death.

Neither the chromosome aberration study nor the cell death study yielded a biomarker of radiation quality. While non-Poisson chromosome aberration over-dispersion of radiation-induced DNA aberrations is normally the result of either high-LET radiation exposure or a partial body exposure, it was found that neither the $^{252}$Cf nor the thermal neutron exposures consistently induced over-dispersion. As such, over-dispersion should not be used to differentiate high-and low-LET radiation exposures in lymphocytes. Unfortunately, due to a late-breaking thermal neutron dose rate decrease, it was not possible to assess whether the percentage of apoptosis and/or necrosis could be used as a biomarker of radiation quality, as the very low doses of thermal neutron radiation failed to demonstrate a significant dose response. That said, the $^{60}$Co cell death experiments demonstrated a linear-quadratic dose response for both apoptosis and necrosis at doses up to 2.5 Gy. Additionally, these experiments established that donor variability had little effect on cell death induction.

This work contributes to our understanding of the biological effects of neutron and gamma radiation, and suggests that both thermal and fast neutron radiations induce chromosome aberrations in a dose-dependent manner. In contrast, it was found that in surviving cells at 48 hours post-irradiation, apoptosis and necrosis

induction are independent of thermal neutron dose, a phenomenon that deserves further investigation. Additionally, since the low-dose $^{252}Cf$ and thermal neutron DCA data failed to indicate consistent over-disperson typically characteristic of high-LET exposures, the results suggest that following accidental low-dose gamma exposures, estimates of dose, made using the DCA method, could be unreliable if the subject has a history of occupational exposures to neutrons.

**ACKNOWLEDGEMENTS**

Thank you to my supervisors Dr. Doug Boreham (McMaster University), Dr. Colin Seymour (McMaster University), and Dr. Richard Richardson (Canadian Nuclear Laboratories) for providing guidance throughout this M.Sc. thesis.

I would also like to acknowledge Radiobiology & Health Branch Manager, Professor Nick Priest (Canadian Nuclear Laboratories), for supporting a work-based M.Sc., as well as Canadian Nuclear Laboratories and for funding this research.

In addition, thank you to Dr. Jovica Atanackovic (formally of Canadian Nuclear Laboratories, now with Ontario Power Generation) and Dr. Samy El-Jaby (Canadian Nuclear Laboratories) for performing the Monte Carlo simulations necessary to derive thermal neutron fluence to kerma conversion coefficient. Without this information, it would not have been possible to embark on this project. In addition, thank you to Chad Boyer (Canadian Nuclear Laboratories) for coordinating thermal neutron beam access, designing the thermal neutron irradiation rig, and operating the spectrometer.

This project was completed in collaboration with McMaster University (Hamilton, ON), and Canadian Nuclear Laboratories, formally Atomic Energy of Canada Limited (Chalk River, ON). The irradiations and laboratory work described herein were performed at Canadian Nuclear Laboratories, in conjunction with the Canadian Neutron Beam Centre (CNBC). This work was

funded by, and formed part of Canadian Nuclear Laboratories' Federal Science & Technology Program.

**TABLE OF CONTENTS**

## LIST OF FIGURES

## LIST OF TABLES

## TABLE OF ACRONYMS

| | |
|---|---|
| $^{60}$Co | Cobalt-60 |
| $^{111}$In | Indium-111 |
| $^{137}$Cs | Cesium-137 |
| $^{197}$Au | Gold-197 |
| $^{198}$Au | Gold-198 |
| $^{235}$U | Uranium-235 |
| $^{252}$Cf | Californium-252 |
| 7AAD | 7-aminoactinomycin |
| ACE-R | Acentric Ring Chromosome |
| AECL | Atomic Energy of Canada Limited |
| BNCT | Boron Neutron Capture Therapy |
| C | Carbon |
| CD | Cluster of Differentiation |
| Ca | Calcium |
| Cl | Chlorine |
| CNBC | Canadian Neutron Beam Centre |
| CNL | Canadian Nuclear Laboratories |
| $CO_2$ | Carbon Dioxide |
| CPM | Counts per Minute |
| CTB | Chromatid break |

| | |
|---|---|
| DCA | Dicentric Chromosome Assay |
| DNA | Deoxyribonucleic Acid |
| DSB | Double Strand Break |
| $E_n$ | Energy |
| Fe | Iron |
| FITC | Fluorescein-5-Isothiocyanate |
| FISH | Fluorescence In-Situ Hybridization |
| FPG | Fluorescence Plus Giemsa |
| Gy | Gray |
| H | Hydrogen |
| HPNG | Health Physics Neutron Generator |
| HRR | Homologous Recombination Repair |
| IAEA | International Atomic Energy Agency |
| ICRP | International Commission on Radiological Protection |
| IR | Ionizing Radiation |
| K | Potassium |
| LCL | Lower Confidence Limit |
| LET | Linear Energy Transfer |
| LMDS | Locally Multiply Damaged Site |
| mBAND | Multicolour Banding |
| MCNP | Monte Carlo N-Particle Radiation Transport Code |

| | |
|---|---|
| mFISH | Multi-colour Fluorescence In-Situ Hybridization |
| Mg | Magnesium |
| N | Nitrogen |
| Na | Sodium |
| NHEJ | Non-homologous End Joining |
| NRU | National Research Universal |
| O | Oxygen |
| P | Phosphorous |
| PHA | Phytohemagglutinin |
| PBL | Peripheral Blood Lymphocyte |
| PBS | Phosphate Buffered Saline |
| PS | Phosphatidylserine |
| RBE | Relative Biological Effectiveness |
| $RBE_M$ | Relative Biological Effectiveness at Minimal Doses |
| RPMI | Roswell Park Memorial Institute |
| S | Sulphur |
| SD | Standard Deviation |
| SE | Standard Error of Mean |
| Si | Silicon |
| SSA | Single Strand Annealing |
| SSB | Single Strand Break |

| | |
|---|---|
| TEPC | Tissue Equivalent Proportional Counter |
| TL | Translocation |
| UCL | Upper Confidence Limit |

.

# 1. CHAPTER 1 – INTRODUCTION & LITERATURE REVIEW

## 1.1. Hypothesis, Rationale and Overview

At high doses, neutron radiation presents an occupational hazard in many occupational fields, including medicine, research and nuclear power production. However, there is currently little data describing cell death and chromosome aberrations following fast and thermal neutron exposures, specifically at low doses. As such, the objective of this thesis is two-fold to: 1) investigate potential biomarkers of radiation quality using exposures to thermal and fast neutrons, and 2) contribute data pertaining to the cytogenetic and cell death effects of low-dose thermal and fast neutron radiation. It is known that fast neutron radiation induces more cell death and more chromosome aberrations, per unit dose, than low-LET gamma radiation. It was hypothesized that thermal neutron radiation would have a higher RBE, per unit dose, than gamma radiation.

This thesis is divided into four sections. This chapter summarizes the relevant background information and discusses the current literature. Chapter Two focuses on chromosome aberrations following thermal and fast neutron exposure. Chapter Three examines cell death following thermal neutron and Cobalt-60 ($^{60}$Co) gamma exposures. Lastly, Chapter Four describes the conclusions deduced from the results of the studies undertaken.

## 1.2. Ionizing Radiation

Ionizing radiation (IR) has the capacity to deposit energy in a medium, and the amount of energy deposited per unit mass in a biological system is defined as

absorbed dose. This is quantified by the unit gray (Gy), where one Gy is equivalent to the absorption one joule of energy in one kilogram of matter (1 Gy = 1 J $kg^{-1}$). Some radiation types are more biologically damaging per unit of absorbed dose than other radiation types. In radiological protection, this is addressed through the use of radiation weighting factors ($w_R$) which are dimensionless values that convert absorbed dose (*D)* in Gy, to equivalent dose, (*H)* in sieverts (Sv), as given by Equation 1.

$$H = w_R D \tag{1}$$

Radiation weighting factors are recommended by the International Commission on Radiological Protection (ICRP), and as described in Table 1, photons and electrons have been assigned a radiation weighting factor of one, protons have a radiation weighting factor of two, and alpha-particles, fission fragments, and heavy ions are allocated a radiation weighting factor of 20. In contrast, neutrons do not have a single $w_R$ value, instead the radiation weighting factors for neutrons are based on a continuous energy distribution, as shown in Figure 1. Specifically, thermal neutrons have a $w_R$ of 2.5, whereas $^{252}$Cf has a $w_R$ of approximately 17.1 (if calculated using the average energy of 2.1 MeV).

Radiation types that are more biologically damaging have larger radiation weighting factors than radiations that are less biologically damaging, and therefore provide a larger equivalent dose. For example, 1 Gy of dose deposited

by 1 MeV of gamma radiation will have an equivalent dose of 1 Sv ($w_R$ = 1). In contrast, 1 Gy of dose deposited by 1 MeV neutrons will have an equivalent dose of approximately 20.7 Sv ($w_R$ = 20.7).

**Table 1. Radiation weighting factors recommended by ICRP Publication 103 [1]. Neutron energy is represented by $E_n$.**

| Radiation Type | Radiation Weighting Factor ($w_R$) |
|---|---|
| Photons | 1 |
| Electrons | 1 |
| Protons | 2 |
| Alpha-particles, fission fragments, heavy ions | 20 |
| Neutrons<br>$E_n < 1$ MeV<br>1 MeV ≤ $E_n$ ≤ 50 MeV<br>$E_n > 50$ MeV | <br>$2.5 + 18.2e^{-\{\ln(E_n)\}^2/6}$<br>$5.0 + 17.0e^{-\{\ln(2E_n)\}^2/6}$<br>$2.5 + 3.25e^{-\{\ln(0.04E_n)\}^2/6}$ |

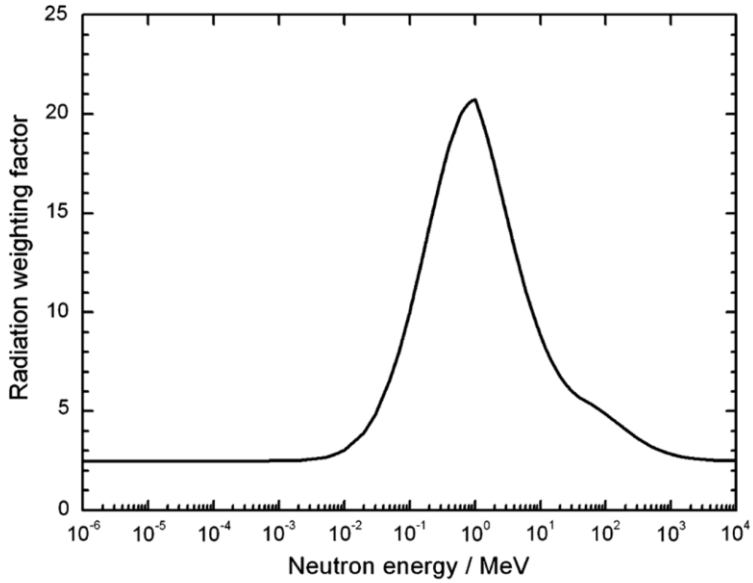


**Figure 1. Radiation weighting factor value for neutrons vs. neutron energy. Image from ICRP Publication 103 [1].**

Radiation can be classified as either directly or indirectly ionizing. Charged particles, such as protons, alpha particles, and heavy nuclei are directly ionizing, whereas uncharged particles, such as photons and neutrons are indirectly ionizing. Directly ionizing radiation deposits energy, and therefore dose, through Coulomb interactions with the orbital electrons of the absorber medium. In contrast, indirectly ionizing radiations interact with tissue via a two-step process. The primary radiation undergoes an initial interaction with the absorber, forcing the release of a charged particle into the medium. During the second step, the directly ionizing charged particle deposits energy in the medium through Coulomb interactions with the orbital electrons of the medium. During the primary

interaction, photons tend to release electrons or electron/positron pairs, through the photoelectric effect, Compton scattering, and pair production interactions. The probability of these interactions occurring depends on photon energy and the absorber material (discussed further in Section 1.2.1). Neutrons, in contrast, will undergo elastic and inelastic collisions, but can also undergo nuclear interactions. These latter nuclear interactions may result in the emission of other particle types such as gamma rays, alpha particles, protons, and other heavier nuclei [2]. The probability of undergoing a particular interaction depends on the neutron energy and the composition of the absorber medium (as detailed in Section 1.2.2).

The manner in which radiation dose is deposited by charged particles is thought to be responsible for its severity, or radiation quality. Radiation quality is a function of LET, which is a measure of the density of ionizations induced by a radiation, averaged over a defined unit path length (given in keV $\mu m^{-1}$). High-LET radiation qualities are densely ionizing and transfer more energy per unit path length of track than low-LET radiation [3, 4]. For example, $^{60}$Co gamma rays are sparsely ionizing and deposit energy of 0.2 keV $\mu m^{-1}$, whereas densely ionizing 14 MeV neutrons and 2.5 MeV alpha-particles deposit 12 keV $\mu m^{-1}$ and 166 keV $\mu m^{-1}$, respectively [5]. Traditionally, gamma rays, x-rays, and beta particles have been considered low-LET radiations whereas neutrons, alpha particles and heavy nuclei are considered high-LET radiations. While this rule holds true most of the time, there are exceptions such as Auger electrons from Indium-111 ($^{111}$In) and some other radionuclides, which are characterized as high-LET radiations with LET

values of about 4 to 26 keV $\mu m^{-1}$ [6]. Qualitatively, if more energy is deposited per unit track length, more significant damage to the absorber will occur. In contrast, if less energy is deposited per unit track length, less significant damage to the absorber, e.g., within individual cells, will occur. This topic will be discussed in depth in subsequent sections.

### 1.2.1. Gamma Radiation

Gamma radiation occurs when an excited atomic nuclei returns to the ground state with the release of energy in the form of a photon. Photons interact with matter through three main processes: the photoelectric effect, Compton scattering, and pair production. The most likely process is a function of both the photon energy and the absorber material, as shown in Figure 2.

The photoelectric effect is dominant at low photon energies where an incident photon interacts with a bound inner-shell electron causing the ejection of the electron. The ejected electron has an energy equal to that of the incident photon minus the binding energy of the electron. Compton scattering predominates at higher photon energies where the incident photon is scattered by a loosely bound or "free" orbital electron. A portion of the photon's energy is transferred to the scattered electron in the form of kinetic energy. The lower-energy photon may take part in additional interactions. Lastly, pair production occurs above threshold photon energies of 1.022 MeV. Here, the incident photon interacts with the Coulomb field of the nucleus, is absorbed by the atom resulting in the creation of

an electron-positron pair. These electrons and positrons may travel through the material, losing energy, or the positron may undergo annihilation, resulting in two gamma rays emitted in opposite directions with energies of 0.511 MeV (equivalent to the mass of the electron).

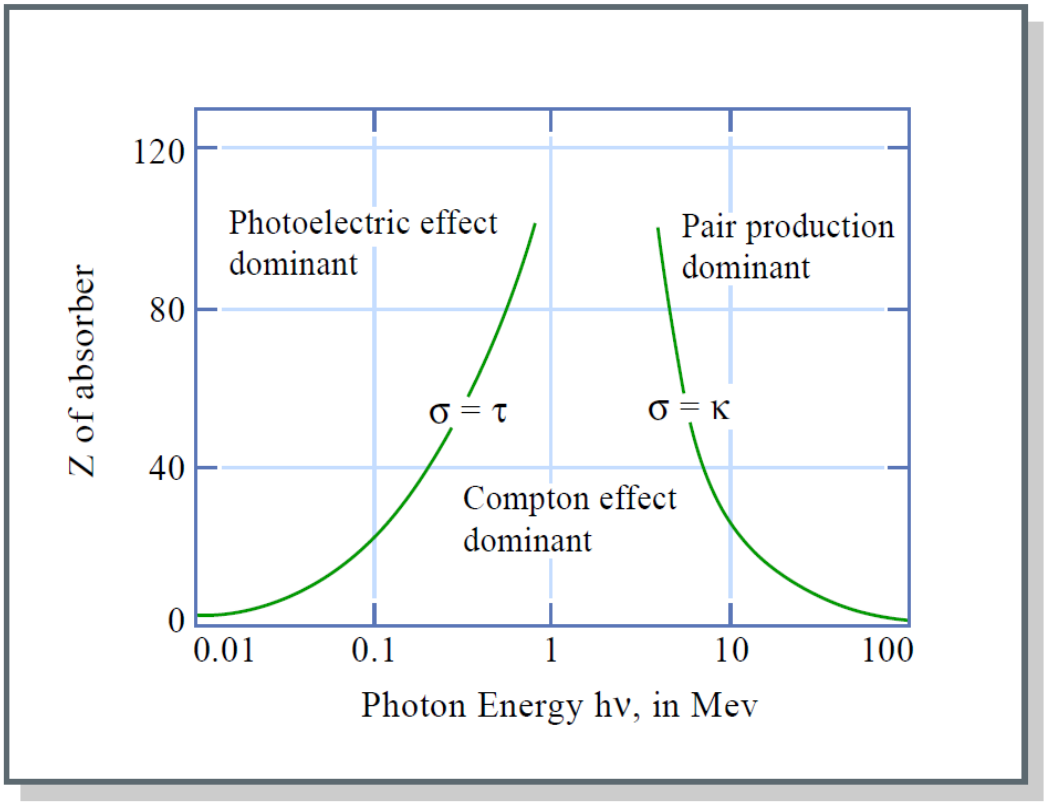


**Figure 2. Representation detailing how photoelectric effect, Compton scattering, and pair production vary with photon energy and absorber atomic number. τ is the interaction probability for the photoelectric effect, σ is the interaction probability for Compton scattering, and κ is the interaction probability for pair production. Figure taken from Massachusetts Institute of Technology Open Course Ware.**

Both $^{60}$Co and Cesium-37 ($^{137}$Cs) gamma radiation sources were used for the work described in this thesis. $^{60}$Co decay results in the emission of 1.17 MeV and 1.33 MeV photons, and because tissue and cells are predominantly composed of low-atomic number elements [7], most photons will lose kinetic energy by Compton scattering. Similarly, the less-energetic 0.66 MeV photon from $^{137}$Cs decay will also interact with matter predominantly via Compton scattering.

$^{60}$Co has a half-life of 5.27 years, and undergoes beta decay to produce stable $^{60}$Ni (Figure 3). There are two possible modes of decay, with branching ratios of 99.88% and 0.12%. Most commonly, a 0.31 MeV beta minus particle and two gamma rays are emitted (1.17 MeV and 1.33 MeV). The remaining 0.12% of the time, a higher-energy 1.48 MeV beta minus particle and one gamma ray (1.33 MeV) are emitted. $^{60}$Co sources typically used in radiobiology are encapsulated in a steel capsule that absorbs the emitted electrons and prevents beta-particle sample irradiation.

$^{137}$Cs has a half-life of 30.07 years and undergoes beta decay to $^{137}$Ba. Decay can proceed by two pathways with 94.6% of the $^{137}$Cs atoms first decaying to the meta-stable state of barium ($^{137m}$Ba), which then decays with the emission of a 0.66 MeV gamma ray to transition to the ground state. The remaining 5.4% of the time, $^{137}$Cs undergoes beta decay directly to the ground state (Figure 4), with no emission of a gamma-ray.

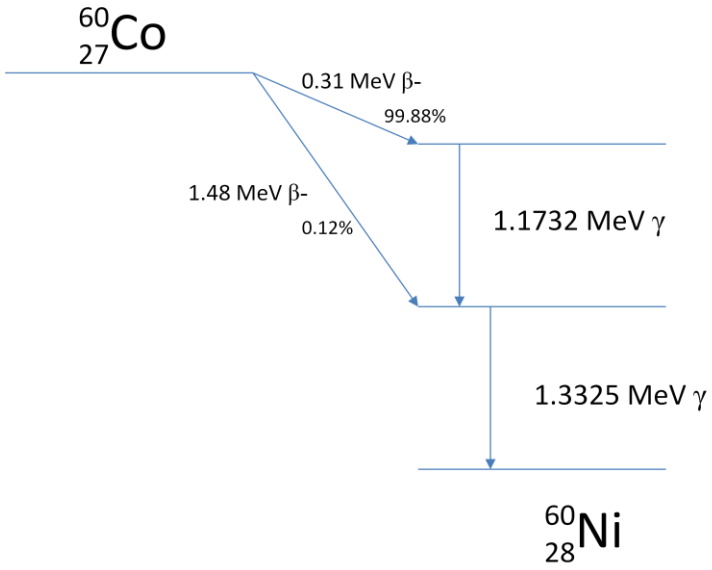


**Figure 3. $^{60}$Co decay scheme.**

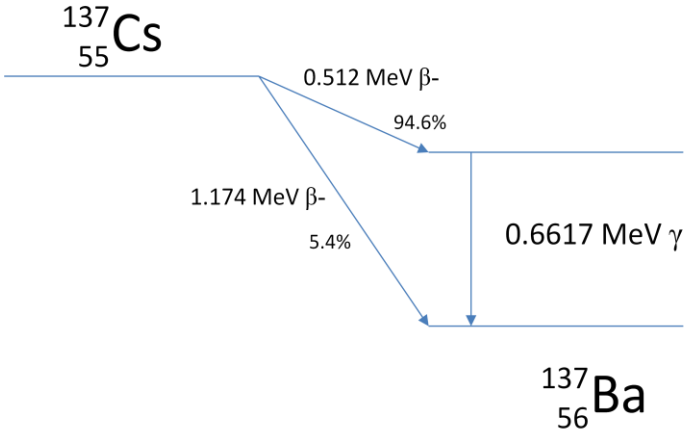


**Figure 4 $^{137}$Cs decay scheme.**

### 1.2.2. Neutron Radiation

A common scheme for the energy-based classification of neutrons is described in Table 2. Thermal neutrons, which are in thermal equilibrium (~ 20°C) with their surroundings, have an energy of approximately 0.025 eV. Epithermal neutrons have energies between 1 eV and 1 keV, intermediate neutrons have energies between 1 keV and 100 keV, and fast neutrons have energies above 100 keV. There are additional higher and lower energy neutron categories, however for the purpose of this thesis, only the range between thermal and Californium-252 ($^{252}$Cf) fast neutrons are discussed in the subsequent chapters.

**Table 2. Abbreviated list of neutron classifications [2].**

| Name | Energy |
|---|---|
| Thermal | ~ 0.025 eV |
| Epithermal | 1 eV – 1 keV |
| Intermediate | 1 keV – 0.1 MeV |
| Fast | > 0.1 MeV |

Fast neutrons are typically generated artificially through nuclear reactions. For instance, at the Canadian Nuclear Laboratories' (CNL) National Research Universal (NRU) reactor, a single Uranium-235 ($^{235}$U) fission event results in the release of approximately 2.5 neutrons and nearly 200 MeV in energy. The emitted neutrons have mean energies of approximately 5 MeV. The remaining reaction energy is distributed among the other fission fragments. Alpha-induced neutron

sources are also very common. For example, alpha particles emitted by the radioactive decay of americium-241 ($^{241}$Am) interact with the beryllium target material (AmBe) to cause the release of neutrons. There also exists naturally occurring fast neutron sources that contain radioisotopes that may decay by spontaneous fission; for example $^{252}$Cf, discussed further in Section 1.2.2.2.

As uncharged particles, neutrons are more penetrating than some other radiation types, including alpha and beta particles. However, the methods by which neutrons interact with matter depend on the neutron energy and the elemental composition of the absorber (target) material. These interactions include neutron capture, elastic and inelastic scattering, spallation, and fission.

Neutron capture reactions are often expressed by the notation A(n,x)B. Here, an incident neutron, n, strikes and is captured by a nucleus, A, resulting in the release of radiation x and recoil nucleus B. At thermal energies, neutron capture reactions predominate, resulting in the nuclear emission of either a photon or particle. Often, this can take the form of a gamma (n,$\gamma$), proton (n,p), or alpha (n,$\alpha$) release.

At fast neutron energies, elastic scattering is the prevailing interaction. Incoming neutrons are deflected by the absorber nuclei, resulting in some kinetic energy transfer to the nucleus, with the scattered neutron bearing less energy than before the interaction. This process repeats until the neutron is thermalized, at which point neutron capture occurs.

At energies above 6 MeV, inelastic scattering may occur. In this process, a neutron is captured by a nucleus and re-emitted in a different direction and at a lower energy. The nucleus, however, is left in an excited state. During relaxation, the nucleus will emit high-energy gamma rays to de-excite.

Spallation occurs at even higher energies. In this process, a neutron strikes a nucleus causing it to break up into many smaller particles such as alpha particles, protons, and neutrons.

Lastly, fission occurs when neutrons interact with high atomic number nuclei resulting in the creation of lighter nuclei and one or more neutrons. This reaction releases a large amount of energy (equivalent to the mass lost in the reaction), and is the driving reaction in nuclear reactors.

#### 1.2.2.1. Thermal Neutrons

Thermal neutrons are normally generated through the slowing of faster energy neutrons. For instance, in CNL's NRU reactor, fast neutrons interact with the 60 °C (333 K) heavy water moderator and lose energy through a series of elastic collisions with $D_2O$ before achieving thermal equilibrium within the moderator [8]. One $^{235}U$ fission event results in the release of approximately 2.5 fast neutrons, and following thermalization, these neutrons are available to interact with other $^{235}U$ nuclei. This may cause additional fissions, thereby propagating the nuclear chain reaction.

In tissue, two neutron capture reactions predominate, with 89% of thermal neutrons absorbed during the $^{1}H(n,\gamma)^{2}H$ reaction and 11% of thermal neutrons absorbed by the $^{14}N(n,p)^{14}C$ reaction [9]. However, as the gamma rays from the $^{1}H(n,\gamma)^{2}H$ reaction only deposit a small amount of energy in tissue before escaping, the $^{14}N(n,p)^{14}C$ reaction is responsible for 80% of the energy deposition in the body [10]. The $^{14}N(n,p)^{14}C$ reaction yields a 0.58 MeV proton and a 0.05 MeV recoil $^{14}C$ nucleus [2]. The proton will travel approximately 11 μm in water, which comprises approximately 80% of the blood volume [7]. This distance is larger than the diameter of a lymphocyte cell nucleus (approximately 4 μm), but smaller than the diameter of most lymphocyte cells (approximately 10-30 μm).

Neutron capture cross sections describe the likelihood of a thermal neutron interacting with an absorber nucleus. This is expressed by the unit, barn (b), which is equivalent to an area of $1.0 \times 10^{-24}$ $cm^2$. This quantity is modified by the natural abundance of each isotope, which is the relative percentage of each isotope of a particular element that occurs naturally on earth. Notable thermal neutron capture reactions and their associated cross sections are described in Table 3.

**Table 3. Relevant neutron capture reactions and their associated cross sections.**

| Reaction | Cross Section (barn) ($1\ barn = 1.0 \times 10^{-24}\ cm^2$) |
|---|---|
| $^{1}H(n,\gamma)^{2}H$ | 0.33 |
| $^{14}N(n,p)^{14}C$ | 1.83 |
| $^{17}O(n,\alpha)^{14}C$ | 0.24 |
| $^{23}Na(n,\gamma)^{24}Na$ | 0.53 |
| $^{31}P(n,\gamma)^{32}P$ | 0.17 |
| $^{35}Cl(n,p)^{35}S$ | 0.48 |
| $^{35}Cl(n,\gamma)^{36}Cl$ | 43.6 |
| $^{37}Cl(n,\gamma)^{38}Cl$ | 0.43 |
| $^{33}S(n,\alpha)^{30}Si$ | 0.14 |

Thermal neutron fluence rates can be characterizing using the gold foil activation technique. Gold-197 ($^{197}Au$) has a large thermal neutron capture cross section, and when foils are exposed to thermal neutrons, $^{198}Au$ is produced via the $^{197}Au(n,\gamma)^{198}Au$ reaction. $^{198}Au$ has a half life of 2.69 days, and decays by beta minus decay to $^{198}Hg$. During the process, three gamma rays are emitted with energies of 412 keV, 676 keV, and 1088 keV. Using either a sodium iodide or germanium gamma detector, the amount of activation can be quantified and mathematically converted into a fluence rate measurement.

### 1.2.2.2. $^{252}$Cf Spontaneous Fission Neutron Source

The half-life of $^{252}$Cf is 2.645 years, and decay proceeds by alpha emission (96.9% probability), and spontaneous fission (3.1% probability). Spontaneous fission is the result of Coulomb repulsion of protons, which, when greater than the attractive nuclear force, results in the splitting of atoms. $^{252}$Cf releases an average of 3.73 neutrons per fission event, with the neutrons exhibiting a predictable spectrum of energies, as described by the Watt distribution (Figure 5). The mean $^{252}$Cf neutron energy is 2.1 MeV, whereas the most probable neutron energy is 0.7 MeV [11]. The resulting secondary fission fragments are usually in an excited state, and de-excitation occurs through the emission of prompt gamma rays, accounting for approximately 33% of the total radiation released by the decay of $^{252}$Cf [12].

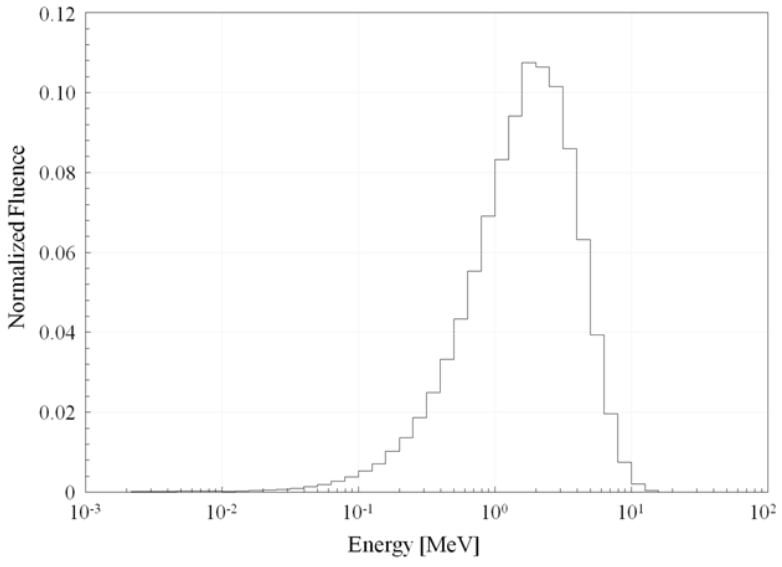


\

**Figure 5. $^{252}$Cf neutron fluence distribution based on the Watt continuous fission energy distribution [13].**

## 1.3. Elemental Blood Composition

The elemental composition of blood is given in Table 4. With the exception of sodium (Na) and phosphorous (P), all blood elements have two or more naturally occurring isotopes. The percentage of blood nitrogen is of special relevance to this work, as the $^{14}N(n,p)^{14}C$ reaction is the major source of tissue dose following thermal neutron exposure. $^{14}N$ is the most common nitrogen isotope, with a natural abundance of 99.6%.

**Table 4. Elemental composition of blood.**

| Isotope | % Blood Composition | Isotope | % Blood Composition |
|---|---|---|---|
| $^{16}O$ | 75% | $^{41}K$ | 0.01% |
| $^{17}O$ | 0.04% | $^{54}Fe$ | 0.003% |
| $^{18}O$ | 0.2% | $^{56}Fe$ | 0.05% |
| $^{1}H$ | 10% | $^{57}Fe$ | 0.001% |
| $^{2}H$ | 0.001% | $^{58}Fe$ | 0.0001% |
| $^{12}C$ | 10% | $^{31}P$ | 0.03% |
| $^{13}C$ | 0.1% | $^{40}Ca$ | 56% |
| $^{14}C$ | 3% | $^{42}Ca$ | 0.4% |
| $^{15}C$ | 0.01% | $^{43}Ca$ | 0.1% |
| $^{35}Cl$ | 0.2% | $^{44}Ca$ | 1% |
| $^{37}Cl$ | 0.1% | $^{46}Ca$ | 0.002% |
| $^{23}Na$ | 0.2% | $^{48}Ca$ | 0.1% |
| $^{32}S$ | 0.2% | $^{28}Si$ | 23% |
| $^{33}S$ | 0.001% | $^{29}Si$ | 1% |
| $^{34}S$ | 0.01% | $^{30}Si$ | 1% |
| $^{36}S$ | 0.00004% | $^{24}Mg$ | 30% |
| $^{39}K$ | 0.1% | $^{25}Mg$ | 4% |
| $^{40}K$ | 0.00002% | $^{26}Mg$ | 4% |

## 1.4. Radiation-Induced DNA Damage & Repair

Deoxyribonucleic acid (DNA) is a possible site of damage following all types of radiation exposure. Its double-helix structure consists of a sugar-phosphate backbone and paired nucleotides (adenine with thymine, cytosine with guanine). DNA exists in an unwound state for much of the cell cycle, however during mitosis, DNA is wound and compacted in a highly regulated manner to form visible chromosomes (Figure 6) [14].

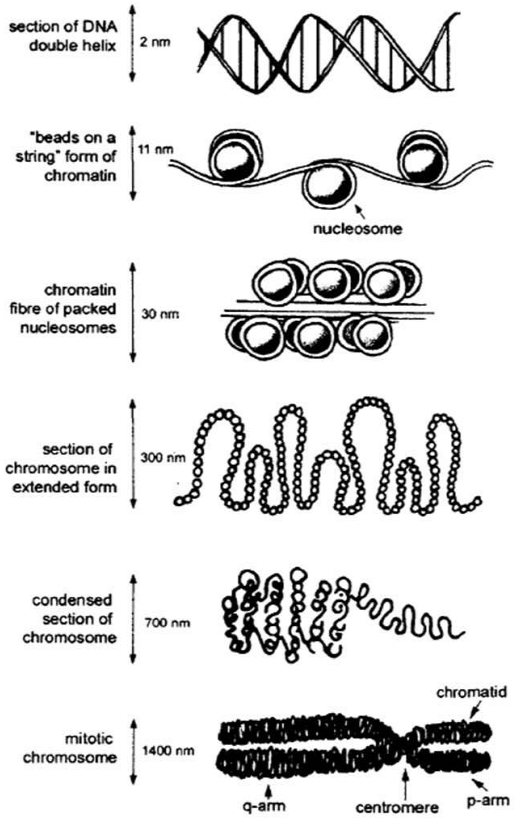


**Figure 6. Graphic detailing DNA compaction, adapted from Alberts *et al* [15]. DNA is wrapped around nucleosomes, which are packed together to form chromatin. The chromatin is further condensed to form a chromosome.**

Chromosomes can be easily viewed with a light microscope during metaphase (Figure 7). These normally have short p-arms, longer q-arms and are constricted and joined at their centromeres, as depicted in Figure 6. A normal human karyotype contains 23 pairs of chromosomes, which are numbered sequentially from 1 to 22, with chromosome 1 being the longest, and chromosome 21 being the shortest. The 23rd pair comprises either two X chromosomes or an X and Y chromosome pair. Centromeres are of particular importance to biological dosimetry, as their number and position is used to determine the presence of aberrations.

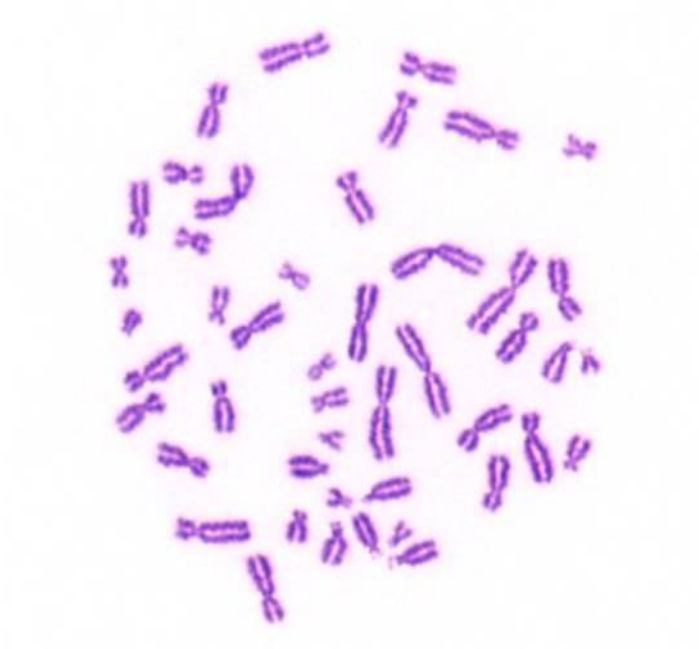

**Figure 7. Undamaged metaphase chromosome spread.**

Radiation can induce DNA damages via either direct or indirect actions. If a radiation either ionizes or excites the atoms of the DNA molecule, this is termed a direct effect, because the radiation is directly interacting with the critical target (Figure 8). Conversely, indirect effects are produced when radiation first interacts with non-DNA atoms in the cell causing the formation of ions and free radicals – the latter being highly reactive uncharged atoms with unpaired orbital electrons. Most commonly, radicals are produced by the radiolysis of $H_2O$ within cells to form $H^{\cdot}$ and $OH^{\cdot}$ radicals. Subsequently, ions and free radicals may go on to cause DNA damage [16]. Both free radicals and ions have the capacity to cause DNA lesions, however, the hydroxyl radical ($OH^{\cdot}$) is thought to be the most damaging, causing approximately 65% of DNA breaks following low-LET radiation exposure [17].

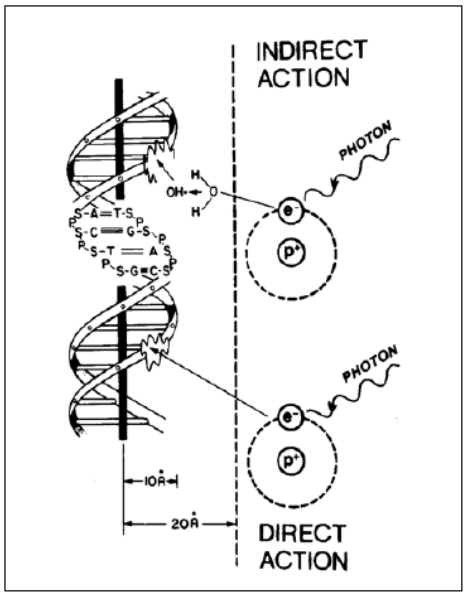


**Figure 8. Indirect vs. direct action of radiation. Adapted from Hall & Giaccia [5].**

The direct and indirect actions of radiation can cause base alterations, DNA-DNA or DNA-protein cross-links, and DNA strand breaks. Adenine, thymine, cytosine, and guanine can be either modified or destroyed by radiation-induced ions and free radicals. However, base alterations do not lead to significant cell killing as these types of lesions are often efficiently repaired. Cross-links between either DNA strands or between DNA and proteins occur when a DNA atom covalently binds (shares electron pairs) with another DNA atom, or with the atoms of nearby proteins. Unless repaired, cross-links can inhibit DNA transcription and translation. DNA single strand breaks (SSB) are bond breakages within the phosphodiester bond that binds sugar residues. DNA double strand breaks (DSB) arise when two SSBs occur on complementary DNA strands, within a 1-2 base pairs of each other, resulting in a physical separation between DNA segments. DSBs are important radiation-induced lesions and will be discussed in subsequent sections. It is important to note that cells also naturally accumulate DBSs as a result of endogenous processes, including the natural production of $H^{\cdot}$ and $OH^{\cdot}$ radicals [18]. Gamma and x-ray radiations cause approximately 20 to 40 DSBs per cell, per Gy of absorbed whole body dose [19] and cause DNA damages predominantly through indirect actions. In contrast, high-LET exposures are described as producing substantially more breaks per unit dose (Figure 9), and interact principally through direct action [5].

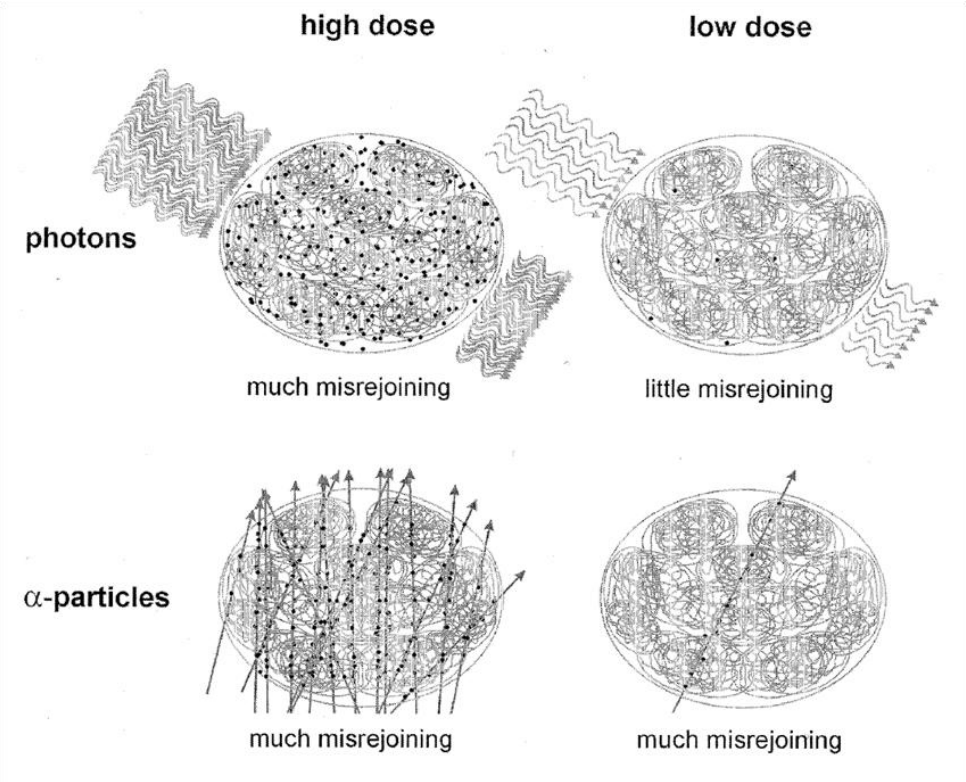


**Figure 9. Schematic detailing DNA breaks and mis-repair in a single cell nucleus following both high-LET alpha particle and low-LET photon irradiation. Even at low doses, a high-LET alpha particle traversal can result in many temporally and spatially-associated breaks which increases the likelihood of mis-repair. Figure adapted from [20].**

Following the induction of DNA SSBs or DSBs, there are three possible outcomes, either error-free repair, mis-repair, or cell death. Error-free repair correctly addresses the DNA damage, and the affected cells continue to function normally. Mis-repair results in a mutation that may lead to a variety of outcomes including genomic instability and/or carcinogenesis [21]. Alternatively, if the radiation-induced damage is too extensive, the cell may die. While this can

prevent carcinogenesis [22], substantial cell death can negatively impact the function of critical body organs and may lead to inflammation, fibrosis, stem cell depletion and even cancer.

Cells are able to repair DNA breaks through a number of different intrinsic processes. SSBs are repaired using the complementary DNA strand as a template, and this occurs by either base excision repair or nucleotide excision repair. Briefly, base excision repair resects the damaged bases and associated sugar residues. Next, new nucleotides are added using the complementary stand as a guide, and the repaired strand is then ligated. Nucleotide excision repair typically removes sections of 24 to 32 nucleotides that are inappropriately bound to chemicals, which are termed DNA adducts. This process also uses the complementary DNA strand as a template to ensure correct repair. In contrast, DSBs may be repaired by homologous recombination repair (HRR), non-homologous end joining (NHEJ), or single-strand annealing (SSA) (Figure 10) [23]. HRR (Figure 10) is a high-fidelity repair pathway and requires the presence of a sister chromatid to act as a repair template. For this reason, HRR occurs in late S and $G_2$ phases of the cell cycle. In contrast, NHEJ is an error-prone method of DNA repair that proceeds without the use of a homologous template. The NHEJ pathway can be mobilized when cells are in all cell cycle phases, however it is predominantly observed when a sister chromatid template is not available. Alternatively, DSB repair may progress by SSA, where the 5’ end next to the DSB is resected to reveal specific homologous sequences. The homologous

sequences are aligned, and the ends are ligated [24]. Incorrect DSB repair can result in gross chromosomal abnormalities including dicentric and ring chromosomes, as well as translocations, inversions, deletions, and insertions [25].

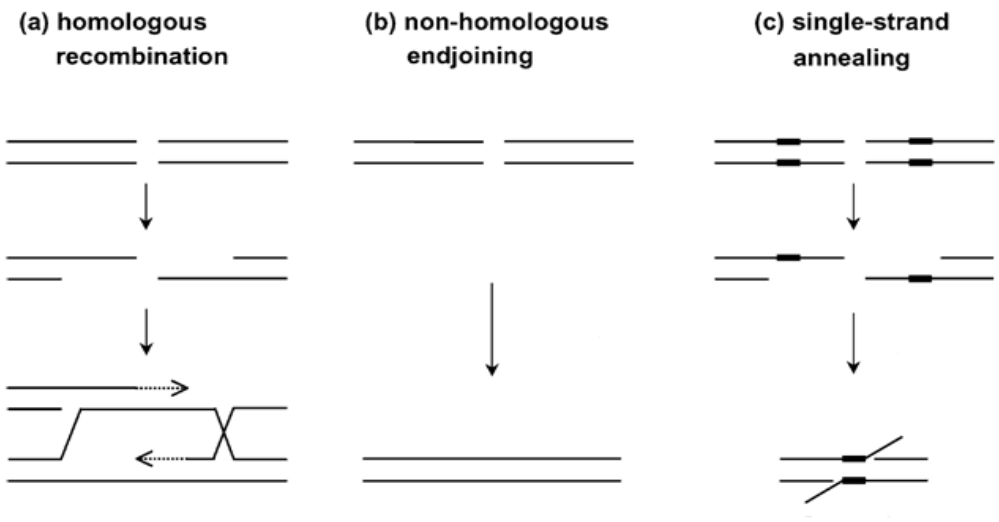


**Figure 10. DNA repair mechanisms following a double-strand break: (a) homologous recombination, (b) non-homologous end-joining, (c) single-strand annealing. Adapted from A. Pastink *et al*. [24].**

### 1.4.1. Chromosome Aberrations

In the event of mis-repair, abnormal DNA structures may be formed. These are easily visualized in metaphase when DNA is compacted into highly visible chromosome structures (Figure 6 and Figure 7). In non-cycling cells such as lymphocytes, cell cycle entry can be achieved by stimulation with a mitogen such as phytohemagglutinin, a lectin that prompts T-lymphocyte division. Cycling cells are then arrested in metaphase using a metaphase blocker, such as colcemid.

This inhibits spindle fibre formation, halting cell cycle progression. At this point, the chromosomes are easily stained and examined under a microscope.

Chromosome aberrations can be characterised as stable or unstable. Stable damages such as translocations, inversions, and insertions do not lead to mitotic cell death and can be passed on to daughter cells. In contrast, unstable damage, such as the formation of dicentric and ring chromosomes, cannot be passed on to progeny and result in cell death at division.

Dicentric and centric ring chromosomes are of particular interest to the work described in this thesis, and may be formed following the mis-repair of two or more chromosome breaks (Figure 11). In their simplest form, dicentric chromosomes are the result of two DSBs, with each break located on a separate chromosome. The centromere-containing portion of one chromosome is then mis-repaired to the centromere-containing portion of another chromosome, resulting in the characteristic two-centromere "dicentric" morphology. Similarly, centric rings are also formed by a minimum of two chromosome-breaks, however both breaks occur on the same chromosome – one on either side of the centromere. On rare occasions, a tricentric chromosome may be observed. This is a chromosome with three centromeres that results from a minimum of four chromosome breaks on three separate chromosomes. The fate of acentric fragments in both situations is normally of less importance – they may be observed in an un-repaired or mis-repaired state. However, these can sometimes be visualized as micronuclei in binucleated cells. It should be noted that dicentric and centric ring chromosomes

are often complex rearrangements that are actually a result of three of more breaks in two or more chromosomes [26, 27]. The background frequency of dicentric chromosome aberrations in peripheral blood lymphocytes reported in the literature is variable with approximations ranging from 1 in 1,000 lymphocytes to 1 in 3,200 lymphocytes [28, 29].

Unwound DNA is localized to specific nuclear domains during interphase [30, 31], and following an ionizing radiation exposure, the probability of observing a chromosomal inter-change is significantly higher in co-localized chromosomes [32, 33]. For mis-repair to occur, the break-points must come in contact with one another. Thus, the probability that two particular chromosomes will be involved in a mis-repair is correlated to the spatial positioning of DNA within the nucleus [34]. Following high-LET radiation exposure, inter-chromosomal exchanges occur between chromosomes damaged by the same radiation track, with little interaction between chromosome breaks resulting from different radiation tracks [35]. This is likely a result of spatial and/or temporal separation between radiation particle traversals [29]. Neutrons have been shown to effectively induce complex chromosome aberrations, even at low doses [35-37]. In contrast, low-LET radiations do not efficiently induce complex chromosome aberrations at doses below 2 Gy [38]. This is a result of the higher ionization density of neutrons, compared to low-LET radiations.

| | Interphase chromosome configuration | Chromosome structure post stimulation (post-synthesis) |
|---|---|---|
| Normal chromosome (no radiation exposure) |  | 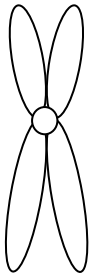 |
| Dicentric Chromosome Formation | 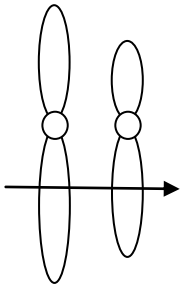 Two chromosomes, each with a single DSB | 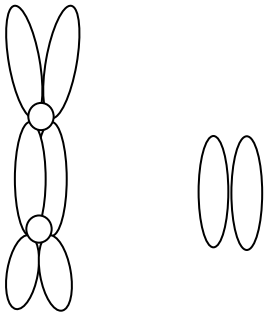 Dicentric Chromosome + Acentric Fragment |
| Ring Chromosome Formation | 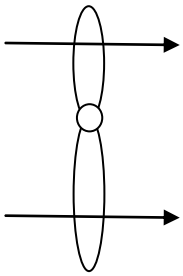 One Chromosome with two DSBs |  Ring chromosome + Acentric Fragment |

**Figure 11. Simplified graphic detailing dicentric and ring chromosome formation following interphase radiation exposure and subsequent mitotic entry.**

It is speculated that high-LET radiations produce complex chromosome damage (both inter- and intra-chromosomal damages) for two reasons: DNA localization and ionization density. The unwound DNA of individual chromosomes is localized within specific and regulated nuclear domains. Thus, the entire unwound DNA complement of a single chromosome is located in close proximity to itself, and consistently adjacent to other co-localized chromosomes [30, 31, 39]. A track of high-LET radiation is densely ionizing, and as such, multiple close proximity ionizations can occur as a single high-LET particle traverses the nucleus. Alternatively, low-LET radiations are sparsely ionizing, and far fewer ionizations occur in the nucleus as a result of a single low-LET radiation track.

When high-LET radiations cause breaks in one part of the unwound interphase DNA strand, it is likely that other parts of the DNA complement from the same chromosome will also be affected because of the spatial proximity of the remainder of the unwound DNA [31]. Multiple DNA breaks in close proximity are termed clustered lesions. These lesions have a greater possibility of resulting in complex chromosome rearrangements such as insertions, inversions and deletions [40] indicating that damage complexity increases with LET [17, 41, 42]. Clustered lesions can comprise a combination of base-damages, SSBs, and DSBs. When clustered lesions occur within about 20 base pairs, this is termed a locally multiply damaged site (LMDS). LMDSs have been theoretically modeled for high- and low-LET radiations, and it is hypothesized that high-LET radiations produce more complex LMDSs compared to low-LET radiations [43].

At equal doses, high-LET radiations are more likely to produce multiple breaks in a given chromosome compared to low-LET radiations [44]. Thus, high-LET radiations are more efficient than low-LET radiations at inducing chromosome aberrations and causing complex chromosome damage, defined as inter- or intra-chromosomal changes involving three of more breakpoints in two or more chromosomes [45]. Additionally, due to their dense ionization patterns, high-LET radiations have been shown to produce a unique suite of chromosome rearrangements, including intra-chromosomal rearrangements [44]. Using fluorescence in-situ hybridization (FISH) techniques, it has been shown that alpha particles [46], heavy ions [47] and neutrons [36] induce more complex aberrations than low-LET radiations, below doses of 2 Gy.

The complexity of the DNA lesion can affect DNA repair speed, with more complex lesions requiring longer repair times [48]. Accordingly, it has been shown that DSB repair time is much longer following high-LET radiation exposure, as compared to low-LET radiations [36, 47, 49, 50].

### 1.4.2. Cell Death

Radiation-induced cell death can occur by multiple processes including apoptosis, necrosis, mitotic catastrophe, autophagy and senescence [51, 52]. Apoptosis is a highly regulated form of cell death where cellular contents are packaged in apoptotic bodies that are later engulfed by a phagocyte. In contrast, necrosis results in the release of cellular contents into the surrounding tissue. This process

may be passive and uncontrolled, or tightly regulated, depending on the circumstances [53]. Mitotic catastrophe is a type of apoptotic cell death that occurs following an error in mitotic cell division [53] [51]. Autophagy is a process of self-degredation whereby cellular components are digested within the cell, and lastly, cells that have lost their replicative potential, but still remain metabolically active are identified as senescent cells [53, 54]. The remainder of this section will discuss only apoptosis and necrosis – the two cell death modalities examined in this thesis.

Apoptosis is the main mode of cell death in lymphocytes following radiation exposure [55-57], and apoptosis preferentially eliminates cells containing dicentric chromosomes [58]. Low-LET radiation qualities induce dose-dependent increases in apoptosis [57, 59]. Similarly, high-LET fast neutron [60] and heavy-ion [61] irradiations also induce significant dose-dependent cell death. There are currently no studies examining apoptosis and/or necrosis following thermal neutron exposure. A RBE of 1 has been found for lymphocyte apoptotic induction following exposure to 280 keV neutrons [59], 5.5 MeV neutrons [62], and 62.5 MeV neutron irradiation of mouse thymocytes [63], as seen in Table 6. Likewise, high-LET nitrogen-ion lymphocyte exposures have also produced an RBE of unity [61].

Information about apoptotic induction following thermal neutron irradiation can be gleaned from boron neutron capture therapy (BNCT) studies in lymphocytes, where untreated lymphocytes showed approximately 5% apoptosis following

0.248 Gy [64]. However, there is currently no dose response data or RBE values for apoptotic induction in lymphocytes following thermal neutron radiation exposure.

Necrotic cell death is the main mode of cell death following very high doses of radiation, and is only viewed as an accidental occurrence following low-dose exposures [65]. Necrosis is largely thought of an accidental or uncontrolled cellular response, however, recent evidence indicates that necrosis may sometimes be under genetic control and that biochemical cascades mediate the necrotic response [66]. While much work is still required to understand necrotic regulation, the endpoint of cellular rupture creates an inflammatory response within tissues that has the potential to induce fibrosis and tumorigenesis [67]. To date, there is little information in the literature about primary or secondary cellular necrosis following radiation exposure, let alone information pertaining to RBE or dose responses.

## 1.5. Relative Biological Effectiveness

Relative biological effectiveness (RBE) is most commonly defined as the ratio of two doses needed to give the same biological effect (Figure 12). Gamma radiation is often used as the reference radiation to which a different radiation quality is compared. RBE is a unit-less quantity that advises radiation weighting factors ($w_R$), but is not equal to $w_R$. RBE is commonly reported in radiobiology as the relative biological effectiveness at minimal doses ($RBE_M$), a singular value

describing the maximum RBE of a particular radiation quality. This describes the ratio of the initial slopes of the dose response curves. Since dose response curves for low-LET gamma reference radiations are described by a linear quadratic model, using the initial low-dose linear portion of the dose response curve allows for comparison to other linear or linear-quadratic dose response curves [68].

To date, there are no precise experimental conditions recommended by the ICRP to minimize the multiple factors that can affect RBE values. Thus, it is important to keep in mind that RBE varies with dose rate, endpoint and cell type [68]. For instance, the probability that two DSBs will interact to form a chromosome aberration decreases with decreasing low-LET dose rate, as described earlier [29]. Different endpoints and cell types can also vary in their sensitivity to radiation. As such, radio-resistant cell types or endpoints would offer different RBE values than radio-sensitive cell types or endpoints. Additionally, inter-laboratory scoring variations can also affect RBE values as scorer bias can modify results. Lastly, the choice of reference radiation can affect $RBE_M$ values, as notable differences have been found when calculating neutron RBE relative to $^{137}Cs$ and $^{60}Co$ gamma data [69]. For these reasons, it is unsurprising that there is so much variability in the neutron RBE values recorded in the literature, as detailed below in Figure 14.

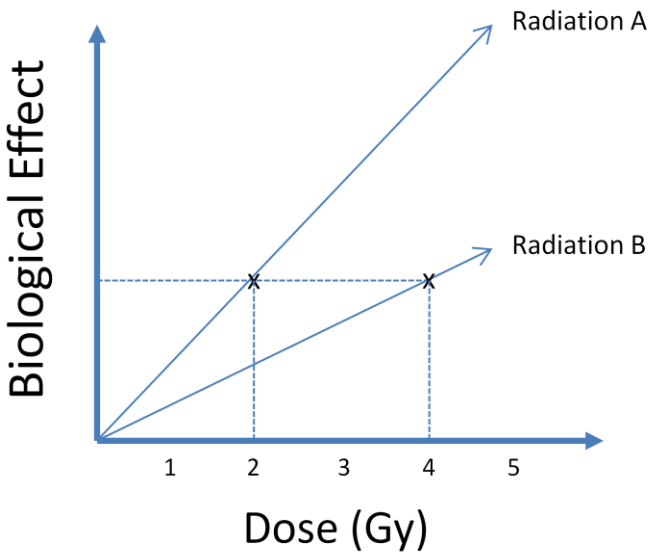


**Figure 12. Schematic of RBE calculation. Radiation A produces a biological effect at 2 Gy, whereas Radiation B (the reference radiation) produces the same effect at 4 Gy. Thus, the RBE of Radiation A is 2.**

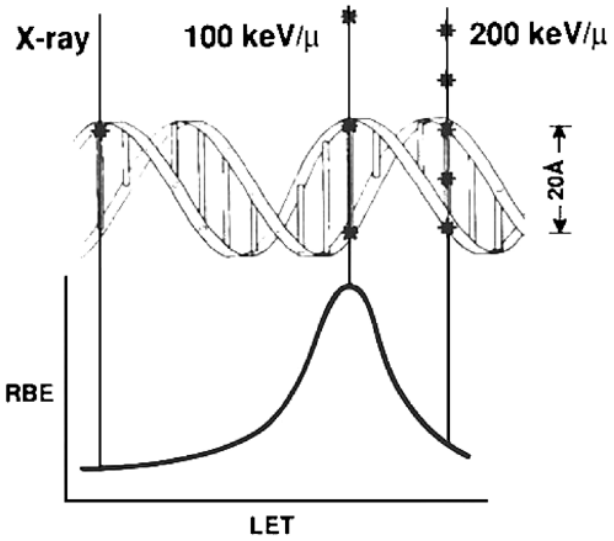


**Figure 13. Relationship between RBE and LET. Maximum RBE values occur at 100 keV $\mu m^{-1}$. This LET is most likely to cause a double strand DNA break. Adapted from Hall & Hei [70].**

RBE values are the greatest when the LET is approximately 100 keV $\mu m^{-1}$, as described in Figure 13. At this ionization density, a DSB is likely because the distance between ionizations is similar to the width of a DNA strand (2 nm). For low-LET radiation qualities, such as γ-rays, it is unlikely that a single track would cause a DSB. On the opposite end of the spectrum, very high-LET radiation qualities (ie. 200 keV $\mu m^{-1}$) are able to produce DSBs with a single track of radiation, however, because of the density of ionizations not all of the energy is needed for DSB induction. As RBE is defined as the ratio of doses to produce the same biological effect, radiation qualities with a LET beyond 100 keV $\mu m^{-1}$ have lower RBE's because the radiation is less effective at producing DSBs due to the "wasted" radiation.

Neutron RBE values for dicentric chromosome induction vary across the neutron energy spectrum, with the highest RBE values occurring in the 200-500 keV energy range [71]. As indicated in Table 5, the average reported thermal neutron DCA $RBE_M$ (±SE) value is 33 ± 24. (SD = 20, n = 3), the average intermediate energy DCA $RBE_M$ is approximately 26 (SD = 35, n = 3), and the average fast neutron energy DCA $RBE_M$ is approximately 29 (SD = 24, n= 22). However, it should be noted that there is much RBE variation across these ranges, especially for fast neutrons, as described in Figure 14. In contrast, the available apoptosis data indicates that the RBE values for apoptotic induction do not vary with fast neutron energy [59, 62, 63].

To date, much of the data pertaining to the biological effects of neutrons is from dicentric chromosome RBE studies in human lymphocytes. A review of the available dicentric and apoptosis data is presented in Table 5 and Table 6, respectively. In addition, Figure 14 illustrates diagrammatically the present variation in published DCA RBE values. Unfortunately, there is currently no RBE data pertaining to neutron-induced cellular necrosis in the literature. It is important to note that, unlike low-LET studies, there are no international guidelines detailing appropriate irradiation, cell culture, and data analysis methods for high-LET radiations.

There are presently three thermal neutron DCA RBE publications that examine dicentric chromosome induction. As with other neutron energies, there is little agreement on an exact thermal neutron RBE (±SE) quantity, with values of 36.4 ± 13.3 [28], 51.1 ± 31.3 [72], and 10.8 ± 1.8 [73, 74], reported in the literature, all in reference to the dicentric induction of $^{60}$Co gamma rays. It should be noted that the $RBE_M$ attributed to Sevan'kaev *et al*. [73, 74] was recalculated for the purposes of this thesis. Sevan'kaev *et al*. detailed how RBE varied with dose, but did not ascribe an overarching $RBE_M$ value. Similarly, there are only two publications examining the effect of $^{252}$Cf spectrum neutrons which report $RBE_M$ values of 7.7 and 27 [12, 75]. The $RBE_M$ of 7.7 is in reference to $^{137}$Cs radiation, while the $RBE_M$ of 27 is in reference to $^{60}$Co radiation. To-date, there have been no studies examining the dose response of apoptotic death in lymphocytes following thermal neutron exposure, however, apoptotic data from a wide range

of fast neutron energies including 280 keV [59], 5.5 MeV [62], and 62.5 MeV [63] indicate that the RBE for apoptosis induction remains at unity, as noted in Table 6.

**Table 5. Reported DCA RBE values following neutron irradiation of human blood lymphocytes.**

| Average Neutron Energy | Neutron Source | Anti-coagulant | Irradiation container | RBE (±SE) | RBE or $RBE_M$ | Reference radiation | Citation |
|---|---|---|---|---|---|---|---|
| THERMAL NEUTRONS Mean RBE (±SE) = 33 ± 24 (SD = 20, n = 3) | | | | | | | |
| 0.025 eV | FRM II research reactor (Germany) | Heparin | Quartz | 36.4 ± 13.3 | $RBE_M$ | $^{60}$Co Gamma-rays | Schmid *et al.* [28] |
| 0.025 eV | Kyoto University Research Reactor Institute (Japan) | Heparin | Polystyrene | 51.1 ± 31.3 | $RBE_M$ | $^{60}$Co Gamma-rays | Sasaki *et al.* [72]<br>Recalculated by Schmid *et al [28].* |
| 0.025 eV | BR-10 reactor (Russia) | n/a | Polyethylene | 10.8 ± 1.8 | $RBE_M$ | $^{60}$Co Gamma-rays | Sevan'kaev *et al.*[73]<br>Re-calculated by Schmid *et al [28].* |
| INTERMEDIATE ENERGY NEUTRONS Mean RBE = 26 (SD = 35, n = 3) | | | | | | | |
| 36 keV | Physikalisch-Technische Bundesanstalt accelerator (Germany) | n/a | Polyvinylcarbazo with polyethylenterephthalate | 67.1 ± 28.9 | $RBE_M$ | $^{60}$Co Gamma-rays | Schmid *et al.* [69] |
| 40 keV | KG – 2.5 accelerator $^{7}$Li(p,n)$^{7}$Be (Russia) | n/a | Polyethylene | 5.13 | $RBE_M$ | $^{60}$Co Gamma-rays | Sevan'kaev *et al.* [74]<br>*Re-calculated for this thesis using ratio of $\alpha$ coefficients |
| 90 keV | KG – 2.5 accelerator $^{7}$Li(p,n)$^{7}$Be (Russia) | n/a | Polyethylene | 6.1 | $RBE_M$ | $^{60}$Co | Sevan'kaev *et al.* [74]<br>*Re-calculated for this thesis using ratio of $\alpha$ coefficients |

continued

| Average Neutron Energy | Neutron Source | Anti-coagulant | Irradiation container | RBE (±SE) | RBE or $RBE_M$ | Reference radiation | Citation |
|---|---|---|---|---|---|---|---|
| FAST NEUTRONS Mean RBE ~ 28.6 (SD = 24, n = 22) | | | | | | | |
| 144 keV | Physikalisch-Technische Bundesanstalt accelerator (Germany) | Heparin | Polyvinylcarbazo with polyethylenterephthalate | 57.0 ± 18.8 | $RBE_M$ | $^{60}Co$ | Schmid *et al.* [76] |
| 350 keV | BR-10 reactor (Russia) | n/a | Glass | 19.3 | $RBE_M$ | $^{60}Co$ | Sevan'kaev *et al.* [74] *Re-calculated for this thesis using ratio of $\alpha$ coefficients |
| 385 keV | Physikalisch-Technische Bundesanstalt accelerator (Germany) | n/a | Polyvinylcarbazo with polyethylenterephthalate | 94.4 ± 38.9 | $RBE_M$ | $^{60}Co$ | Schmid *et al.* [69] |
| 565 keV | Physikalisch-Technische Bundesanstalt accelerator (Germany) | n/a | Polyvinylcarbazo with polyethylenterephthalate | 76.0 ± 29.5 | $RBE_M$ | $^{60}Co$ | Schmid *et al.* [77] |
| | | | | 54.2 ± 18.4 | $RBE_M$ | $^{137}Cs$ | |
| | | | | 20.3 ± 2.0 | $RBE_M$ | 220 kV X-rays | |
| 700 keV | BEPO reactor (Harwell, United Kingdom) | Heparin | Polycarbonate | 8.0 | RBE (200 rad) | $^{60}Co$ | Lloyd *et al.* [78] |
| | | | | 47 | $RBE_M$ | | |
| 850 keV | BR-10 reactor (Russia) | n/a | Glass | 9.7 | $RBE_M$ | $^{60}Co$ | Sevan'kaev *et al.* [74] *Re-calculated for this thesis using ratio of $\alpha$ coefficients |

continued

| Average Neutron Energy | Neutron Source | Anti-coagulant | Irradiation container | RBE (±SE) | RBE or $RBE_M$ | Reference radiation | Citation |
|---|---|---|---|---|---|---|---|
| 900 keV | AWRE Aldermaston (United Kingdom) | Heparin | Polycarbonate | 6.1 | RBE (200 rad) | $^{60}$Co | Lloyd *et al.* [78] |
| | | | | 36 | $RBE_M$ | | |
| 1.151 MeV | Physikalisch-Technische Bundesanstalt accelerator (Germany) | n/a | Polyvinylcarbazo with polyethylenterephthalate | 46.3 ± 19.1 | $RBE_M$ | $^{60}$Co | Schmid *et al.* [69] |
| | | | | 11.5 ± 1.3 | $RBE_M$ | 220 kV X-rays | |
| 1.6 MeV (average – fission spectra) | RENT 1 therapy beam from Forschungsreaktor München (FRM) reactor (Germany) | n/a | Polyvinylcarbazo with polyethylenterephthalate | 40.4 ± 16.4 | $RBE_M$ | $^{60}$Co | Schmid *et al*. [79] & Schmid *et al.* [69] |
| | | | | 10 ± 0.9 | $RBE_M$ | 220 kV X-rays | |
| 1.6 MeV (average – fission spectra) | RENT 1 therapy beam from Forschungsreaktor München (FRM) reactor (Germany) | n/a | Polyvinylcarbazo with polyethylenterephthalate | 37.4 ± 15.2 | $RBE_M$ | $^{60}$Co | Bauchinger *et al.* [80] & Schmid *et al.* [69] |
| | | | | 9.3 ± 0.9 | $RBE_M$ | 220 kV X-rays | |
| 2.1 MeV (average – fission spectra) | Californium-252 | n/a | 15 ml conical tube (no material mentioned) | 7.7 | RBE (1 Gy) | $^{137}$Cs | Tanaka *et al*. [12] |
| 2.1 MeV (average – fission spectra) | Californium-252 | n/a | Perspex | 27 | $RBE_M$ | $^{60}$Co | Lloyd *et al.* [75] |

continued

| Average Neutron Energy | Neutron Source | Anti-coagulant | Irradiation container | RBE (±SE) | RBE or $RBE_M$ | Reference radiation | Citation |
|---|---|---|---|---|---|---|---|
| 4.85 MeV | Physikalisch-Technische Bundesanstalt (PTB) accelerator facility (Germany) | n/a | Polyvinylcarbazo with polyethylenterephthalate | 32.3 ± 13.3 | $RBE_M$ | $^{60}Co$ | Schmid *et al.* [69] |
| | | | | 8.0 ± 0.7 | $RBE_M$ | 220 kV X-rays | |
| 6.5 MeV | Université Catholique de Louvain (UCL) cyclotron (Belgium) | Lithium Heparin | Polystyrene | 14.0 | $RBE_M$ | $^{60}Co$ | Fabry *et al.* [81] |
| 7.6 MeV | Hammersmith cyclotron (England, United Kingdom) | Heparin | Polycarbonate | 4.1 | RBE (200 rad) | $^{60}Co$ | Lloyd *et al.* [78] |
| | | | | 23 | $RBE_M$ | | |
| 14 MeV | Université Catholique de Louvain (UCL) cyclotron (Belgium) | Lithium Heparin | Polystyrene | 6.2 | $RBE_M$ | $^{60}Co$ Gamma-rays | Fabry *et al.* [81] |
| 14.6 MeV | Physikalisch-Technische Bundesanstalt (PTB) accelerator facility (Germany) | n/a | Polyvinylcarbazo with polyethylenterephthalate | 16.4 ± 6.8 | $RBE_M$ | $^{60}Co$ | Schmid *et al.*[69] |
| | | | | 4.1 ± 0.5 | $RBE_M$ | 220 kV X-rays | |
| 14.7 MeV | NG-150M neutron generator (Russia) | n/a | Glass | 2.6 | $RBE_M$ | $^{60}Co$ | Sevan'kaev *et al.* [74] *Re-calculated for this thesis using ratio of $\alpha$ coefficients |

continued

| **Average Neutron Energy** | **Neutron Source** | **Anti-coagulant** | **Irradiation container** | **RBE (±SE)** | **RBE or $RBE_M$** | **Reference radiation** | **Citation** |
|---|---|---|---|---|---|---|---|
| 14.7 MeV | Elliot P-tube generator (Scotland, United Kingdom) | Heparin | Polycarbonate | 2.7 | RBE (200 rad) | $^{60}$Co | Lloyd *et al.* [78] |
| | | | | 13 | $RBE_M$ | | |
| 14.9 MeV | $^{3}H(d,n)^{4}He$ reaction from 300 keV deuteron accelerator | Heparin | Poly(methyl methacrylate) | 4.1 | $RBE_M$ | 250 kVp X-rays | Lloyd *et al.* [82] |
| 15.0 MeV | BBC-Tandem accelerator | n/a | Nylon | variable | RBE | 220 kV X-rays | Bauchinger *et al. [83]* |
| 21 MeV | Université Catholique de Louvain (UCL) cyclotron (Belgium) | Lithium Heparin | Polystyrene | 4.7 | $RBE_M$ | $^{60}$Co | Fabry *et al.* [81] |
| 60 MeV | Université Catholique de Louvain (UCL) cyclotron (Belgium) | n/a | Plastic syringes | 14 ± 4 | $RBE_M$ | $^{60}$Co | Nolte *et al.* [84] |

**Table 6. Reported apoptosis RBE values following neutron irradiation of human blood lymphocytes.**

| Average Neutron Energy | Neutron Source | Anti-coagulant | Irradiation container | RBE | RBE or $RBE_M$ | Reference radiation | Citation | Year |
|---|---|---|---|---|---|---|---|---|
| 280 keV | McMaster University Accelerator Facility - $^{7}Li(p,n)^{7}Be$ reaction | Heparin | Information not available | 1 | RBE | $^{137}Cs$ Gamma-rays | Ryan *et al.* [59] | 2006 |
| 5.5 MeV | University of Gent CGR-MeV 520 cyclotron (Belgium) | Heparin | Information not available | 1 | RBE | $^{60}Co$ Gamma-rays | Vral *et al.* [62] | 1998 |
| 62.5 MeV | Douglas cyclotron (United Kingdom) | None | Information not available | 1 | RBE | Photons from a clinical linear accelerator | Warenius *et al.* [63] | 1995 |

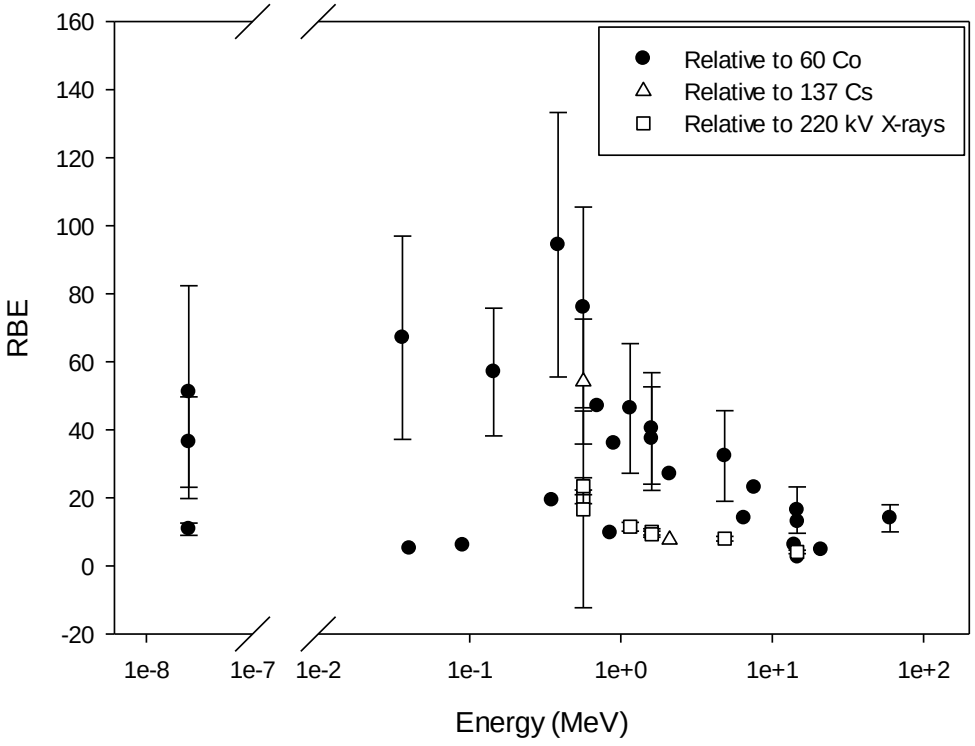


**Figure 14. Literature review of DCA RBE values vs. neutron energy.**

It is possible that the RBE value discrepancies are a result of multiple experimental factors. For instance, in the two studies with the highest RBE values, heparin was used as an anticoagulant. This would have artificially changed the percent sample nitrogen, since the $^{14}N(n,p)^{14}C$ reaction is the major dosing mechanism.

Lastly, apoptotic RBE values remain at unity following 280 keV and 5.5 MeV neutron irradiations of human lymphocytes and 62.5 MeV irradiations of mouse thymocytes.

## 1.6. Model System & Biological Endpoints

Human peripheral blood lymphocytes (PBL) were used for this work. Biological dosimetry and radiobiology assays frequently make use of lymphocytes and this cell type has been widely cited in the literature [29]. Lymphocytes make up approximately 30% of the leukocyte population, and they are a long-lived cell-type. For example, lymphocytes with stable damage may live up to 20 years in circulation, and lymphocytes with unstable damage may live up to 2.5 years in circulation [85].

### 1.6.1. Chromosome Aberrations

Dicentric and ring chromosome aberrations were examined using the DCA. Following irradiation, the T-cell sub-population of lymphocytes was stimulated with phytohemagglutinin to prompt the normally non-cycling cells to undergo division. The thymidine analogue bromodeoxyuridine (BrdU) was added during culture, and was incorporated into the sister chromatid during DNA synthesis. This facilitates fluorescence-plus-giemsa (FPG) staining, which allows differentiation between cells in the first mitotic cycle and cells in subsequent mitotic cycles, for which the latter display a “harlequin” chromatid effect (Figure 15). In contrast, cells in first mitosis display chromosomes with consistently dark chromatid staining [29].

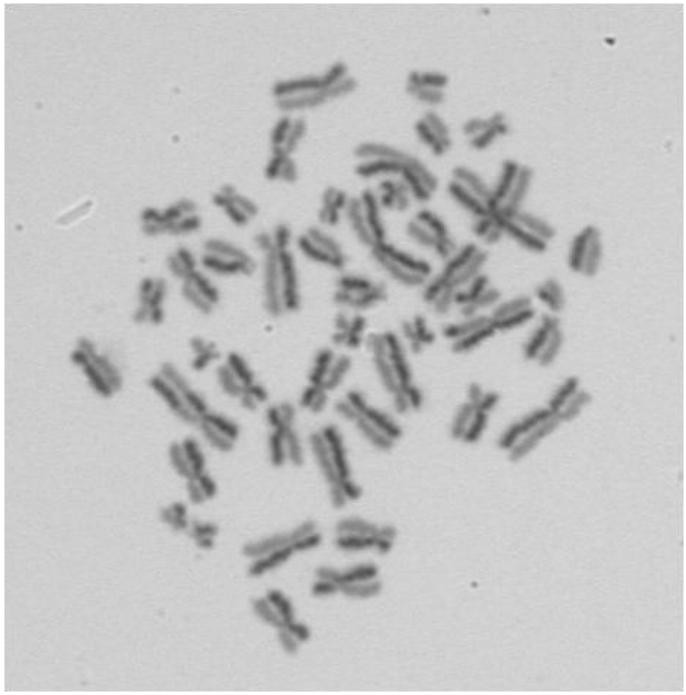

**Figure 15. A "harlequin" metaphase chromosome spread from a cell that has undergone two cell culture divisions. Image from the IAEA Cytogenetic Dosimetry publication [29].**

### 1.6.2. Dose Response Curves

Dose response curves demonstrate how a particular endpoint varies with dose. Commonly, low-LET radiation qualities show a linear-quadratic dose response for dicentric and ring chromosome induction, while high-LET radiation qualities exhibit a linear dose response, as described in Figure 16. To date, three separate laboratories have published thermal neutron dose response curves, all indicating a linear dose response for dicentric chromosome induction [28, 72, 74]. A similar linear response was found by Tanaka *et al*. and Lloyd *et al.* when examining the

effect of $^{252}$Cf fission neutron irradiations [12, 75]. As expected, linear dose response curves have also been found following intermediate [69, 74] and fast [69, 76-78, 83, 84] neutron exposures. In contrast, other neutron studies have demonstrated a linear quadratic response at fast energies [74, 78, 81, 82].

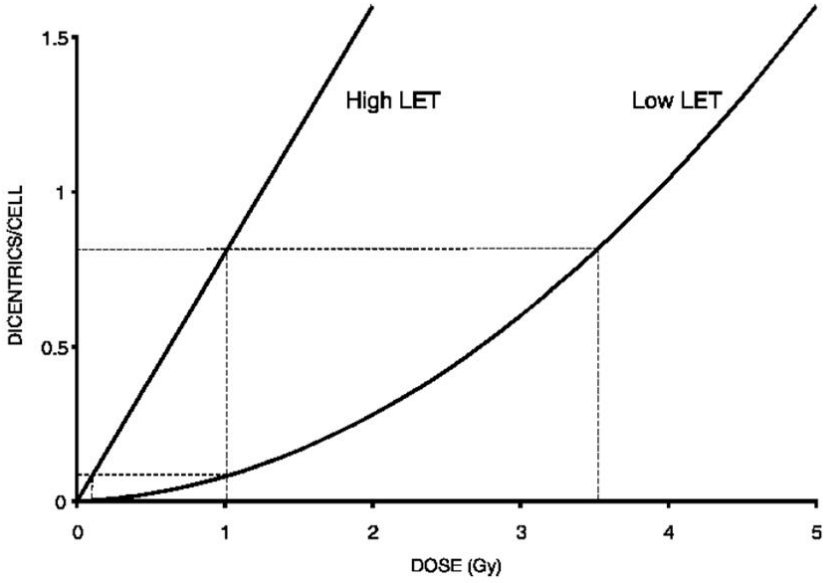


**Figure 16. Typical dose response curves. High-LET radiation qualities often result in a linear dose response, whereas low-LET radiation qualities demonstrate a linear quadratic dose response [29].**

Low-LET linear quadratic dose response relationships are normally described using Equation 2:

$$Ab = c + \alpha D + \beta D^2 \qquad (2)$$

Where:
*Ab* = number of aberrations per cell
*D* = absorbed dose, in Gy.
*α, β, c* = coefficients describing linear quadratic function

The $\alpha$ coefficient describes the linear portion of the dose-effect relationship where two DNA DSBs have been produced by a single charged particle, whereas the $\beta$ coefficient describes the quadratic relationship and where two breaks have been caused by separate charged particles. The $c$ coefficient is the background frequency of aberrations [29, 86]. With increasing LET, the likelihood that two breaks are produced by the same track also increases. Thus, for high-LET radiations, the relationship between dose and aberrations per cell is often linear and can be represented as Equation 3:

$$Ab = c + \alpha D \tag{3}$$

### 1.6.3. Cell Death

Two cell death modalities were examined in work undertaken for this thesis. Apoptosis was visualized through the use of the Annexin V antibody (also called Annexin A5), which has a high affinity for phosphatidylserine (PS), a cell membrane phospholipid. In healthy cells, PS is located in the inner leaflet of the plasma membrane, however in the early phases of apoptosis, cells lose asymmetry of their membrane proteins and PS becomes exposed on the exterior cell surface. This occurs in early apoptosis without compromising the integrity of the cell membrane and is meant to signal phagocytosing cells. Annexin V does not have innate fluorescence, so the Annexin V protein is bound to fluorescein-5-isothiocyanate (FITC) in a 1:1 ratio.

Necrotic cells, which include both primary and secondary necrotic populations, were distinguished *in vitro* by examining 7-aminoactinomycin D (7-AAD) uptake. 7-AAD intercalates in DNA, preferentially in guanine/cytosine-rich regions. It does not pass through intact cell membranes, thus for DNA intercalation to occur, the cell membrane must be disrupted. For this reason, live cells with intact membranes and early apoptotic cells will not exhibit 7-AAD staining. However late-apoptotic (also called secondary necrotic cells) and primary necrotic cells will show 7-AAD fluorescence due to loss of cell membrane integrity.

### 1.6.4. Flow Cytometry

Cell death analysis was performed using the Amnis ImageStream X flow cytometer which allows for the high-throughput analysis of cells, in comparison to traditional microscopy techniques. Briefly, fluorescently labelled cells are passed by an illumination point in single file where they may encounter a halogen light (brightfield) and/or a single wavelength laser. The scattering of brightfield and laser light as well as the excitation of florescent tags results a light signal that interacts with a photodetector. The signal is then processed and separated into six spectrally unique images of each cell.

The Amnis ImageStream X flow cytometer self-calibrates at the beginning of each use and uses speed beads to continually monitor the sample flow during analysis. Imaging of the speed beads provides constant feedback to the instrument and ensures that the focus and fluidics remain in an optimal state.

### 1.6.5. Risk Assessment

A risk assessment was completed to ensure the hazards associated with this work were thoroughly considered (see Appendix A). Briefly, the risk assessment addressed the possibility of musculoskeletal injuries, biological hazards, radiological hazards, chemical hazards, and environmental hazards. Mitigation and avoidance techniques were recommended to address the various hazards.

### 1.6.6. Ethical Considerations

The studies described in this thesis were approved by the Atomic Energy of Canada Limited (AECL) Committee on Research Involving Human Subjects. Blood donor anonymity was maintained throughout the study; only age ranges, gender, and past radio- and/or chemotherapy status was released.

# 2. CHAPTER 2 – CHROMOSOME ABERRATIONS FOLLOWING THERMAL AND FAST NEUTRON EXPOSURE

Declarations:

Laura Paterson was responsible for the experimental design, laboratory work, and data analysis.

Dr. Jovica Atanackovic and Dr. Samy El-Jaby performed Monte Carlo simulations to derive the fluence to kerma conversion coefficient that was used to calculate the neutron radiation doses.

Chad Boyer designed and fabricated the test tube holder used for the thermal neutron irradiations and operated the N5 triple axis spectrometer. In addition, Chad, in conjunction with the Analytical Chemistry Branch at CNL, performed gold foil activation experiments to confirm the thermal neutron flux.

Dr. Andre Yonkeu operated the $^{252}Cf$ irradiation source and assisted with the irradiation set-up.

## 2.1. INTRODUCTION

### 2.1.1. Overview

Neutron radiation exposure is a potential hazard in many fields, including medicine, nuclear research and nuclear power production. While stringent guidelines are in place to prevent occupational over exposures, accidental acute exposures may still occur, and as such, it is advantageous to understand the biological effects of neutron radiation. Furthermore, comparing the effects of neutron and gamma radiation allows for the exploration of issues concerning variation in radiation quality.

The field of biological dosimetry was born in 1962 when Bender and Gooch suggested that dicentric chromosome frequency could be used for radiation dose assessment [87]. The dicentric chromosome is a radiation-specific chromosome aberration that is induced in a dose-dependent manner [88]. To-date, the DCA remains the gold-standard for assessing radiation dose following an accidental acute exposure. This is achieved by examining solid-stained metaphase spreads from peripheral blood lymphocytes for specific radiation-induced changes. This chapter will describe the induction of dicentric and ring chromosomes following thermal neutron and $^{252}$Cf fission neutron exposures.

Currently, there is considerable interest in finding a biomarker of radiation quality – that is, a marker that behaves differently following exposure to gamma rays, neutrons, heavy ions, etc. To date, many of the studies investigating potential

biomarkers have focused on specific cytogenetic aberrations. It is well accepted that high-LET radiations can cause complex chromosome damage, specifically inter- or intrachanges involving three of more breakpoints in two or more chromosomes [45], with alpha particles [46], heavy ions [47], and neutrons [36] all inducing more complex aberrations than low-LET radiations at doses below 2 Gy. However, despite much research into the subject, no cytogenetic methods have been formally recognized by the IAEA as a definitive technique to identify radiation quality [29].

One of the first proposed cytogenetic biomarkers of radiation quality was the F ratio. In 1994, Brenner and Sachs proposed that the number of interchromosomal to intrachromosomal interarm aberrations, which can be interpreted as either the ratio of translocations to pericentric inversions, or the ratio of dicentric to centric rings, could differentiate between high- and low-LET radiations [89]. For densely ionizing radiation, F-ratios of about 6 were expected, whereas for low-LET gammas and x-rays, F-ratios of 15 or higher were likely. However, while this method proved promising for solid-stained samples, following the development and widespread use of the fluorescence in-situ hybridization (FISH) technique in the late 1990's and early 2000's, the utility of the F-ratio hypothesis was called into question [90-92]. As a result, a variety of alternative FISH-based biomarkers were investigated including the G ratio (acentric interstitial deletions to centric rings) [93], the H ratio (dicentrics to acentric interstitial deletions) [92], the S ratio (complete exchanges to incomplete rejoinings, or apparent complete exchanges to

hidden complete exchanges) [94], and the I ratio (total translocations to insertions) [95]. In addition, the ratio of complex to simple interchanges using multicolour fluorescence in-situ hybridization (mFISH) or spectral karyotyping (SKY) has generated interest [90, 96], as has insertion frequency [36].

In the absence of an inexpensive and time-sensitive biomarker of radiation quality, the ultility of the cellular distribution of chromosome damage was investigated as a potential biomarker of radiation exposures. Based on our current understanding of the biophysical action of ionizing radiation, specifically that as high-LET radiations deposit more energy per unit path length and typically have much shorter track lengths than low-LET radiations, a non-random distribution of high-LET chromosome aberrations is expected. That is, it is hypothesized that high-LET radiation will produce an over-dispersed population of dicentric chromosomes. This is in contrast to low-LET gamma radiation, which is known to produce a Poission-like distribution of dicentric chromosome aberrations. Even though mBAND studies have indicated greater overdispersion following alpha irradiation as compared to gamma radiation [97], it is currently unknown if this phenomenon can be applied to neutron-irradiated solid stained metaphase spreads.

## 2.2. METHODS

### 2.2.1. Irradiation Conditions

#### 2.2.1.1. $^{252}$Cf Neutron Irradiations

Fast neutron irradiations were completed at CNL using a $^{252}$Cf source housed within the Health Physics Neutron Generator (HPNG) facility. The cylindrical californium-palladium alloy source was obtained from Frontier Technology (Xenia, OH) in 2010. The source is encapsulated with two layers of stainless steel and is 9.4 mm in diameter and 25.7 mm long. The source certificate, dated February 18, 2010, indicates a preliminary neutron fluence rate of $2.3 \times 10^8$ neutrons $s^{-1}$. The CNL $^{252}$Cf source is moved in and out of the irradiation apparatus using a remotely controlled rabbit system. A test tube holder was built around the irradiation apparatus which allowed test tubes to be suspended at controlled distances throughout irradiation.

As indicated in Figure 17 and Figure 18, 15 mL polypropylene test tubes (Fisher Scientific) were suspended in a semi-circle 10 cm from the exterior of the source housing. The vertical centre of the blood volume aligned with the vertical centre of the $^{252}$Cf pellet. A REM500 (Health Physics Instruments) tissue equivalent proportional counter (TEPC) was also placed alongside the blood tubes, 10 cm from the $^{252}$Cf source, with the vertical center of the detector aligned with the vertical centre of the $^{252}$Cf pellet. The $^{252}$Cf dose rates were measured to be 15.6

mGy/h (for doses between 10 mGy, delivered in approximately 45 minutes, and 75 mGy, delivered over 5 hours) and 16.7 mGy/h for the 108 mGy dose point. Table 7 describes the doses and irradiation timings.

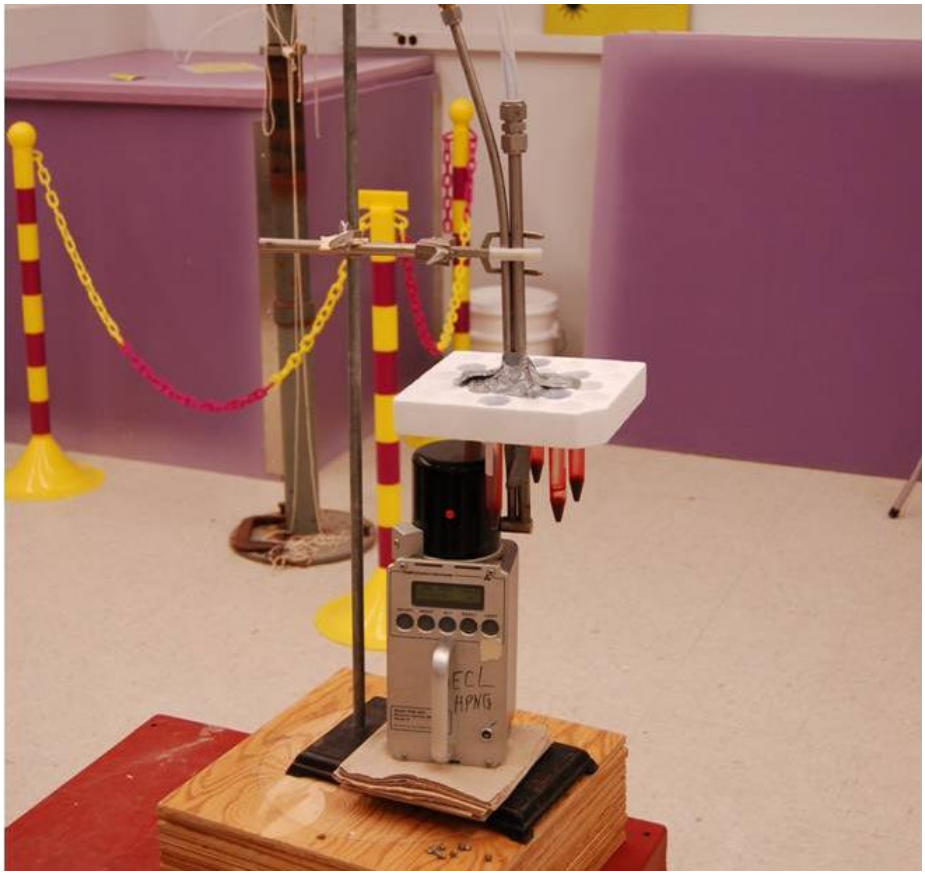


**Figure 17. $^{252}$Cf irradiation set-up.**

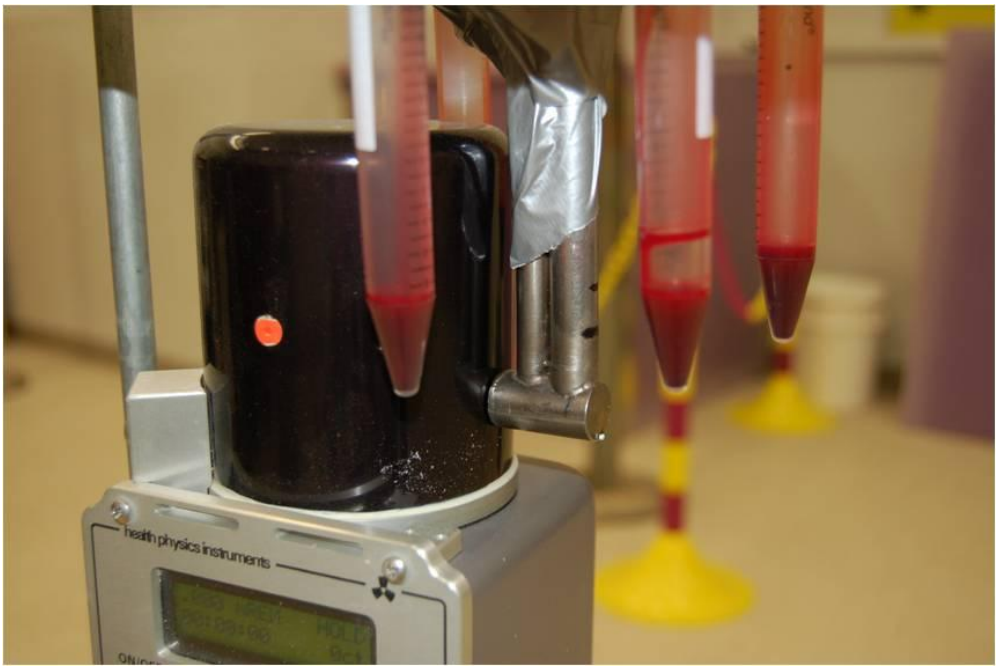


**Figure 18. Close-up image of the $^{252}$Cf irradiation set-up.**

**Table 7. $^{252}$Cf irradiation details.**

| NEUTRON DOSE (Gy) | GAMMA DOSE (Gy) | IRRADIATION TIME (h) | IRRADIATION DATE |
|---|---|---|---|
| 0 | 0 | - | - |
| 0.01 | 0.006 | 0.647 | April 30, 2012 |
| 0.025 | 0.015 | 1.62 | April 30, 2012 |
| 0.05 | 0.031 | 3.24 | April 30, 2012 |
| 0.075 | 0.046 | 4.87 | April 30, 2012 |
| 0.108 | 0.061 | 6.48 | May 9, 2012 |

#### 2.2.1.1.1. $^{252}$Cf Neutron Dose

The $^{252}$Cf spectra in the HPNG Facility was previously measured by Atanackovic *et al*. [98] using Bonner spheres, as detailed in Figure 19. The authors found that on January 1, 2012, the fluence rate at 100 cm from the $^{252}$Cf source was approximately $1.15 \times 10^3$ neutrons $cm^{-2}$ $s^{-}$, and the equivalent neutron dose rate was approximately 1.587 mSv/h [98]. These values represent the average of the MAXED and STAY'SL Bonner sphere unfolding codes used by Atanackovic *et al*. [98]. To account for source decay between January 1, 2012 and the blood irradiation dates, the standard decay equation (Equation 4) can be employed. As such, the fluence rates for the blood irradiations on April 30, 2012 and May 9, 2012 irradiations at 100 cm from the $^{252}$Cf pellet were calculated to be $1.054 \times 10^3$ neutrons $cm^{-2}$ $s^{-1}$, and $1.045 \times 10^3$ neutrons $cm^{-2}$ $s^{-1}$, respectively. Similarly, the dose rates on April 30, 2012 and May 9, 2012 were found to be 1.455 mSv/h and 1.446 mSv/h, respectively at 100 cm from the $^{252}$Cf source pellet. However, as the blood irradiations were performed at 10 cm from the $^{252}$Cf source, the inverse square law (Equation 5) was next applied. The use of the inverse square law is based on the assumptions that the $^{252}$Cf behaves as a point source at 10 cm. Thus, the fluence rate and dose rate at 10 cm would be one hundred times the measured fluence rate at 100 cm, resulting in a maximum experimental fluence rate of approximately $1.054\times 10^5$ neutrons $cm^{-2}$ $s^{-1}$ on April 30, 2012 and $1.045 \times 10^5$ neutrons $cm^{-2}$ $s^{-1}$ on May 9, 2012. Similarly, the dose rate at 10 cm on April 30, 2012 was 145.5 mSv/h and on May 9, 2012 the dose rate was 144.6 mSv/h.

As described in Figure 19, the $^{252}$Cf spectrum energy falls between approximately 0.1 and 10 MeV, with a small thermal peak at approximately 0.025 eV. The average weighting factor for the $^{252}$Cf fast neutron spectrum is approximately 13.8 [99], demonstrating that the dose rates given by Atanackovic *et al*. [98] of 145.5 mSv/h and 144 mSv/h can be considered in line with the REM500 measured dose rates on the blood irradiation days of 15.6 mGy/h and 16.7 mGy/h. Subtle variations in these values likely reflect rig and detector differences.

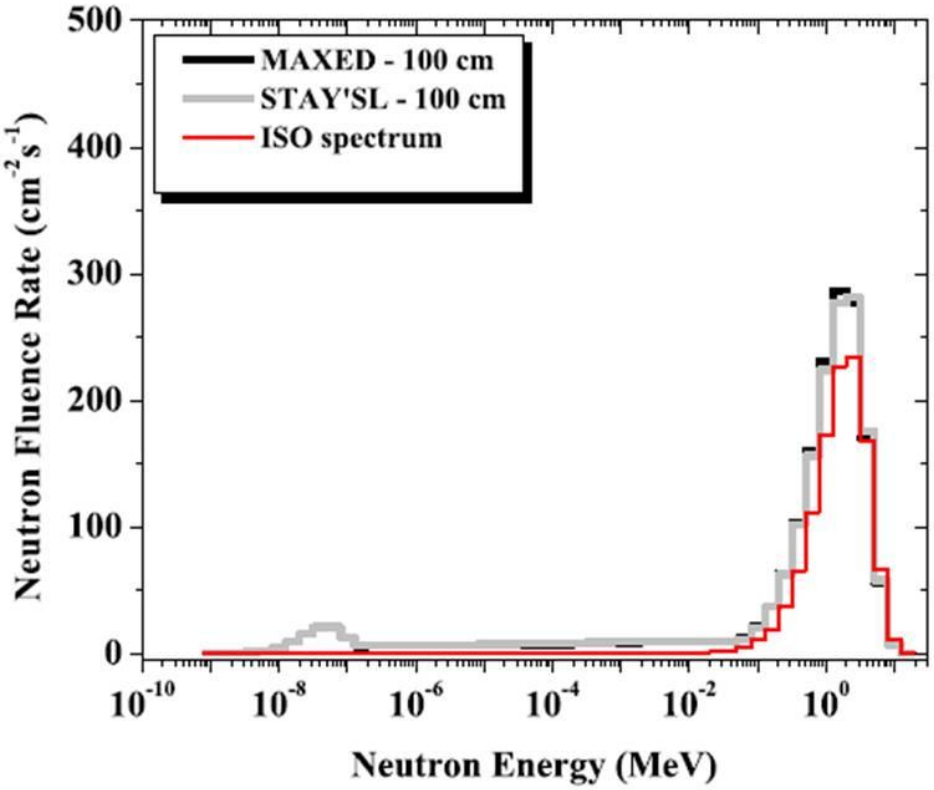


**Figure 19. Measured $^{252}$Cf spectrum in CNL's HPNG Facility using a Bonner sphere spectrometer [98]. The MAXED and STAY'SL graphs describe different unfolding methods used to interpret the Bonner sphere spectrometer data. The ISO spectrum represents the theoretical ISO-8529 $^{252}$Cf spectrum.**

$$N = N_o e^{\frac{-t\ln 2}{t_{1/2}}} \quad (4)$$

Where:
$N$ = calculated value
$N_o$ = original value
$t$ = time elapsed
$t_{1/2}$ = half life

$$\frac{I_1}{I_2} = \frac{{D_2}^2}{{D_1}^2} \quad (5)$$

Where:
$I_1$ = fluence rate at $D_1$
$I_2$ = fluence rate at $D_2$
$D_1$ = distance 1 from the source
$D_2$ = distance 2 from the source

#### 2.2.1.1.2. $^{252}$Cf Gamma Doses

The $^{252}$Cf gamma dose rate was measuring the using a P-200 gamma detector and SM713 probe (BOT Engineering) on January 14, 2016. At 60 cm, the average dose rate indicated was 0.1 mGy·h$^{-1}$. Using the standard decay equation (Equation 4) inverse square law (Equation 5), the dose rate at the 10 cm sample irradiation position on the April 30, 2012 and May 9, 2012 irradiation days was calculated to be 9.52 mGy·h$^{-1}$ and 9.45 mGy·h$^{-1}$, respectively. As the gamma dose contribution was found to be well below the threshold required to observe dicentric chromosome induction, as noted in Table 7, the gamma component to

the total dose received by the blood samples is treated as negligible and has been ignored throughout the remainder of this chapter.

#### 2.2.1.2. Thermal Neutron Beam Set-up

Thermal neutron irradiations were performed using the beam port and pyrolytic graphite monochromater associated with the N5 Triple-Axis Spectrometer at CNL's Canadian Neutron Beam Centre (CNBC).

The CNBC N5 spectrometer set-up is shown in Figure 20. Fission neutrons generated in the reactor, labelled "source" on Figure 20, can have energies up to 10 MeV. However, by the time the neutrons enter the beam tube, most have been cooled to thermal energies through interactions with the 60 °C (333 K) heavy water moderator [8]. A sapphire filter, identified by the blue rectangle in Figure 20, removes the remaining fast neutron energies. Further down the beam tube, the pyrolytic graphite monochromator, labelled "M" in Figure 20, refines the beam energies. As described in Figure 21, the monochromator crystal can select for one of two energies, 14.5 meV or 34.1 meV, depending on reflection angle. For the work described in Chapter 2 and 3, the monoenergetic 14.5 meV (0.0145 eV) energy was used. This translated into a fluence rate of $1.50 \times 10^{7}$ n $cm^{-2}$ $s^{-1}$ at the blood sample position labelled "B" in Figure 20.

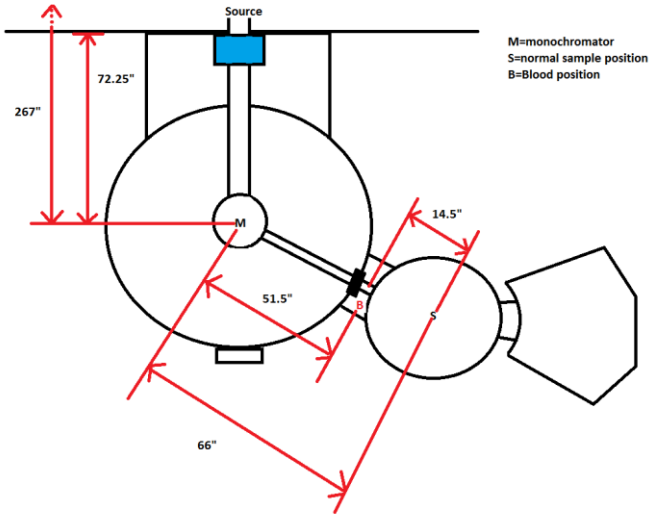


**Figure 20. CNBC N5 spectrometer blood irradiation set-up. Image modified from [8].**

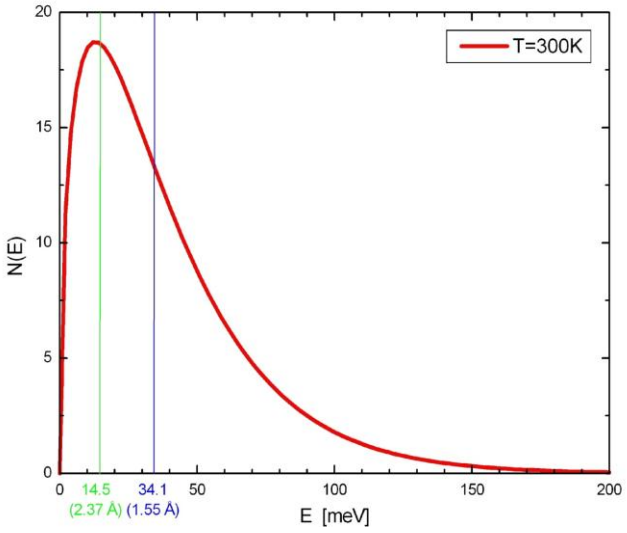


**Figure 21. The pyrolytic graphite monochromator can select for two distinct thermal energies – 14.5 meV and 34.1 meV. The red line details the energy spectrum incident on the monochromator crystal. Image supplied by CNBC.**

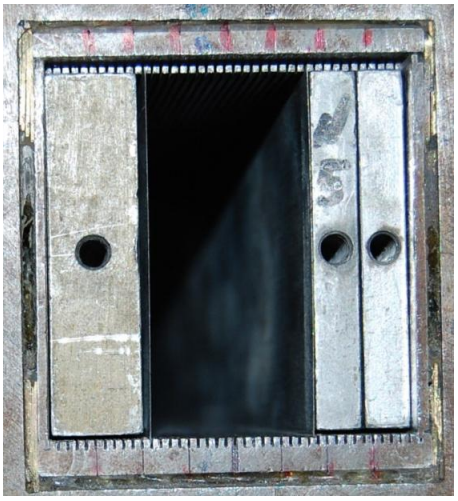

**Figure 22. Close-up photograph of CNBC N5 beam port.**

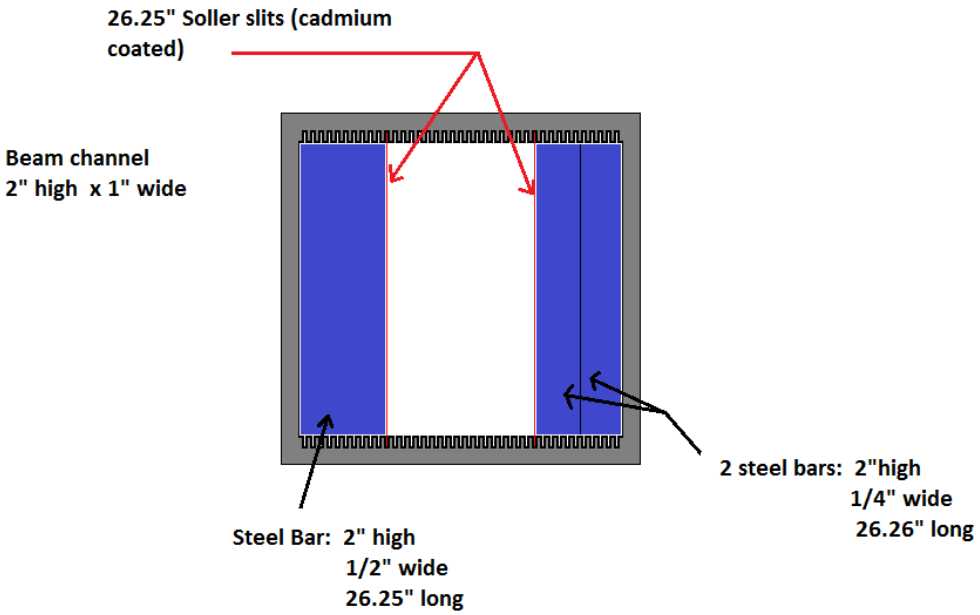


**Figure 23. CNBC N5 spectrometer beam port shaping. Image supplied by CNBC.**

As shown in Figure 22 and Figure 23, the beam port was modified to achieve a beam 2.54 cm wide × 5.08 cm high (1" × 2"). This was accomplished by using steel bars to narrow the beam port with cadmium-coated Soller slits placed on the inner face. The dimensions of the left steel bar was 1.27 cm wide × 5.08 cm high × 66.68 cm long (0.5" × 2" × 26.25"). The right side of the beam port was shaped using two separate steel bars, with combined dimensions of 1.27 cm wide × 5.08 cm high × 66.68 cm long (0.5" × 2" × 26.25"). The Soller slits were 0.5 mm wide × 5.08 cm high × 66.68 cm long.

#### 2.2.1.3. Cell Irradiations

15 mL polypropylene test tubes (Fisher Scientific), each containing 1.5 mL of blood, were suspended on a computer-controlled gantry in front of the N5 Triple-Axis Spectrometer beam port that was adjusted to a beam dimension of 2.54 cm × 5.08 cm. The test tubes had 1.5 mm thick polypropylene walls, with the blood sitting in the conical tip (Figure 24). The thermal neutron doses ranged between 1.2 mGy and 13.4 mGy at a dose rate of 12 mGy $h^{-1}$. These exposures are lower than optimal and will be explained later. This resulted in irradiation timings ranging between 53 s and 4034 s, as described in Table 8.

All blood samples were irradiated at room temperature, and transportation temperature variations were minimized through the use of a Styrofoam cooler. Control tubes were left at room temperature for the entire irradiation period.

**Table 8. Thermal neutron doses and irradiation timings for chromosome aberration experiment.**

| THERMAL NEUTRON DOSE (mGy) | REACTOR POWER (MW) | TOTAL NEUTRON COUNTS | IRRADIATION TIME (s) |
|---|---|---|---|
| 0.00 | -- | -- | -- |
| 1.2 | 90-92 | 6894675 | 403 |
| 1.6 | 90-92 | 9172275 | 536 |
| 1.8 | 96-98 | 10795161 | 538 |
| 4.4 | 96-98 | 26331032 | 1344 |
| 8.9 | 96-98 | 52480947 | 2688 |
| 13.4 | 96-98 | 79338168 | 4034 |

#### 2.2.1.3.1. Thermal Neutron Dose Calculations

The dose delivered to the blood volumes was indirectly determined using the Monte Carlo N-Particle (MCNP 5) radiation transport code [100][1]. In these simulations, the neutron beam and target geometry illustrated in Figure 24 was modelled. The composition of blood was input using elemental compositions given in ICRP Publication 23 (Reference Man), which included a nitrogen concentration of 2.9% [7]. The thermal neutron fluence rate at the sample holder was calculated to be $1.50 \times 10^7$ neutrons $cm^{-2}$ $s^{-1}$, following gold foil measurements performed in August 2015. Fluence to kerma conversion

[1] MCNP modelling was completed by J. Atanackovic & S. El-Jaby

coefficient for thermal neutrons, which in this particular situation is equivalent to dose absorbed, was calculated to be $2.31 \times 10^{-13}$ Gy $cm^2$. This neutron kerma factor is well aligned with published values [28, 101]. The dose reflects the average dose across the whole sample (ie. not the entry, exit, or mid-point dose).

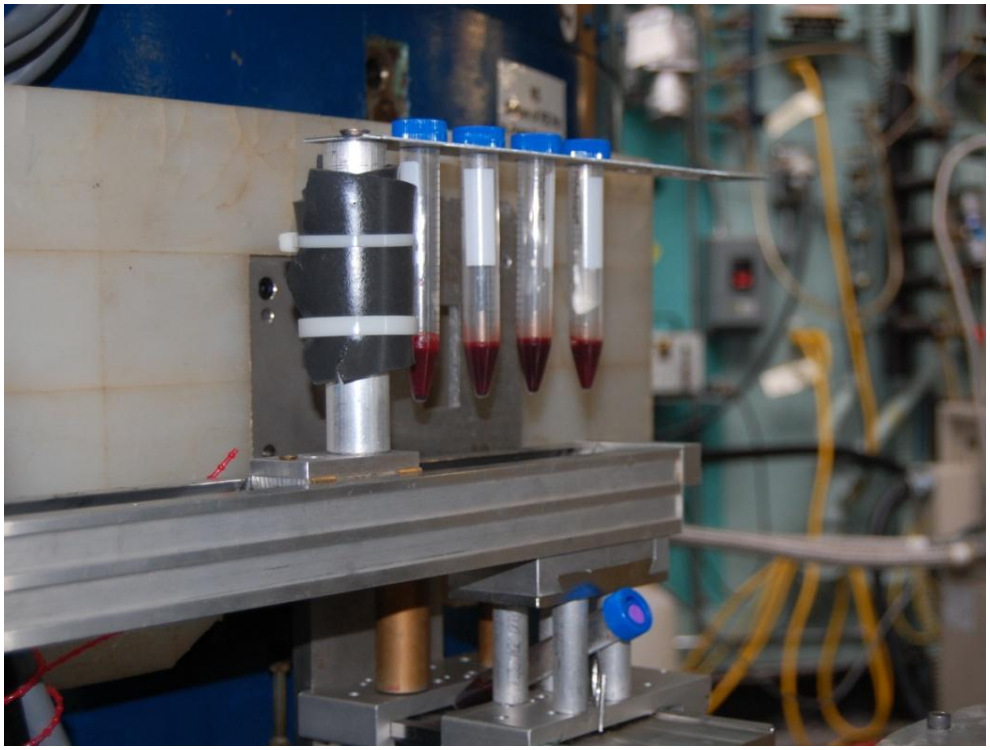

**Figure 24. Thermal neutron irradiation set-up. The sample tubes are suspended on a computer-controlled gantry in-front of the beam port. The gamma field control tube (bottom) sits outside of the neutron beam.**

### 2.2.2. Cell Culture

Blood was drawn *via* venipuncture from a healthy male blood donor (aged between 25 and 30 years old) who routinely donates for other biological dosimetry work at CNL. As such, it is well documented that this individual's

white blood cells respond normally to radiation exposure. Blood from the same donor was used for both the $^{252}Cf$ and thermal neutron irradiations.

The International Atomic Energy Agency (IAEA) guidelines on cytogenetic dosimetry recommend the use of heparinised anticoagulants, specifically lithium heparin [29]. However, for thermal neutron exposures, sodium citrate-containing vacutainers (BD Biosciences) were used. As the major dosing mechanism is a $^{14}N(n,p)^{14}C$ reaction, nitrogen-containing anticoagulants like sodium and lithium heparin were avoided because the number of heparin molecules found in different lots of sodium heparin can vary. As such, it is not possible to accurately calculate the effect of varying nitrogen levels. For fast neutron exposures, sodium heparin was chosen as an anticoagulant. Lithium heparin was avoided as lithium can undergo a (n,α) reaction, which could affect both dosimetry and user safety.

Following venipuncture, 1.5 mL aliquots of anticoagulated whole blood were transferred into 15 mL polypropylene test tubes (Fisher Scientific), and the tubes were taken to the appropriate irradiation facility. Following both thermal and fast neutron exposures, whole blood cultures were treated according to IAEA recommendations [29]. 1 mL of whole blood was transferred to a T-25 cell culture flask (Nunc) containing 9 mL of Roswell Park Memorial Institute RPMI-1640 medium (Hyclone), with 15% fetal bovine serum (Sigma-Aldrich), 100 units $mL^{-1}$ penicillin and 100 μg $mL^{-1}$ streptomycin (Sigma-Aldrich), and 20 μM of bromodeoxyuridine (BD Biosciences). 100 μL of phytohemagglutinin (PHA) was added to stimulate lymphocyte T-cell division. Cultures were incubated for 48

hours at 37 °C with 5% carbon dioxide ($CO_2$) in air. To induce cell cycle arrest in metaphase, 100 µl of colcemid (Life Technologies) was added for the final 4 hours of incubation.

### 2.2.3. Cell Harvest

Following incubation, cells were transferred back to polypropylene tubes for harvest. Tubes were centrifuged for 8 minutes at 200 xg, the supernatant was removed, and the pellet was re-suspended. To swell the cells, 10 mL of 0.075 M potassium chloride hypotonic solution (Gibco) was added. Following a 15 minute room temperature incubation, 2 mL of Carnoy's fixative (3 parts methanol to 1 part glacial acetic acid (both Fisher Scientific) was added. The samples were mixed, and allowed to sit at room temperature for another 10 minutes. The tubes were then centrifuged for 8 minutes at 200 xg. The supernatant was removed, and the pellet was re-suspended. Next, cells were washed twice with 10 mL of Carnoy's fixative and again centrifuged at 200 xg for 8 minutes.

### 2.2.4. Slide-Making

Slide making was completed using the Hanabi Metaphase Spreader (Transition Technologies Inc.) which allowed for consistent and reproducible environmental control. The Hanabi Metaphase Spreader was run with 30 °C base temperature, 30 °C wall temperature, and 30 °C bath temperature. These values indicate the temperature increase above ambient, and therefore translate into a humid internal environment of approximately 50 °C. The airflow setting was adjusted to 5.

Slides were allowed to age for a minimum for 1 day at room temperature prior to FPG staining.

### 2.2.5. Staining

To achieve FPG staining, slides were immersed in 20 μg $mL^{-1}$ Bisbenzimide H 33258 for 2 minutes and then placed face-up on the lab bench. 100 μL of 0.6 M sodium phosphate (pH 9.0) was added to the slide face and covered with a plastic coverslip. The slide placed 2.5 cm under a 365 nm ultraviolet light for 4 minutes, washed three times in ultra-pure water, and stained for 10 minutes in 10% Giemsa Stain (Fisher Scientific) in Gurr buffer (Gibco). This was followed by two quick washes in Gurr buffer and water. Lastly, slides were quick-dried using filtered and pressurized laboratory air to blow off excess fluid. Cover slips were mounted using Permount (Fisher Scientific) and allowed to dry a minimum of 6 hours before aberration scoring to ensure coverslips did not dislodge during automated microscope capture.

### 2.2.6. Aberration Scoring

Microscope slides were blinded and the Metafer Slide Scanning System (Metasystems Group Inc) was used to automate metaphase finding. The Metafer first scans each slide under 100 X power to determine the location of all metaphase spreads. At this stage, the Metafer presents the user with a series of thumbnails that, without providing too much detail about the actual chromosome complement, allows the user to select the metaphase spreads to be captured at

higher magnification (1000 X). Thumbnails that contained either more than one metaphase spread or a very condensed metaphase spread (not well spread, often containing multiple chromosome overlaps) were not selected for 1000 X capture. Complete metaphase spreads were manually scored according to the criteria laid out in the IAEA Cytogenetic Dosimetry publication [29]. Briefly, centromeres were counted to ensure metaphase spread completeness, with a complete spread requiring the detection of 46 centromeres. Metaphase spreads were then examined for the presence of dicentric chromosomes, centric rings, and acentric fragments. Dicentric and centric ring chromosomes were only scored if they were accompanied by at least one acentric fragment. Tricentric chromosomes were considered equivalent to the formation of two dicentric chromosomes (both require a minimum of four DSBs), and thus required a minimum of two associated acentric fragments.

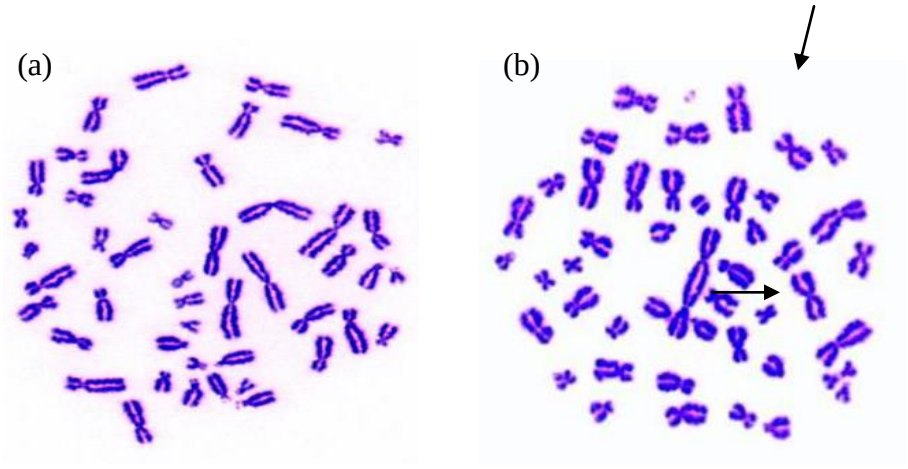


**Figure 25. Metaphase spreads with (a) no damage, and (b) a dicentric chromosome in the middle and an associated acentric fragment on the periphery (arrows).**

### 2.2.7. Statistics

The results of the DCA were tested for compliance with the Poisson distribution, which describes the probability of a given number of events occurring in a specified time interval, at a known average rate, but independent of time since the previous event. To achieve this, the dispersion index and the u test statistic were calculated for all doses. The dispersion index was calculated by dividing the variance by the mean, and indicates whether the data aligns with a Poisson distribution (which would demonstrate a dispersion index of unity), or whether data is over- or under-dispersed . The u test statistic, or the normalized unit of the dispersion index, as described by Equation 6, indicates the significance of the dispersion. Results above 1.96 indicated over-dispersion at the 5% significance level [29, 102].

$$u = (\sigma^2/y - 1)\sqrt{\frac{N-1}{2(1-\frac{1}{X})}} \qquad (6)$$

Where:
$\sigma^2$ = variance
$y$ = mean
$N$ = number of cells analyzed
$X$ = number of dicentric and ring chromosomes

## 2.3. RESULTS

### 2.3.1. Exposure to a Bare $^{252}$Cf Source

The distribution of chromosome aberrations following the $^{252}$Cf irradiations is given in Table 9. A total of 2875 metaphase spreads were examined yielding 200 chromosome aberrations. As a function of dose, aberration yield varied from 0 dicentric chromosomes in 500 metaphase spreads at 0 Gy, to 95 dicentric chromosomes in 600 spreads at 0.108 Gy. As such, the background yield was 0 aberrations per cell and the maximum yield at 0.108 Gy was 0.158 aberrations per cell. The quality of the data was tested by calculating the dispersion index (variance divided by the mean) and the *u* value (normalized unit of the dispersion index) (Equation 6), as given in Table 9. All data points, except for 0.075 Gy, conformed to the Poisson distribution. This indicates an absence of clustered damage at the majority of the dose points. Overall, the data conformed to a linear dose response, illustrated in Figure 26, with a $R^2$ value of 0.98. Equation 7 details the linear dose-response relationship calculated using the iteratively reweighted least squares method recommended by the IAEA [29, 103], and Table 10 illustrates the standard error values for each dose response equation term. The Dose Estimate software package was used to verify proper curve fitting [103]. Table 11 gives the 95% lower (LCL) and upper confidence limits (UCL) for each dose point. The $^{252}$Cf chromosome analysis raw data is listed in Table 12.

**Table 9. $^{252}$Cf chromosome aberration distribution.**

| NEUTRON DOSE (Gy) | CELLS SCORED | ABERR-ATIONS | DISTRIBUTION OF ABERRATIONS | | | | ABERR-ATIONS PER CELL | DISPERSION INDEX($\sigma^2$/y) | u VALUE |
|---|---|---|---|---|---|---|---|---|---|
| | | | 0 | 1 | 2 | 3 | | | |
| 0 | 500 | 0 | 438 | 0 | 0 | 0 | 0 | - | - |
| 0.010 | 300 | 3 | 297 | 3 | 0 | 0 | 0.010 | 0.99 | 0.100 |
| 0.025 | 500 | 21 | 480 | 19 | 1 | 0 | 0.042 | 1.06 | 0.896 |
| 0.050 | 464 | 34 | 435 | 26 | 3 | 0 | 0.073 | 1.06 | 0.854 |
| 0.075 | 511 | 47 | 470 | 37 | 3 | 1 | 0.092 | 1.15 | 2.39* |
| 0.108 | 600 | 95 | 518 | 74 | 7 | 1 | 0.158 | 1.03 | 0.437 |

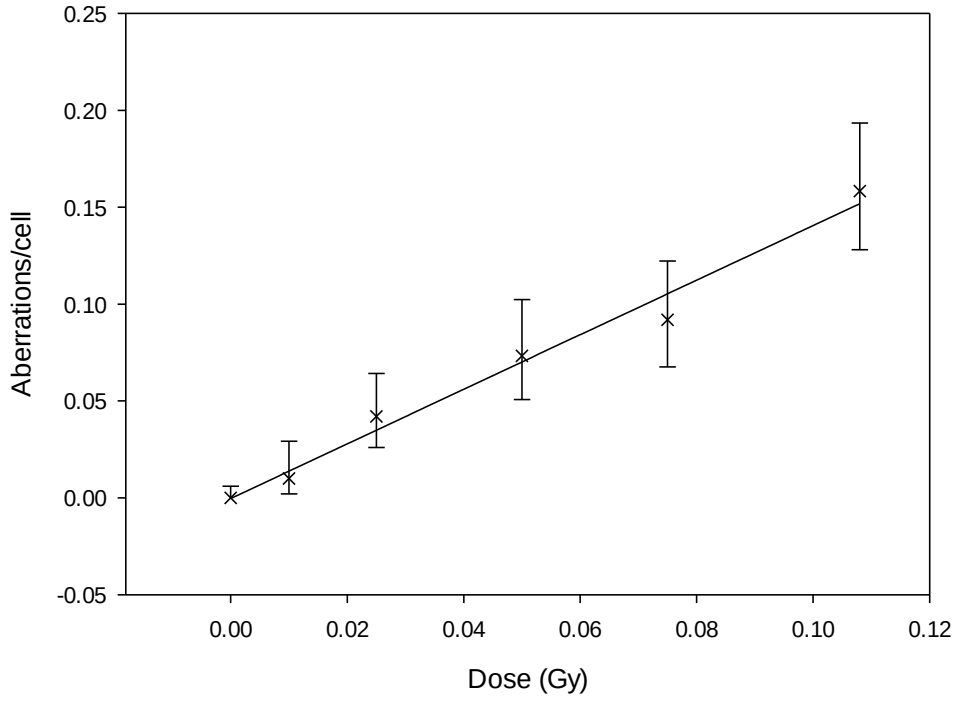


**Figure 26. $^{252}$Cf dose response curve detailing the relationship between radiation dose and aberrations per cell. Error bars represent the 95% confidence limits. The $R^2$ value is 0.98.**

* Non-Poisson distribution

$$Ab = 1.41D \quad (7)$$

Where:
*Ab* = aberrations/cell
*D* = dose (in Gy)

**Table 10. $^{252}$Cf dose response curve values (±SE) for linear relationship Ab = c + αD.**

| ***α*** **(±SE)** | ***c*** **(±SE)** |
|---|---|
| 1.41 ± 0.1 | 0 ± 0 |

**Table 11. $^{252}$Cf dose-response curve 95% lower and upper confidence limits**

| NEUTRON DOSE (Gy) | CELLS SCORED | TOTAL ABERR-ATIONS | ABERR-ATIONS PER CELL | 95% LCL | 95% UCL |
|---|---|---|---|---|---|
| 0 | 500 | 0 | 0 | 0 | 0.007 |
| 0.010 | 300 | 3 | 0.010 | 0.002 | 0.029 |
| 0.025 | 500 | 21 | 0.042 | 0.026 | 0.064 |
| 0.050 | 464 | 34 | 0.073 | 0.051 | 0.102 |
| 0.075 | 511 | 47 | 0.092 | 0.068 | 0.122 |
| 0.108 | 600 | 95 | 0.158 | 0.128 | 0.194 |

## Table 12. $^{252}$Cf DCA complete scoring data.

| 0 Gy | Cells Scored | Aberrations | | Acentrics | Aberrations per cell | | |
|---|---|---|---|---|---|---|---|
| | | Dicentrics | Rings | | 1 event | 2 events | 3 events |
| Slide 1 | 188 | 0 | 0 | 1 | 0 | 0 | 0 |
| Slide 2 | 62 | 0 | 0 | 2 | 0 | 0 | 0 |
| Slide 3 | 150 | 0 | 0 | 1 | 0 | 0 | 0 |
| Slide 4 | 100 | 0 | 0 | 1 | 0 | 0 | 0 |
| **TOTAL** | **500** | **0** | **0** | **5** | **0** | **0** | **0** |

| 0.01 Gy | Cells Scored | Aberrations | | Acentrics | Aberrations per cell | | |
|---|---|---|---|---|---|---|---|
| | | Dicentrics | Rings | | 1 event | 2 events | 3 events |
| Slide 1 | 100 | 0 | 0 | 5 | 0 | 0 | 0 |
| Slide 2 | 100 | 2 | | 7 | 2 | 0 | 0 |
| Slide 3 | 100 | 1 | | 6 | 1 | 0 | 0 |
| **TOTAL** | **300** | **3** | **0** | **18** | **3** | **0** | **0** |

| 0.025 Gy | Cells Scored | Aberrations | | Acentrics | Aberrations per cell | | |
|---|---|---|---|---|---|---|---|
| | | Dicentrics | Rings | | 1 event | 2 events | 3 events |
| Slide 1 | 100 | 1 | 0 | 15 | 1 | 0 | 0 |
| Slide 2 | 100 | 7 | 2 | 16 | 7 | 1 | 0 |
| Slide 3 | 75 | 2 | 0 | 9 | 2 | 0 | 0 |
| Slide 4 | 100 | 2 | 2 | 9 | 4 | 0 | 0 |
| Slide 5 | 125 | 5 | 0 | 16 | 5 | 0 | 0 |
| **TOTAL** | **500** | **17** | **4** | **65** | **19** | **1** | **0** |

| 0.05 Gy | Cells Scored | Aberrations | | Acentrics | Aberrations per cell | | |
|---|---|---|---|---|---|---|---|
| | | Dicentrics | Rings | | 1 event | 2 events | 3 events |
| | | | | | | | |
| Slide 1 | 100 | 4 | 1 | 18 | 5 | 0 | 0 |
| Slide 2 | 100 | 10 | 2 | 20 | 6 | 2 | 0 |
| Slide 3 | 64 | 3 | 1 | 8 | 4 | 0 | 0 |
| Slide 4 | 100 | 7 | 0 | 14 | 7 | 0 | 0 |
| Slide 5 | 100 | 6 | 0 | 14 | 4 | 1 | 0 |
| **TOTAL** | **464** | **30** | **4** | **74** | **26** | **3** | **0** |

| 0.075 Gy | Cells Scored | Aberrations | | Acentrics | Aberrations per cell | | |
|---|---|---|---|---|---|---|---|
| | | Dicentrics | Rings | | 1 event | 2 events | 3 events |
| | | | | | | | |
| Slide 1 | 100 | 6 | 1 | 14 | 6 | 0 | 0 |
| Slide 2 | 100 | 7 | 0 | 19 | 4 | 0 | 1 |
| Slide 3 | 100 | 12 | 0 | 20 | 10 | 1 | 0 |
| Slide 4 | 61 | 3 | 1 | 8 | 2 | 1 | 0 |
| Slide 5 | 50 | 6 | 0 | 9 | 6 | 0 | 0 |
| Slide 6 | 100 | 8 | 3 | 18 | 9 | 1 | 0 |
| **TOTAL** | **511** | **42** | **5** | **88** | **37** | **3** | **1** |

Continued

| 0.108 Gy | Cells Scored | Aberrations | | Acentrics | Aberrations per cell | | |
|---|---|---|---|---|---|---|---|
| | | Dicentrics | Rings | | 1 event | 2 events | 3 events |
| | | | | | | | |
| Slide 1 | 100 | 13 | 3 | 27 | 12 | 2 | 0 |
| Slide 2 | 100 | 13 | 2 | 25 | 11 | 2 | 0 |
| Slide 3 | 100 | 10 | 3 | 24 | 13 | 0 | 0 |
| Slide 4 | 100 | 14 | 1 | 28 | 12 | 1 | 0 |
| Slide 5 | 100 | 16 | 0 | 22 | 12 | 2 | 0 |
| Slide 6 | 100 | 17 | 3 | 39 | 14 | 0 | 1 |
| **TOTAL** | **600** | **83** | **12** | **165** | **74** | **7** | **1** |

### 2.3.2. Exposure to Thermal Neutron Beam

Table 13 gives the distribution of chromosome aberrations following thermal neutron exposure. A total of 4437 metaphase spreads were examined yielding 57 chromosome aberrations. As a function of dose, aberration yield varied from 1 dicentric chromosome in 629 metaphase spreads at 0 Gy, to 35 dicentric chromosomes in 1174 spreads at 0.0134 Gy (13.4 mGy). As such, the background yield was 0.002 aberrations per cell and the maximum yield at 13.4 mGy was 0.029 aberrations per cell. The quality of the data was tested by calculating the dispersion index (variance/mean) and the associated value of the u statistic, as given in Equation 6. This showed that all data points, except for 13.4 mGy, conformed to the Poisson distribution, indicating an absence of clustered damage among the lower doses. Overall, the data conformed to a linear dose response, illustrated in Figure 27, and described in Equation 8, with a $R^2$ value of 0.96. The 95% confidence intervals given in Table 15 were calculated according to the iteratively reweighted least squares method recommended by the IAEA for cytogenetic dosimetry [29]. The Dose Estimate software package was used to

confirm both curve fit and the 95% confidence limits [103]. The chromosome analysis raw data is listed in Table 16.

**Table 13. Thermal neutron chromosome aberration distribution.**

| NEUTRON DOSE (Gy) | CELLS SCORED | ABERR-ATIONS | DISTRIBUTION OF ABERRATIONS | | | ABERR-ATIONS PER CELL | DISPER-SION INDEX ($\sigma^2/y$) | u VALUE |
|---|---|---|---|---|---|---|---|---|
| | | | 0 | 1 | 2 | | | |
| 0 (Gamma Control) | 1127 | 2 | 1125 | 2 | 0 | 0.002 | 0.99 | -0.030 |
| 0 | 629 | 1 | 628 | 1 | 0 | 0.002 | 1 | - |
| 0.0012 | 770 | 9 | 761 | 9 | 0 | 0.012 | 0.99 | -0.216 |
| 0.0018 | 485 | 5 | 480 | 5 | 0 | 0.010 | 0.99 | -0.144 |
| 0.0089 | 221 | 5 | 216 | 5 | 0 | 0.023 | 0.98 | -0.213 |
| 0.0134 | 1205 | 35 | 1174 | 27 | 4 | 0.029 | 1.20 | 4.992* |

* Non-Poisson distribution

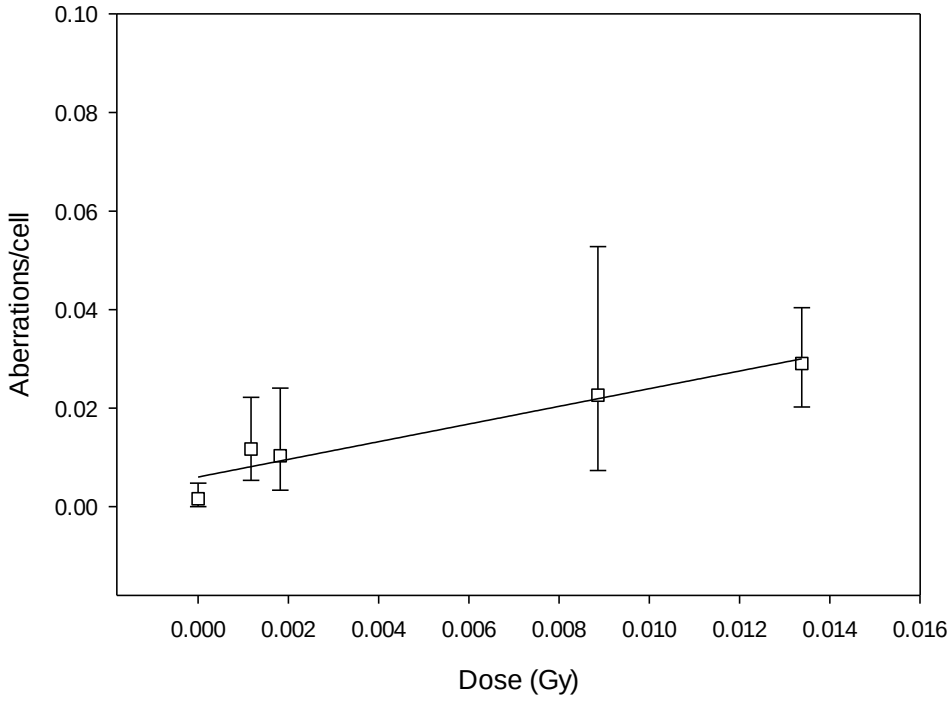


**Figure 27. Thermal neutron dose response curve indicating the relationship between radiation dose and the number aberrations per cell. Error bars represent the 95% confidence limits. $R^2$ value of 0.96.**

$$Ab = 0.005 + 1.86D \quad (8)$$

Where:
*Ab* = aberrations/cell
*D* = dose (in Gy)

**Table 14. Thermal neutron dose response curve values (±SE) for linear relationship Ab = c + αD.**

| ***α*** **(±SE)** | ***c*** **(±SE)** |
|---|---|
| 1.86 ± 0.44 | 0.005 ± 0.023 |

**Table 15. Thermal neutron dose-response curve 95% confidence intervals.**

| NEUTRON DOSE (Gy) | CELLS SCORED | TOTAL ABERR-ATIONS | ABERR-ATIONS PER CELL | 95% LCL | 95% UCL |
|---|---|---|---|---|---|
| 0 | 629 | 1 | 0.002 | 0 | 0.005 |
| 0.0012 | 770 | 9 | 0.012 | 0.005 | 0.022 |
| 0.0018 | 485 | 5 | 0.010 | 0.003 | 0.024 |
| 0.0089 | 221 | 5 | 0.023 | 0.007 | 0.053 |
| 0.0134 | 1205 | 35 | 0.029 | 0.020 | 0.040 |

**Table 16. Thermal neutron DCA scoring data.**

| SLIDE # | DOSE (Gy) | # CELLS | ABERRATIONS | | | ABERRATIONS PER CELL | | | |
|---|---|---|---|---|---|---|---|---|---|
| | | | DI-CENTRIC | RING | ACENTRIC | 0 EVENTS | 1 EVENT | 2 EVENTS | 3 EVENTS |
| 12 | **0 (NRU Control)** | 89 | 0 | 0 | 1 | 89 | 0 | 0 | 0 |
| 18 | **0 (NRU Control)** | 64 | 0 | 0 | 0 | 64 | 0 | 0 | 0 |
| 20 | **0 (NRU Control)** | 64 | 0 | 0 | 1 | 64 | 0 | 0 | 0 |
| 22 | **0 (NRU Control)** | 170 | 0 | 0 | 3 | 170 | 0 | 0 | 0 |
| 31 | **0 (NRU Control)** | 68 | 0 | 0 | 2 | 68 | 0 | 0 | 0 |
| 45 | **0 (NRU Control)** | 174 | 1 | 0 | 3 | 173 | 1 | 0 | 0 |
| 35 | **0 (Gamma Control)** | 146 | 0 | 0 | 2 | 146 | 0 | 0 | 0 |
| 36 | **0 (Gamma Control)** | 450 | 0 | 0 | 6 | 450 | 0 | 0 | 0 |
| 30 | **0 (Gamma Control)** | 349 | 1 | 0 | 4 | 348 | 1 | 0 | 0 |
| 44 | **0 (Gamma Control)** | 182 | 1 | 0 | 4 | 181 | 1 | 0 | 0 |
| 13 | **0.00117** | 131 | 4 | 0 | 9 | 127 | 4 | 0 | 0 |
| 26 | **0.00117** | 174 | 2 | 0 | 6 | 172 | 2 | 0 | 0 |
| 27 | **0.00117** | 161 | 1 | 0 | 2 | 160 | 1 | 0 | 0 |
| 32 | **0.00117** | 36 | 0 | 0 | 2 | 36 | 0 | 0 | 0 |
| 43 | **0.00117** | 111 | 0 | 0 | 1 | 111 | 0 | 0 | 0 |
| 46 | **0.00117** | 121 | 1 | 1 | 5 | 119 | 2 | 0 | 0 |
| 121 | **0.00117** | 36 | 0 | 0 | 1 | 36 | 0 | 0 | 0 |
| 122 | **0.00155** | 11 | 0 | 0 | 0 | 11 | 0 | 0 | 0 |
| 101 | **0.00182** | 230 | 2 | 0 | 4 | 228 | 2 | 0 | 0 |
| 102 | **0.00182** | 255 | 1 | 2 | 15 | 252 | 3 | 0 | 0 |

continued

| SLIDE # | DOSE (Gy) | # CELLS | ABERRATIONS | | | ABERRATIONS PER CELL | | | |
|---|---|---|---|---|---|---|---|---|---|
| | | | DI-CENTRIC | RING | ACENTRIC | 0 EVENTS | 1 EVENT | 2 EVENTS | 3 EVENTS |
| 102 | **0.00886** | 116 | 2 | 0 | 9 | 114 | 2 | 0 | 0 |
| 37 | **0.00886** | 7 | 1 | 0 | 2 | 6 | 1 | 0 | 0 |
| 128 | **0.00886** | 98 | 0 | 2 | 4 | 96 | 2 | 0 | 0 |
| 3 | **0.01338** | 279 | 10 | 0 | 31 | 269 | 8 | 1 | 0 |
| 5 | **0.01338** | 400 | 16 | 0 | 32 | 384 | 10 | 3 | 0 |
| 4 | **0.01338** | 365 | 5 | 0 | 17 | 360 | 5 | 0 | 0 |
| 118 | **0.01338** | 161 | 2 | 2 | 6 | 157 | 4 | 0 | 0 |

#### 2.3.2.1. Thermal Neutron Sample Activation

Beta/gamma surveys routinely detected neutron activation in the longest irradiated samples. The majority of the gamma activation died off quickly, with no detectable activation 24-hours post-irradiation. Short-lived gamma activity can result from the $^{37}Cl(n,\gamma)^{38}Cl$, $^{23}Na(n,\gamma)^{24}Na$ and $^{36}S(n,\gamma)^{37}S$ reactions, however as blood is made up of approximately 2.9% nitrogen and only 0.18% sodium and sulphur, it is expected that despite similar cross sections, the majority of the short-lived activity is likely due to the $^{37}Cl(n,\gamma)^{38}Cl$ reaction. $^{38}Cl$ decays to $^{38}Ar$, and has a half life of 37.2 min.

### 2.3.3. RBE Calculation

As standard practice, $RBE_M$ was calculated as a ratio of the $\alpha$ coefficient values [28]. The $\alpha$ values derived in this thesis, along with the associated standard errors, are listed in Table 17. Published $^{137}Cs$ chromosome aberration data from a previous CNL in-house study, in which the author participated, was used as the reference radiation [88]. The $\alpha$ coefficient values represent the linear portion of the dose response curve, as described in Equations 2 and 3.

The $RBE_M$ for dicentric induction following low-dose thermal neutron exposure, in comparison to $^{137}Cs$ data, was found to be 26.1 ± 7.0, and the $RBE_M$ following $^{252}Cf$ exposure was found to be 20.1 ± 2.9. The standard error on the $RBE_M$ value was calculated using the error propagation rule for division, as described in

Equation 9. Graphical representations of the dose response differences can be found in Figure 28 ($^{252}$Cf vs. $^{137}$Cs) and Figure 29 (thermal neutron vs. $^{137}$Cs).

**Table 17. Dicentric chromosome dose response curve $\alpha$ coefficient values.**

| Radiation Type | $\alpha$ (±SE) | RBE (±SE) |
|---|---|---|
| $^{137}$Cs (CNL curve Flegal *et al.* [88]) | 0.0700 ± 0.0088 | 1 |
| $^{252}$Cf Source (this thesis) | 1.41 ± 0.1 | 20.1 ± 2.9 |
| Thermal Neutron Beam (this thesis) | 1.86 ± 0.44 | 26.1 ± 7.0 |

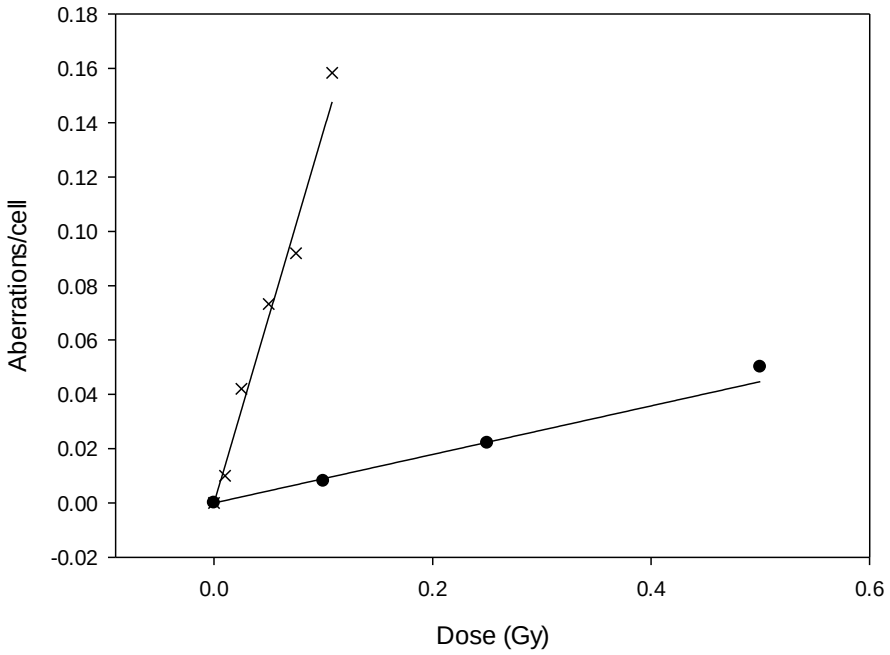


**Figure 28. Comparison of $^{252}$Cf (×) (Figure 26) and $^{137}$Cs gamma (●) dose response curves. The number of aberrations per cell is plotted against the radiation dose, in Gy.**

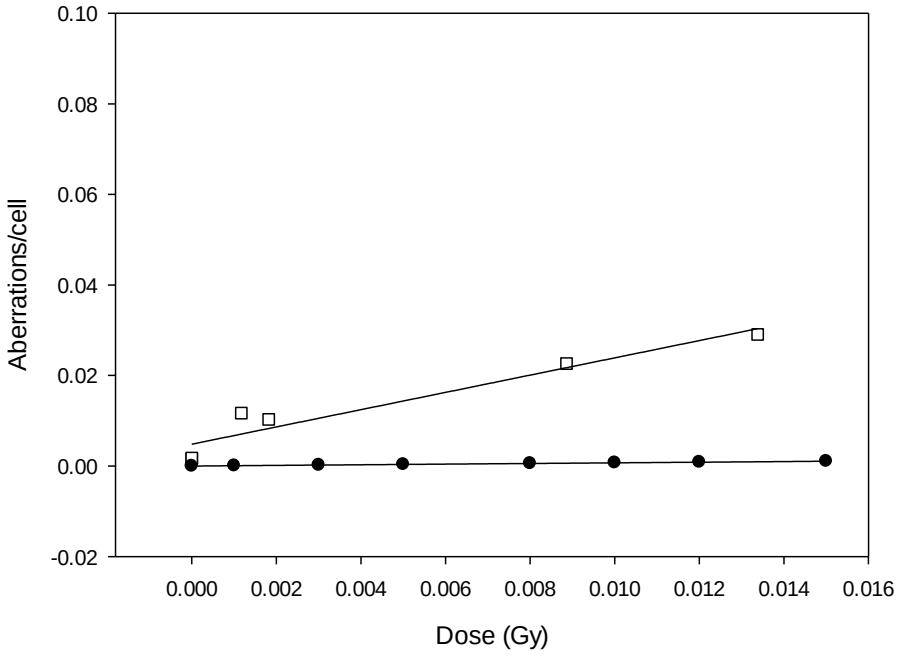


**Figure 29. Comparison of thermal neutron (□) (Figure 27) and $^{137}$Cs gamma (●) dose response curves. The number of aberrations per cell is plotted against the radiation dose, in Gy.**

$$\delta Q = Q \cdot \sqrt{\left(\frac{\delta a}{a}\right)^2 + \left(\frac{\delta b}{b}\right)^2} \qquad (9)$$

Where:
$Q$ = the final quantity
$\delta Q$ = the standard error on Q
$a$ = one of the $\alpha$ coefficients
$\delta a$ = the standard error of a
$b$ = the other $\alpha$ coefficient
$\delta b$ = the standard error of b

Using Equation 10, it was determined that the slopes of the thermal neutron and $^{252}$Cf dose response curves were not significantly different (p = 0.35). As such, it follows that the resulting RBE values are also not significantly different.

$$t = \frac{b_1 - b_2}{\sqrt{s_{b1}^2 + s_{b2}^2}} \qquad (10)$$

$$df = n_1 + n_2 - 4$$

Where:
$t$ = t-value
$b_1$ = slope of line 1
$b_2$= slope of line 2
$s_{b1}$ = SE of line 1
$s_{b2}$ = SE of line 2

$df$ = degrees of freedom
$n_1$ = sample size for line 1
$n_2$ = sample size for line 2

## 2.4. DISCUSSION

### 2.4.1. Overdispersion and Aberration Clustering

In an effort to identify a parameter linked to radiation quality, overdispersion and chromosome aberration clustering trends were studied. When a track of radiation causes multiple chromosome breaks, chromosome aberration clustering, and thus overdispersion, is predicted to occur. Mathematically, overdispersion occurs when the variance exceeds the mean as a result of non-homogenous distribution

of chromosome aberrations, resulting in chromosome aberration clustering [29, 104]. It is generally accepted that non-Poisson overdispersion of radiation-induced DNA aberration clustering is a result of either (a) a partial body exposure, or (b) high-LET radiations [29, 105]. Dose points with u values greater than 1.96 are considered to be overdispersed, indicating a failure to adhere to a Poisson distribution. However, even though the dose response curves described in this chapter are the result of high-LET $^{252}$Cf and thermal neutron radiation, only a single point on both curves is overdispersed (Table 9 and Table 13).

In order to compare ovedispersion of our results with those of other neutron studies, a review of the published literature was carried out (Table 18). Published data indicates that some fast neutron radiations demonstrate a dispersion index near unity, and thus exhibit a linear quadratic fit [78, 81, 82], however other references indicate consistent overdispersion following $^{252}$Cf and thermal neutron exposure [28, 72]. For instance, following thermal neutron exposure, Schmid *et al*.[28] noted consistent overdispersion at all doses between 0.375-1.875 Gy and Sasaki *et al.* [72] indicated overdispersion at six of seven dose points between 0.037-2.19 Gy. The dispersion differences between the published data and the results presented in this thesis may be due to dose range differences, for instance, the lowest dose examined by Schmid *et al.* [28] was 0.375 Gy (375 mGy) and the lowest dose examined by Sasaki *et al.* [72] was 0.073 Gy (73 mGy). In contrast, the highest thermal neutron dose examined in this thesis was 13.9 mGy. Interestingly, in the Sasaki *et al.* [72] dataset, the only dose point that was not

overdispersed was the second lowest dose of 0.183 Gy. Their lowest dose point of 0.073 Gy showed a large amount of overdispersion with a *u* value of 4.695 – similar to the *u* value reported in this thesis for the 13.9 mGy dose point. It is also possible that the dispersion differences are influenced by each laboratory's unique irradiation and cell culture methods as there is currently no global standard protocol for performing neutron RBE investigations.

While there are two publications detailing chromosome aberrations following $^{252}$Cf exposure [12, 75], neither article presents the aberration distributions. As such, it is not possible to compare the dispersion of the $^{252}$Cf chromosome aberrations found in the current work to published data. However, in other fast neutron RBE publications, where dispersion was reported, the majority of studies reported overdispersion at some, but not all, dose points, as described in Table 18.

As the data presented in this thesis did not indicate consistent overdispersion, aberration clustering should not be used as a marker of radiation quality at low doses for either $^{252}$Cf or thermal neutron radiation. This is not to say that lesion clustering did not occur, just that it was not observed during the DCA analysis of low-dose neutron-irradiated samples. It is possible that another process, such as cell death, interfered with the ability to analyze cells that contained the clustered damage.

**Table 18. Summary of dispersion in chromosome aberration studies**

| AVERAGE NEUTRON ENERGY | RBE | DOSE RANGE | RBE or $RBE_M$ | REFERENCE RADIATION | DOSE RELATIONSHIP | DISPERSION | CITATION |
|---|---|---|---|---|---|---|---|
| THERMAL NEUTRONS | | | | | | | |
| 0.025 eV | 36.4 ± 13.3 | 0.375-1.875 Gy | $RBE_M$ | $^{60}Co$ | Linear | Overdispersed at 5/5 dose points | Schmid et al. [28] |
| 0.025 eV | 51.1 ± 31.3 | 0.037-2.19 Gy | $RBE_M$ | $^{60}Co$ | Linear | Overdispersed at 6/7 dose points | Sasaki et al. [72] Recalculated by Schmid et al [28]. |
| 0.025 eV | 10.8 ± 1.8 | 0.16-0.64 Gy | $RBE_M$ | $^{60}Co$ | Linear | No information | Sevan'kaev et al.[73] Re-calculated by Schmid et al [28]. |
| INTERMEDIATE ENERGY NEUTRONS | | | | | | | |
| 36 keV | 67.1 ± 28.9 | 0.0036-0.0248 Gy | $RBE_M$ | $^{60}Co$ | Linear | Overdispersed at 1/7 dose points (0.0168 Gy) | Schmid et al. [69] |
| 40 keV | 5.13 | 9-58 rad | $RBE_M$ | $^{60}Co$ | Linear | No information | Sevan'kaev et al. [74] *Re-calculated for this thesis using ratio of $\alpha$ coefficients |
| 90 keV | 6.1 | 13-165 rad | $RBE_M$ | $^{60}Co$ | Linear | No information | Sevan'kaev et al. [74] *Re-calculated for this thesis using ratio of $\alpha$ coefficients |

continued

| AVERAGE NEUTRON ENERGY | RBE | DOSE RANGE | RBE or $RBE_M$ | REFERENCE RADIATION | DOSE RELATIONSHIP | DISPERSION | CITATION |
|---|---|---|---|---|---|---|---|
| FAST NEUTRONS | | | | | | | |
| 144 keV | 57.0 ± 18.8 | 0.0219-0.0924 Gy | $RBE_M$ | $^{60}Co$ | Linear | Overdispersed at 2/5 dose points (0.0228 Gy & 0.0481 Gy) | Schmid et al. [75] |
| 350 keV | 19.3 | 2.2-172 rad | $RBE_M$ | $^{60}Co$ | Linear | No information | Sevan'kaev et al. [74] *Re-calculated for this thesis using ration of $\alpha$ coefficients |
| 385 keV | 94.4 ± 38.9 | 0.0151-0.119 Gy | $RBE_M$ | $^{60}Co$ | Linear | Overdispersed at 2/5 dose points (0.0912 Gy & 0.1199 Gy) | Schmid et al. [69] |
| 565 keV | 76.0 ± 29.5<br>20.3 ± 2.0 | 0.0213-0.167 Gy | $RBE_M$ | $^{60}Co$<br>220 kV X-rays | Linear | Overdispersed at 5/5 dose points | Schmid et al. [77] |
| 700 keV (spectrum) | 47 | 50-300 rad | $RBE_M$ | $^{60}Co$ | Linear | No information | Lloyd et al. [78] |
| 850 keV | 9.7 | 2.1-300 rad | $RBE_M$ | $^{60}Co$ | Linear | No information | Sevan'kaev et al. [74] *Re-calculated for this thesis using ration of $\alpha$ coefficients |
| 900 keV (spectrum) | 36 | 6-265 rad | $RBE_M$ | $^{60}Co$ | Linear | No information | Lloyd et al. [78] |

continued

| AVERAGE NEUTRON ENERGY | RBE | DOSE RANGE | RBE or $RBE_M$ | REFERENCE RADIATION | DOSE RELATIONSHIP | DISPERSION | CITATION |
|---|---|---|---|---|---|---|---|
| 1.151 MeV | 46.3 ± 19.1<br>11.5 ± 1.3 | 0.0245-0.1460 Gy | $RBE_M$ | $^{60}Co$<br>220 kV X-rays | Linear | Overdispersed at 3/5 dose points (0.0265 Gy, 0.0962 Gy & 0.1460 Gy) | Schmid et al. [69] |
| 1.6 MeV (average – fission spectra) | 40.4 ± 16.4<br>10 ± 0.9 | 0.043-2.68 Gy | $RBE_M$ | $^{60}Co$<br>220 kV X-rays | Linear-quadratic | Overdispersed at 5/8 dose points | Schmid et al. [79] & Schmid et al. [69] |
| 1.6 MeV (average– fission spectra) | 37.4 ± 15.2<br>9.3 ± 0.9 | 0.04-1.97 Gy | $RBE_M$ | $^{60}Co$<br>220 kV X-rays | Linear-quadratic | Overdispersed at 8/13 dose points | Bauchinger et al. [80] & Schmid et al. [69] |
| 2.1 MeV (average– fission spectra) | 7.7 | 0.25-0.85 Gy, 0.5-3 Gy, 0.05-2.5 Gy | RBE (1 Gy) | $^{137}Cs$ | Linear | No information | Tanaka et al. [12] |
| 2.1 MeV (average– fission spectra) | 27 | 11.8-289.4 rad | $RBE_M$ | $^{60}Co$ | Linear-quadratic | No information | Lloyd et al. [75] |
| 4.85 MeV | 32.3 ± 13.3<br>8.0 ± 0.7 | 0.049-0.388 Gy | $RBE_M$ | $^{60}Co$<br>220 kV X-rays | Linear | Overdispersed at 1/5 dose points (0.291 Gy) | Schmid et al. [69] |
| 6.5 MeV | 14 | 0.05-1 Gy | $RBE_M$ | $^{60}Co$ | Linear-quadratic | Some overdispersion at high doses | Fabry et al. [81] |
| 7.6 MeV (spectrum) | 23 | 27-324 rad | $RBE_M$ | $^{60}Co$ | Linear-quadratic | No information | Lloyd et al. [78] |

continued

| AVERAGE NEUTRON ENERGY | RBE | DOSE RANGE | RBE or $RBE_M$ | REFERENCE RADIATION | DOSE RELATIONSHIP | DISPERSION | CITATION |
|---|---|---|---|---|---|---|---|
| 14 MeV | 6.2 | 0.05-2Gy | $RBE_M$ | $^{60}Co$ | Linear-quadratic | Adheres to Poisson distribution | Fabry et al. [81] |
| 14.6 MeV | 16.4 ± 6.8<br>4.1 ± 0.5 | 0.068-0.568 Gy | $RBE_M$ | $^{60}Co$<br>220 kV X-rays | Linear | Over dispersed at 2/5 dose points (0.271 Gy & 0.408 Gy) | Schmid et al.[69] |
| 14.7 MeV | 2.6 | 48-364 rad | $RBE_M$ | $^{60}Co$ | Linear | No information | Sevan'kaev et al. [74]<br>*Re-calculated for this thesis using ratio of $\alpha$ coefficients |
| 14.7 MeV | 13 | 5-303 rad | $RBE_M$ | $^{60}Co$ | Linear-quadratic | No information | Lloyd et al. [78] |
| 14.9 MeV | 4.1 | 0.0386 Gy-2.28 Gy | $RBE_M$ | 250 kVp X-rays | Linear-quadratic | Overdispersion | Lloyd et al. [82] |
| 15.0 MeV | variable | 0-375 rad | RBE | 220 kV X-rays | Linear | No information | Bauchinger et al. [83] |
| 21 MeV | 4.7 | 0.05-2 Gy | $RBE_M$ | $^{60}Co$ | Linear-quadratic | Some overdispersion at high doses | Fabry et al. [81] |
| 60 MeV (spectrum) | 14 ± 4 | 0.104-0.527 Gy | $RBE_M$ | $^{60}Co$ | Linear | Overdispersion at 4/5 points | Nolte et al. [84] |

### 2.4.2. RBE Values

**Table 19. Comparison of $\alpha$ coefficients (the linear portion of the dose response curves) for thermal neutron, $^{252}$Cf, and gamma sources.**

| $\alpha$ (±SE) | CITATION |
|---|---|
| THERMAL NEUTRON | |
| 1.86 ± 0.44 | this thesis |
| 0.400 ± 0.018 | Schmid *et al*. [28] |
| 0.920 ± 0.028 | Sasaki *et al*. [72] |
| 0.745 ± 0.030 | Sevan'kaev *et al*. [74].<br>Recalculated by Schmid *et al.* [28] |
| $^{252}$Cf SOURCE | |
| 1.41 ± 0.09 | this thesis |
| 0.369 | Tanaka *et al.* [12] |
| 0.0600 ± 0.0019 | Lloyd *et al.* [75] |
| GAMMA RADIATION | |
| 0.0700 ± 0.0088 | $^{137}$Cs - Flegal *et al.* [88] – CNL gamma curve |
| 0.011 ± 0.004 | $^{60}$Co - Schmid *et al.*[28] |
| 0.018 ± 0.011 | $^{60}$Co - Sasaki *et al.* [106] |
| 0.069 ± 0.011 | $^{60}$Co - Sevan'kaev *et al.* [74].<br>Recalculated by Lloyd & Edwards [107] |
| 0.0472 | $^{137}$Cs - Tanaka *et al.* [12] |
| 0.00018 ± 0.00008 | $^{60}$Co - Lloyd *et al.* [75] |

The $\alpha$ coefficients, which are the linear component of the dose response curve function (see Equation 2 and 3), and the standard error of the mean from this thesis and comparable dicentric chromosome studies, are presented in Table 19.

The $\alpha$ coefficients describe the number of dicentric and ring aberrations produced by a single track of radiation, and represent the linear portions of a dose response curve. The $\alpha$ coefficient describing the in-house low-dose thermal neutron dose response curve (1.86 ± 0.44) is significantly higher than other published thermal neutron values (mean = 0.69 ± 0.05, n = 3) [28, 72, 74]. Similarly, the derived alpha coefficient describing the $^{252}$Cf mixed field irradiation (1.41 ± 0.09) is also larger than comparable published values (mean = 0.21, n = 2) [12, 75]. However, as the $\alpha$ coefficient for CNL's published $^{137}$Cs gamma dose response curve (0.0700 ± 0.0088) is slightly larger than the mean $\alpha$ coefficient of other published gamma dose response curves (mean = 0.03, n = 5), the resulting $RBE_M$ values for low-dose $^{252}$Cf (20.1 ± 2.9) and thermal neutron (26.1 ± 7.0) exposures align well with published higher-dose data (Table 19) [12, 28, 72, 75]. Inter-laboratory variation, such as scoring methodology and the type of reference radiation are likely the cause of these discrepancies. This underscores the importance of each laboratory having their own set of dose response curves.

There are currently only two published studies examining the ability of $^{252}$Cf to produce chromosome aberrations, as summarized in Table 5 and Figure 30 [12, 75]. Tanaka *et al*. [12] found a $RBE_M$ of 7.7 (with RBE values ranging from 2.3 to 7.7, depending on dose rate), in reference to $^{137}$Cs gamma rays, while Lloyd *et al.* [75] described a $RBE_M$ of 27 with respect to the effects of $^{60}$Co. The low value reported by Tanaka *et al*. is significantly different than the $RBE_M$ of 20.1 ± 2.9 reported in this thesis, while the RBE value of 27 reported by Lloyd *et al.* [75] is

more consistent with the current results. Neither study reported the SE on the RBE values. As a possible explanation for this variation, it should be noted that Tanaka *et al.* [12] irradiated three sets of neutron and gamma samples, at identical dose rates of 1.2 Gy $h^{-1}$, 0.12 Gy $h^{-1}$, or 0.012 Gy $h^{-1}$. The highest RBE of 7.7 was reported following gamma and neutron irradiations at the lowest dose rate of 0.012 Gy $h^{-1}$. It is already well-established that low-LET radiation effects are susceptible to dose rate variations and long irradiation times [29], and the 0.012 Gy $h^{-1}$ $^{137}$Cs reference radiation curve used by Tanaka *et al.* [12] included gamma irradiation times of over 100 hours. This protracted irradiation time would have drastically affected the scope of chromosome aberrations available for assessment, as the resulting DNA DSBs would have been spatially and temporally separated. In fact, this very effect was demonstrated by Tanaka *et al.* [12], as the three distinct gamma dose rates produced curves with differing slopes, and therefore differing RBE values. In addition, while high-LET exposures are generally unaffected by dose rate variation due to energy distribution, the low neutron dose rates would have resulted in irradiation times of up to 70 hours. At these irradiation durations, it is possible that cell death may have affected the yield of $^{252}$Cf-induced chromosomal aberrations in the higher-doses samples, as apoptotic cell death has been shown to peak 48-72 hours post radiation exposure for both high- and low-LET radiations [59], and apoptotic cells preferentially clear out dicentric chromosomes and other complex chromosomal damage [58]. Taken together, it is not surprising that the RBE reported in this thesis for

dicentric induction in lymphocytes following $^{252}$Cf fission neutron exposure does not line up with the data published by Tanaka *et al.* [12] as both dose rate effects and cell death likely modified their dose response.

In contrast, Lloyd *et al*. [75] performed the $^{252}$Cf exposures at higher dose rates of 1.2 Gy $h^{-1}$ and 1.7 Gy $h^{-1}$, and the $^{60}$Co reference radiation exposures at a dose rate 1.8 Gy $h^{-1}$. Even so, at a maximum gamma dose of 30 Gy, a 16 hour irradiation would have been required. As above, the protracted gamma irradiation time would have affected the number of chromosome aberrations available for analysis in the higher dosed sample, and thus the RBE values, as it is known that the majority of DNA DSBs are repaired or unavailable for a potential mis-repair within five to six hours post-irradiation [29]. It is likely that the slightly elevated $^{252}$Cf $RBE_M$ of 27 described by Lloyd *et al*. is due in-part to the lengthy gamma irradiation times.

Contrary to the $^{252}$Cf data published by Tanaka *et al.* [12] and Lloyd *et al*. [75], the $^{137}$Cs reference radiation curve used in this thesis was generated with a much higher dose rate of 48.1 Gy $hr^{-1}$. Even at the highest dose of 4 Gy, all of the dose was delivered within five minutes [88]. In this situation, it is very unlikely that DNA repair would begin before the irradiations were completed. Furthermore, the longest in-house neutron irradiation was approximately 6.5 hours. As such, the $^{252}$Cf results presented in this thesis should be unaffected by both dose rate effects (for the reference gamma irradiation curve), and apoptotic cell death.

It should be noted that RBE values are not equivalent to $w_R$, and thus cannot be used as multipliers to determine equivalent dose. Instead, these values are used to contrast the damaging effects of neutron radiations, in comparison to gamma-rays, in lymphocytes that were assessed using the DCA. That said, if the $w_R$ of thermal neutrons was 26.1, as per the derived RBE value (instead of 2.5, as given by the ICRP continuous function for neutrons), this would drastically modify the equivalent doses given in this thesis. For instance, using the ICRP $w_R$ of 2.5, the highest given thermal neutron dose of 18.9 mGy is equivalent to 47.3 mSv. However, if the thermal neutron $w_R$ was 26.1, as per the RBE value derived in this thesis, the equivalent dose would be much larger at 0.49 Sv. Similarly, the ICRP $w_R$ for $^{252}$Cf neutrons is 17.1 (based on the average energy of 2.1 MeV), meaning the highest $^{252}$Cf dose of 0.108 Gy is equivalent to 1.9 Sv. If this $w_R$ value was instead 20.1, as per the RBE calculated in this thesis, the largest dose of 0.108 Gy would be equivalent to 2.2 Sv. As more radiobiology experiments are performed using thermal neutrons, it is possible that the $w_R$ may be re-defined if other cell types and end points continually demonstrate large RBE values, however significant work in this area is still required.

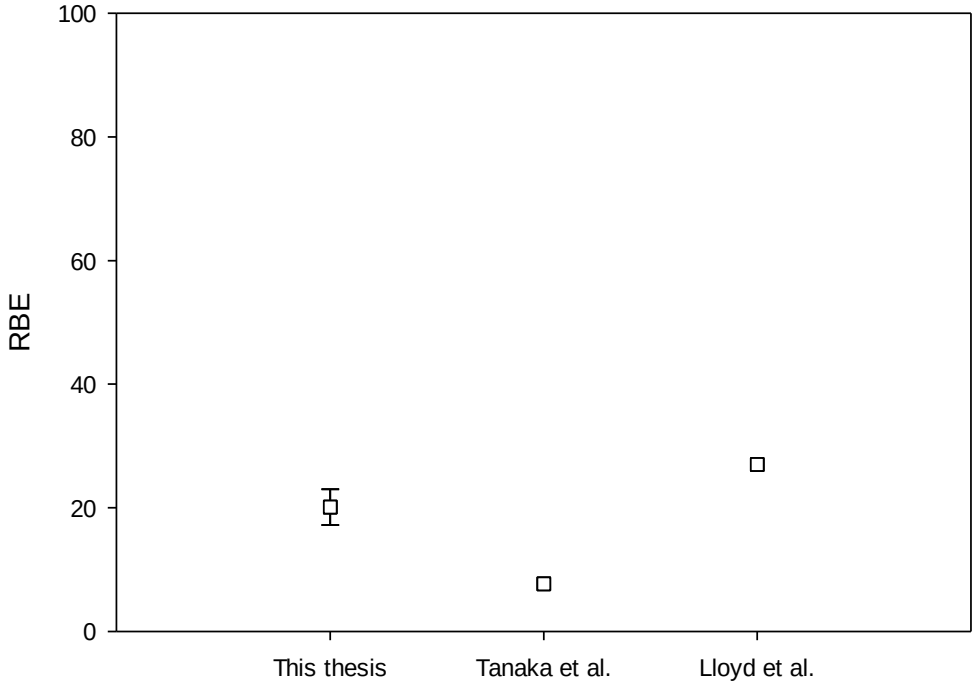


**Figure 30. Comparison of reported $^{252}$Cf RBE values.**

Published thermal neutron $RBE_M$ data for dicentric chromosome induction is variable with values of 10.8 ± 1.8 [28, 73], 36.4 ± 13.3 [28], and 51.1 ± 31.3 [28, 72] reported in the literature (Table 5). With the exception of the $RBE_M$ of 10.8 ± 1.8 reported by Sevan'kaev *et al.* [28, 73], the $RBE_M$ (±SE) of 26.1 ± 7.0 described in this chapter for low-dose thermal neutron exposure agrees well with the published data, and shown in Figure 31.

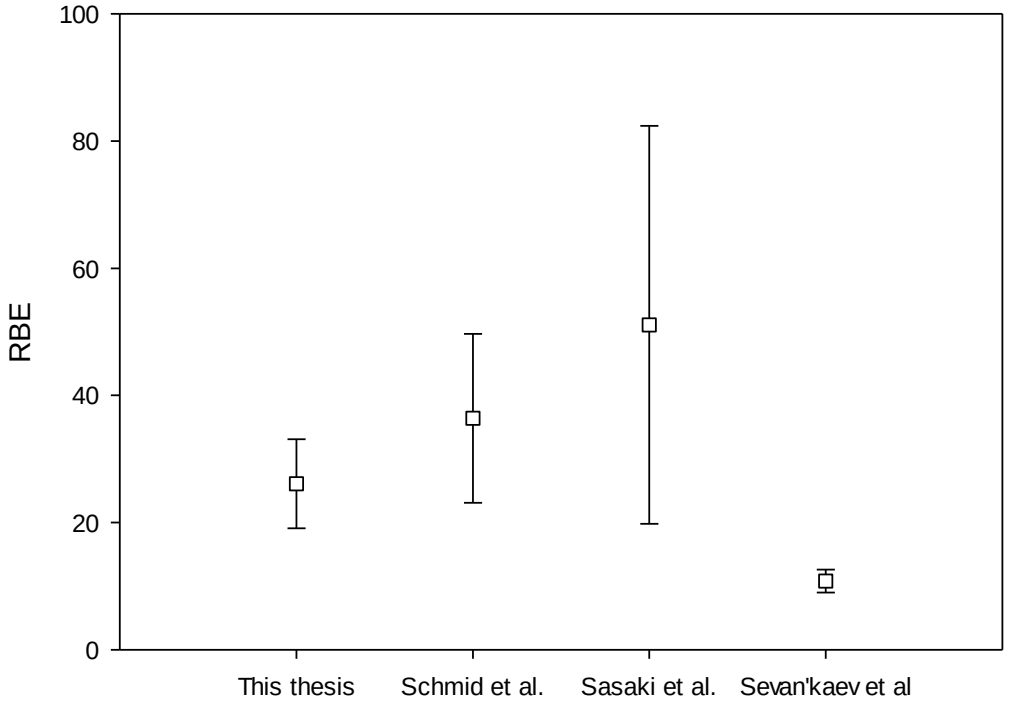


**Figure 31. Comparison of reported thermal neutron RBE values.**

That said, it should be noted that the in-house $RBE_M$ of 26.1 ± 7.0 for thermal neutrons was calculated using $^{137}Cs$ as the reference radiation, whereas the published values are all in comparison to $^{60}Co$ radiation. It is well known that RBE can be modified by the choice of reference radiation, including ICRP-recommended hard gamma radiations such as $^{60}Co$ or $^{137}Cs$, with $^{60}Co$ producing higher RBE estimates than $^{137}Cs$ [68, 77]. For instance, Schmid *et al.* [77] noted that when 565 keV neutron data was compared to both $^{137}Cs$ and $^{60}Co$ reference radiations, $RBE_M$ values of 54.2 ± 18.4 and 76.0 ± 29.5 resulted, respectively.

Unfortunately, CNL does not currently have a DCA $^{60}$Co dose response curve, which would allow for a better comparison to published data. However, it is expected that the $^{252}$Cf and thermal neutron RBE values reported in this thesis would be larger if compared to the effects of $^{60}$Co gamma radiation.

Lastly, as thermal neutron beams often contain a gamma component, it is possible that this gamma dose may have affected the RBE values. At this time, the gamma contamination of the CNBC N5 beam is not known, however work is underway to determine this value. That said, the gamma radiation controls used in this thesis did not show elevated dicentric induction as compared to the un-irradiated control sample (Table 13). For comparison, gamma contamination values ranging from <5 % (Sevan'kaev *et al.* [73]) to 48 % (Sasaki *et al.* [72]) have been reported in the literature. Interestingly, but unexplainable, the study reporting the lowest published gamma contamination value of <5%, also reported the lowest thermal neutron $RBE_M$ value of 10.8 ± 1.8. Conversely, the study with the highest gamma contamination value of 48% reported the largest $RBE_M$ of 51.1 ± 31.3. While the exact gamma contamination of the CNBC N5 thermal neutron beam is not known, because the gamma field control samples presented a low rate of dicentric induction, as reported in Table 16, it is expected that the resulting gamma field did not significantly influence the rate of dicentric induction. As such, the dose response detailed in this chapter can be confidently attributed to thermal neutron exposure.

As described in Section 2.3.3 and Figure 32, there is not a significant difference between the RBE values calculated for thermal neutrons (26.1 ± 7.0) and $^{252}$Cf (20.1 ± 2.9). This finding is consistent with other published neutron RBE data, as noted in Figure 14, and indicates that RBE values obtained using the DCA in human lymphocytes may be independent of neutron energy up to 2.1 MeV.

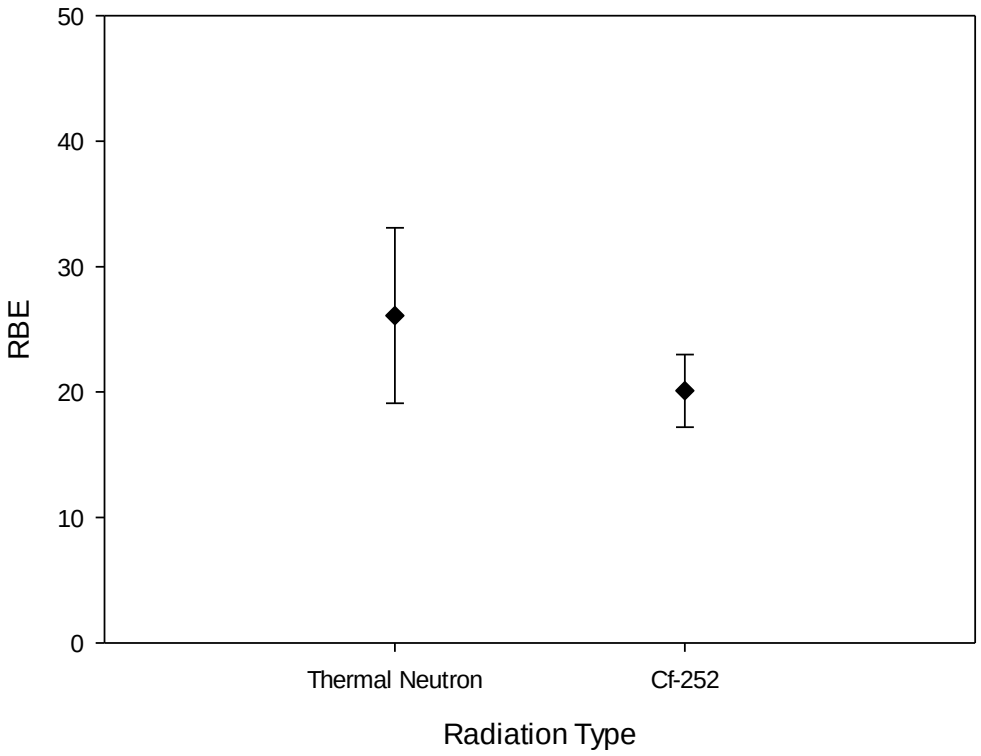


**Figure 32. Graphical comparison of thermal neutron and $^{252}$Cf RBE values.**

### 2.4.3. Low Cell Numbers

The number of cells available for scoring was lower than expected in the thermal neutron samples. This qualitative observation was evident from the very small sample pellet following cell harvest. The thermal neutron irradiations were repeated three times, using blood from the same donor; however cell counts remained consistently low. This is not believed to be a blood donor-specific abnormality, as the donor regularly provides blood for other CNL gamma-irradiated radiobiology research projects where cell yields have always been sufficient, including the $^{252}$Cf irradiations reported earlier in this chapter. Instead, it is possible that cell death prior to sample fixation is the cause of the low cell numbers. While unlikely, other experimental factors may have also affected cell numbers. This includes cell culture contamination and reagent failure. As a consequence of the poor survival of the thermal neutron irradiated cells, the number of metaphase spreads analysed for the production of the dose response curve was much less than the 3000 cells recommended by the IAEA [29].

### 2.4.4. Summary

The in-house thermal neutron and $^{252}$Cf dose response curves yielded RBE values of 26.1 ± 7.0 and 20.1 ± 2.85, respectively. Both curves complied with a Poisson distribution, with the exception of one dose point on each curve. This was an unexpected result, as high-LET radiations, such as the $^{252}$Cf and thermal neutron exposures performed as part of this thesis, are often generalized as not adhering to a Poission distribution. This finding also indicated that there was no aberration

clustering of DNA damage as theoretically predicted by high-LET radiation models. As such, given the longevity of human peripheral blood lymphocytes with stable chromosome aberrations, the results of this chapter indicate that it would be difficult to identify gamma radiation doses to workers with a history of acute low-dose neutron exposures. That said, it is possible that cells displaying chromosome aberration clustering underwent cell death, and thus were unavailable for analysis using the DCA. As such, the following chapter examines whether low doses of thermal neutrons induce notable apoptotic or necrotic cell death.

# 3. CHAPTER 3 – APOPTOTIC AND NECROTIC CELL DEATH FOLLOWING THERMAL NEUTRON EXPOSURE

Declarations:

Laura Paterson was responsible for the experimental design, laboratory work, and data analysis.

Dr. Jovica Atanackovic and Dr. Samy El-Jaby performed Monte Carlo simulations to derive the fluence to kerma conversion coefficient that was used to calculate the neutron radiation doses.

Chad Boyer designed and fabricated the test tube holder used for the thermal neutron irradiations and set-up and ran the N5 triple axis spectrometer.

## 3.1. INTRODUCTION

### 3.1.1. Overview

Low doses of neutrons are encountered globally as a result of cosmic radiation and nuclear energy. For example, the worldwide average lifetime dose of neutrons from natural sources, which is predominantly due to cosmic radiation, is approximately 6.0 mSv [108]. In contrast, nuclear energy workers receive lifetime neutron doses of approximately 44.4 mSv, and similarly aircrew receive neutron doses of approximately 30 mSv [108]. Despite the possibility of occupational neutron exposure, there is currently little known about the biological effects of low doses of neutron radiation specifically relating to either lymphocyte apoptosis or necrosis.

Apoptosis, first described in 1972 by Kerr *et al*. [109], is a highly regulated and conserved form of cell death identified by easily-observed and tightly-regulated morphological changes (Figure 33). It is present at all stages of life and it serves multiple functions including the homeostatic maintenance of cell populations and protection against tumorgenesis [22, 110]. Early-apoptosis is characterized by chromatin condensation and cell shrinkage. Here, organelles are observed to be in close proximity and the cytoplasm becomes denser, however, the cell still maintains a characteristic shape. Next, cell membrane blebbing occurs, followed by karyorrhexis (breakdown of the nuclear membrane and cleavage of DNA). The cellular contents are then packaged into apoptotic bodies that bud off from

the cellular membrane. In the body, the apoptotic bodies are phagocytosed by macrophages and/or other phagocytic cells. Cells *in vitro*, are allowed to enter late apoptosis at which point the cellular membrane degrades. Phosphatidyserine transfer from the inner cell membrane to the outer cell membrane is a highly conserved characteristic of early apoptosis that is readily exploited for labelling. The presence of phosphatidylserine on the external cell membrane aids in recruiting macrophages [111] and very early apoptotic cells expressing only small amounts of phosphatidylserine can be targets for phagocytosis [112]. However, to date, the mechanism by which phosphatidylserine is externalized is not well understood. That said, it is well known that Annexin V has a very high affinity for phosphatidylserine, and was, therefore, selected for this work as an apoptotic marker.

On a molecular level, there are three apoptotic pathways – the extrinsic/death receptor pathway, the intrinsic/mitochondrial pathway, and the perforin/granzyme pathway. The perform/granzyme pathway is further subdivided into the granzyme A and granzyme B pathways. The extrinsic, intrinsic and granzyme B pathways all result in caspase-3 activation and the morphological changes described above. Caspase-3 is activated as part of the apoptotic pathway following both photon [113, 114] and neutron irradiations [60]. In contrast, the granzyme A pathway is caspase-independent. As its name suggests, the extrinsic pathway is activated following interactions with transmembrane proteins. In contrast, the intrinsic pathway is activated following signals that originate within the cell.

The *TP53* gene encodes tumor protein p53 (TP53), a phosphoprotein that acts as a tumor suppressor by inducing either cell cycle arrest or apoptosis following DNA damage. The *TP53* gene is mutated in approximately 50% of human cancers, resulting in an increased resistance to both radiotherapy and chemotherapy. However, high energy neutrons have been noted to induce apoptosis both with and without the presence of functional TP53 [60].

There are numerous intrinsic apoptotic signalling pathways. The stimuli to activate these pathways can be either negative or positive, with radiation acting in a positive manner. Negative stimuli involve the absence of either specific cytokines, hormones or growth factors. In a properly functioning, undamaged cell, these molecules would play a role in suppressing apoptosis (as a healthy cell has no need to undergo apoptosis). On the other hand, the absence of these molecules is an important apoptosis initiator. Positive apoptotic signals include the presence of free radicals, radiation, toxins, hypoxia, etc [115]. Regardless of the stimuli, characteristic mitochondrial membrane changes occur. These include the opening of a mitochondrial permeability transition pore, loss of membrane potential, and the release of two groups of pro-apoptotic proteins from the mitochondrial inter-membrane space into the cytoplasm. Once released, these proteins initiate caspase-dependent and caspase-independent cell death pathways [116].

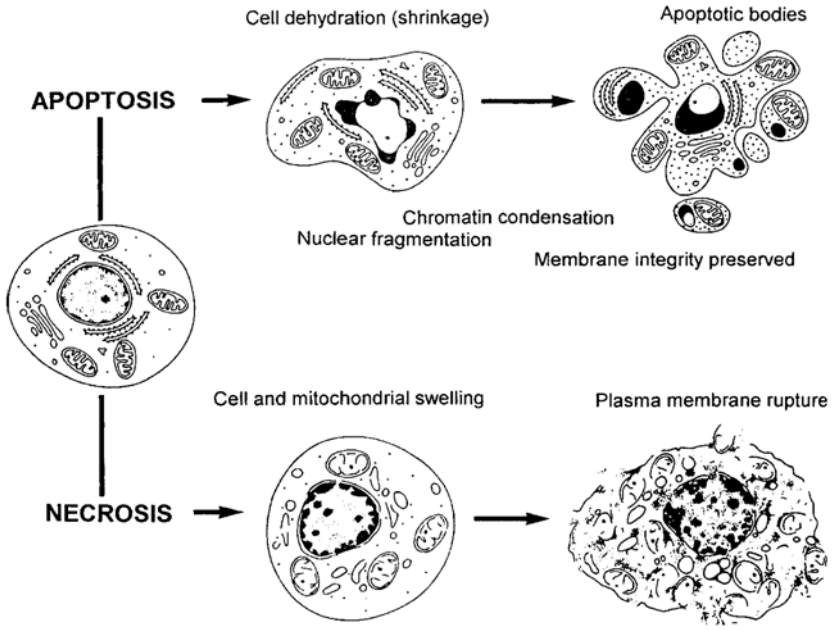


**Figure 33. Morphological characteristics of apoptosis and necrosis. Adapted from Darzynkiewicz *et al.* [117].**

Necrosis is most commonly thought to be an accidental or uncontrolled cellular response, however, recent evidence indicates that necrosis may sometimes be under genetic control and that biochemical cascades mediate the necrotic response [66]. While much work is still required to understand necrotic regulation, the endpoint of cellular rupture creates an inflammatory response that has the potential to induce tumorigenesis [67]. To date, there is little information in the literature about cellular necrosis following radiation exposure, however, necrotic cell death is thought to be the main mode of cell death following very high doses of radiation, and is only viewed as an accidental occurrence following low-dose exposures [65]. There are two main sub-types of necrosis: primary necrosis and

secondary necrosis. In both subtypes, the final outcome is similar - the breakdown of the cellular membrane and the subsequent release of intercellular contents. However, while primary necrosis is the result of the necrotic phenotype described above, secondary necrosis occurs, predominantly *in vitro*, at the end of the apoptotic pathway if cells are not phagocytosed by scavenger cells [118]. In this situation, un-phagocytosed apoptotic cells slowly degrade and begin to resemble traditional necrotic cells.

This chapter will describe apoptotic and necrotic cell death following low doses of thermal neutron radiation and $^{60}$Co exposure.

## 3.2. METHODS

Over the course of the study period, four healthy male volunteers routinely donated blood. One donor was between the ages of 25 and 30, two donors were between the ages of 30 and 35, and one donor was over 60 years. Whole blood was drawn by venipuncture into either sodium heparin (for gamma irradiations) or sodium citrate (for neutron irradiations) vacutainers (BD Biosciences). Aliquots of 1.5 mL of blood were then immediately transferred into 15 mL polypropylene test tubes for irradiation. Sodium heparin anticoagulant was used for the gamma-irradiated samples, while sodium citrate was used for the thermal neutron exposures to eliminate the additional radiation dose produced by neutron interactions with the additional nitrogen content found in heparin.

### 3.2.1. Irradiation

#### 3.2.1.1. Thermal Neutron Beam Irradiation

Thermal neutron irradiations were completed as described in Chapter 2. Samples were exposed for 53-5,379 seconds, resulting in doses that ranged between 0.2 mGy and 18.9 mGy, as described in Table 20. Due to only occasional reactor beam line availability, different samples were irradiated over the period of 1.5 years. The dose variation between donors is a result of the reactor power on the day of irradiation.

**Table 20. Thermal neutron irradiation parameters for cell death assays.**

| | DOSE (mGy) | REACTOR POWER (MW) | NEUTRON COUNTS | TIME (s) |
|---|---|---|---|---|
| DONOR 1 | 0 | - | - | - |
| | 0.4 | 91-98 | 2,631,881 | 134 |
| | 0.9 | 91-98 | 5,278,898 | 269 |
| | 1.4 | 91-98 | 7,955,192 | 403 |
| | 1.8 | 91-98 | 10,570,157 | 538 |
| | 4.8 | 91-98 | 28,292,824 | 1344 |
| | 9.0 | 91-98 | 53,424,901 | 2689 |
| | 18.9 | 87-90 | 111,742,773 | 5379 |
| DONOR 2 | DOSE (mGy) | REACTOR POWER (MW) | NEUTRON COUNTS | TIME (s) |
| | 0 | - | - | - |
| | 0.2 | 93-100 | 1,046,405 | 53 |
| | 0.5 | 93-100 | 2,643,898 | 134 |
| | 0.9 | 93-100 | 5,299,802 | 269 |
| | 1.3 | 93-100 | 7,920,588 | 403 |
| | 2.0 | 96-98 | 11,807,893 | 538 |
| | 5.0 | 96-98 | 29,583,791 | 1344 |
| | 9.9 | 96-98 | 58,767,657 | 2689 |
| | 13.4 | 93-100 | 79,167,714 | 4034 |
| DONOR 3 | DOSE (mGy) | REACTOR POWER (MW) | NEUTRON COUNTS | TIME (s) |
| | 0 | - | - | - |
| | 0.2 | 96-98 | 1,162,827 | 53 |
| | 0.5 | 96-98 | 2,952,467 | 134 |
| | 1.0 | 96-98 | 5,930,930 | 269 |
| | 1.5 | 96-98 | 8,904,246 | 403 |
| | 2.0 | 96-98 | 11,696,959 | 538 |
| | 4.9 | 96-98 | 29,204,807 | 1344 |
| | 10.0 | 96-98 | 59,300,452 | 2689 |
| | 15.1 | 96-98 | 89,240,883 | 4034 |
| DONOR 4 | DOSE (mGy) | REACTOR POWER (MW) | NEUTRON COUNTS | TIME (s) |
| | 0 | - | - | - |
| | 0.2 | 95-98 | 1,066,577 | 53 |
| | 0.5 | 95-98 | 2,694,927 | 134 |
| | 0.91 | 95-98 | 5,403,915 | 269 |
| | 1.4 | 95-98 | 8,085,212 | 403 |
| | 1.8 | 95-98 | 10,793,404 | 537 |
| | 4.5 | 93-100 | 26,337,100 | 1344 |
| | 8.9 | 93-100 | 52,412,918 | 2688 |
| | 13.7 | 95-98 | 80,960,528 | 4034 |

#### 3.2.1.1.1. Control Samples

To ensure that extraneous factors did not negatively affect the results, three control blood samples were used – a laboratory control, a NRU control, and a gamma field control. The laboratory control tube remained in the cell culture laboratory throughout the sample irradiation. This control tube will not have encountered either elevated radiation or extreme temperature changes that could possibly result during sample transport. The NRU control tube was taken to the reactor, but not placed near the neutron beam or in the surrounding gamma field. This was used for verification that the slightly elevated gamma and neutron radiation environment inside the NRU facility did not affect results. Finally, a gamma field control was placed in the gamma field directly below the neutron beam port. This tube was not exposed to neutrons, but was within an elevated gamma field. This control allowed us to determine whether the gamma field influenced our results. Additionally, due to (n,γ) reactions, it is possible that the sample tubes could have irradiated each other. The gamma control would have encountered gamma radiation from both the reactor and from the sample activation. All three control tubes remained in-place throughout the entire irradiation period.

### 3.2.1.2. $^{60}$Co Gamma Irradiations

Gamma irradiations were performed at CNL using $^{60}$Co GammaCell 200 and GammaCell 220 irradiators. Two irradiators were used to achieve both low doses and to ensure the higher doses were delivered in an acute manner. Unfortunately,

both requirements could not be met using one single irradiator. The $^{60}$Co doses ranged from 0.03 Gy to 2.5 Gy. The dose rate varied from 4.57 Gy $h^{-1}$ to 4.75 Gy $h^{-1}$ for the low-dose samples and 214 Gy $h^{-1}$ to 222 Gy $h^{-1}$ for samples receiving 0.63 Gy and higher, as described in Table 21.

**Table 21. $^{60}$Co Gamma doses and dose rates.**

| DOSE (Gy) | DOSE RATE (Gy $h^{-1}$) |
|---|---|
| 0.00 | -- |
| 0.03 | 4.57 – 4.75 |
| 0.06 | 4.57 – 4.75 |
| 0.13 | 4.57 – 4.75 |
| 0.19 | 4.57 – 4.75 |
| 0.25 | 4.57 – 4.75 |
| 0.63 | 214 – 222 |
| 1.25 | 214 – 222 |
| 1.88 | 214 – 222 |
| 2.50 | 214 – 222 |

### 3.2.2. Cell Assays

Immediately following irradiation, lymphocytes were isolated using Ficoll Paque PLUS (GE Health Care) and cell cultures were prepared containing 9 mL of Roswell Park Memorial Institute RPMI-1640 medium (Hyclone), 15% fetal

bovine serum (Sigma-Aldrich), 100 units $mL^{-1}$ penicillin and 100 μg $mL^{-1}$ streptomycin (Sigma-Aldrich). Cultures were incubated for 48 hours at 37 °C with 5% $CO_2$ in air.

Following the 48 hour incubation, cells were washed in phosphate buffered saline (Hyclone) and counted using the Moxi Z cell counter (Orflo). Cultures were adjusted to a concentration of approximately $1.0 \times 10^5$ cells $ml^{-1}$. 100 μL of suspension was transferred to a 1.7 mL microtube for flow cytometry. 10 μL of Annexin V-FITC and 20 μL of 7-aminoactinomycin D (7AAD) (both Beckman Coulter) were added to the cell suspension, which was kept on ice throughout the analysis period. 5 μL of leukocyte marker CD45-PE (Beckman Coulter) was also added to the cultures.

In addition to the experimental samples, three spectral compensation control samples were set-up, each containing only one fluorescent marker. As above, 100 μl of adjusted cell suspension was added to a 1.7 mL microtube, and the appropriate volume of single fluorescent marker was added.

### 3.2.3. Cell Death Kinetics

To ensure cell cultures were analysed at an appropriate times a time-course study was completed. Only one blood donor was involved in this study, however this donor was also used for both the apoptosis/necrosis assays and chromosome damage study. Gamma-irradiated samples were given a dose of 2.0 Gy, whereas thermal neutron-irradiated samples were given 9.95 mGy. Following irradiation,

four different incubation times were chosen: 24 h, 48 h, 72 h, and 96 h. An un-irradiated control sample was also included. Following the appropriate incubation time, the cell death response was analyzed by flow cytometry.

### 3.2.4. Flow Cytometry

Flow cytometry was completed using an ImageStream X (AMNIS Corp.) and its associated Inspire™ (AMNIS Corp.) software. Annexin V-FITC, 7AAD, and CD45-PE were excited by a 488 nm laser. A lower object size limit of 40 pixels was applied to the bright-field channel to ensure speed beads and small debris were not collected. Fluorescent, bright-field, and side-scatter (785 nm) images were captured together with compensation controls for each fluorochrome. Between 10,000 and 20,000 cells were captured per sample run.

Annexin V-FITC was detected in channel 2 (505-560 nm), 7AAD was visualized in channel 4 (595-660 nm), and CD45-PE was seen in channel 3 (560-595 nm) (Figure 36). Brightfield images were captured in channel 1.

#### 3.2.4.1. Spectral Compensation

At the end of every flow cytometry session, the three spectral compensation controls were run. Bright-field and side-scatter illumination were turned off during the spectral compensation collection. A lower object size limit of 40 pixels was applied to the channel corresponding to the individual fluorescent marker to rule out reflected fluorescent signals from the speed beads. Fluorescent

signals were compensated according to the Ideas™ user manual [119]. Following compensation, spill-over accounted for less than 1% of the total signal in adjacent channels.

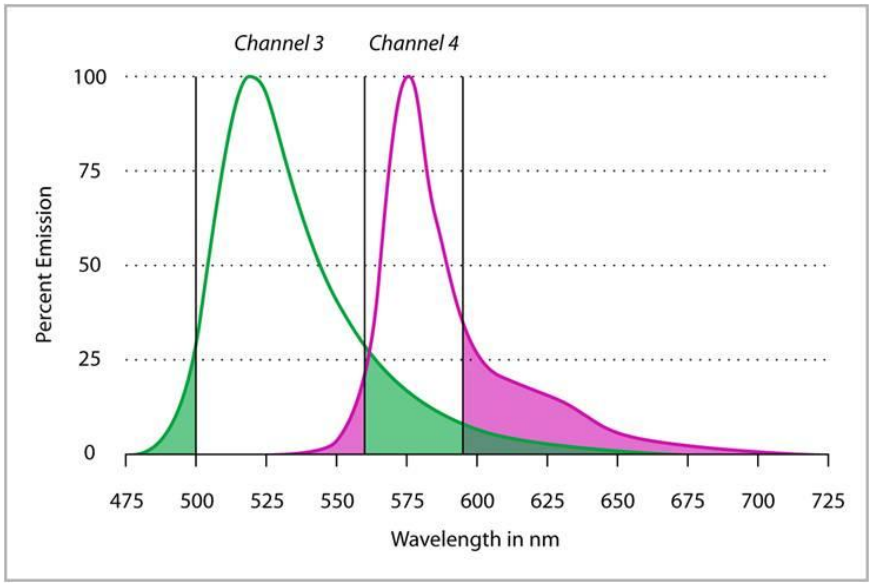


**Figure 34. Overview of compensation rationale. While the green signal primarily fluoresces in the Channel 3 wavelength range, a portion of the signal can be detected in the Channel 4 range. Image taken from [119].**

Spillover is due to the overlap of fluorescent emission spectra. For example, in Figure 34 the green fluorochrome, which is primarily detected in channel 3, spills into channel 4, where the pink fluorochrome is primarily localized. Thus, the channel 3 signal is incorrectly influencing the channel 4 signal. If this data was interpreted without the use of compensation, the fluorescent intensity reported in channel 4 would be the result of both the true pink signal and the spillover of the

green signal from channel 3. Proper compensation removes the unwanted effect of signal spillover.

#### 3.2.4.2. Population Gating

Population gating was performed using the Ideas™ (AMNIS Corp.) software package. As recommended in the Ideas™ User Manual [119], image data was first gated to ensure only focused and single cells were included in the final analysis. Briefly, focused cells were found by creating a histogram of the Gradient RMS characteristic in Ideas™, as shown in Figure 35a. Gradient RMS is defined as root mean square of the rate of change of the image intensity profile [120]. Values above 40 were considered indicative of focused cells. Next, using only cells found in the focused cell population, single cell gating was achieved by plotting the area of the brightfield image against the aspect ratio of the brightfield image. The Ideas™ software calculates area as the number of pixels in the image mask, while the aspect ratio is calculated as the ratio of the image mask height to the image mask width [120]. Cells with areas between approximately 50 and 150 pixels and aspect ratios of 0.7 and above were gated as single cells, as indicated in Figure 35b. This step ensured that debris and multiple-cell clusters were not included in the final analysis population.

Cell death populations were visualized by plotting the intensity of Annexin V-FITC (channel 2) against the intensity of 7AAD (channel 4). As described in Table 22, this method revealed four distinct cell populations. Cells expressing

both low Annexin and low 7AAD were considered live undamaged cells (Figure 36a), while cells expressing low Annexin but high 7AAD were referred to as live, damaged cells. High Annexin, low 7AAD cells were considered early apoptotic cells (Figure 36b) and cells expressing high Annexin and high 7AAD were composed of both primary and secondary necrotic cells (Figure 36c).

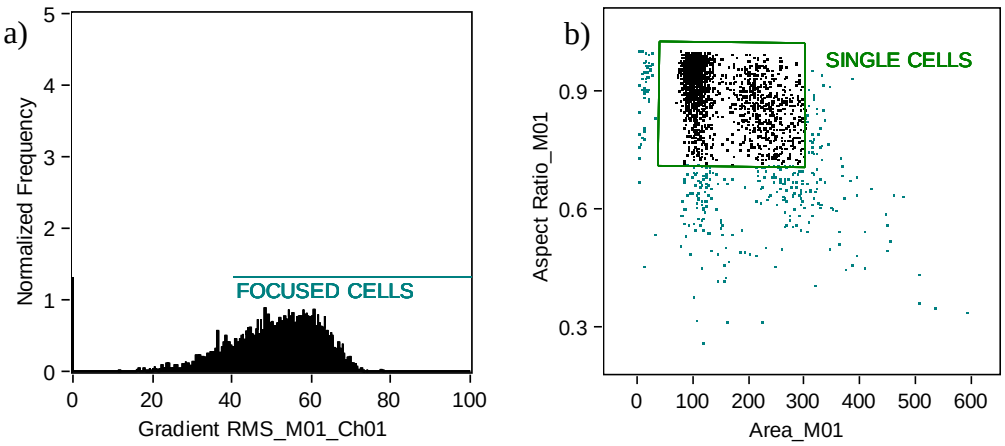


**Figure 35. Gating of (a) focused cells and (b) single cells.**

**Table 22, Annexin V-FITC and 7AAD Staining Interpretation.**

| | | |
|---|---|---|
| **HIGH 7-AAD** | Damaged Viable Cells | Primary & Secondary Necrosis (late Apoptosis) |
| **LOW 7-AAD** | Normal Cells | Early Apoptosis |

| | LOW Annexin V-FITC | HIGH Annexin V-FITC |
|---|---|---|

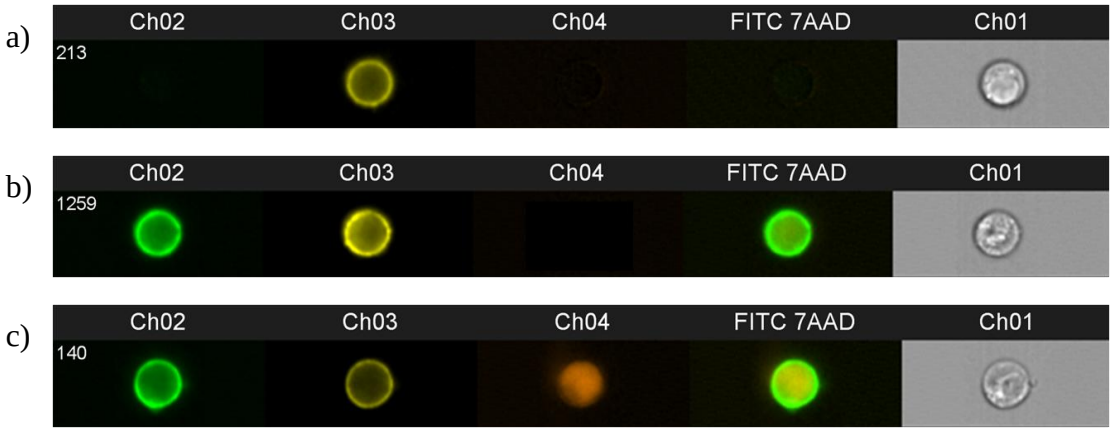


**Figure 36. Fluorescent differentiation between (a) live cells, (b) apoptotic cells, and (c) necrotic cells.**

Figure 37 represents a typical cell death analysis plot following 1.88 Gy gamma irradiation. This sample shows an obvious live cell population in the lower left corner. However, the separation between apoptotic and necrotic cells populations are not easily distinguished through simple graphical interpretation due to the interplay between apoptosis and secondary necrosis. When plasma membrane integrity becomes compromised in late-stage apoptosis, 7AAD is able to enter the cell. For this reason, isolated apoptotic and necrotic cells populations are difficult to achieve *in vitro* by plotting the intensity of Annexin V-FITC vs. the intensity of 7AAD. Fortunately, the ImageStream X allows for individual image analysis, and

this capability was instrumental for the setting of the appropriate apoptosis and necrosis gates.

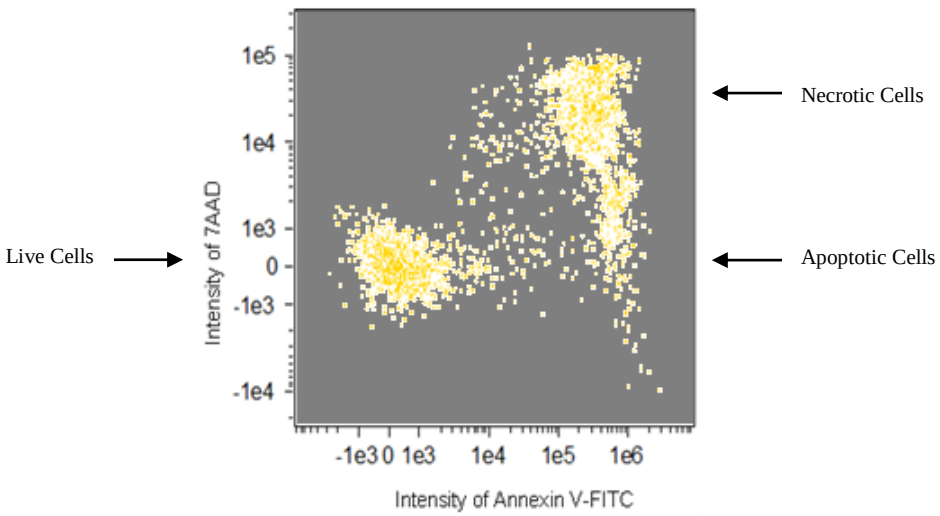


**Figure 37. Cell death response following 1.88 Gy gamma. The intensity of Annexin V-FITC versus 7AAD for Donor 3 is shown.**

### 3.2.5. Statistics

#### 3.2.5.1. Cell Death Kinetics

As described in Section 3.2.3, cell death kinetic graphs were created using blood from the youngest donor. The percentage of each cell fate (apoptosis, necrosis, live damaged, and live cells) was calculated using approximately 15,000 cells. Error bars were not included on the kinetics graphs because the count error was less than one percent.

#### 3.2.5.2. Cell Death Assays

The pooled data represents the mean response of four different donors. Error bars were calculated at the standard error of the mean. *p*-values were calculated using the Student's *t*-test for unequal variances. Results where the two-sided *p* value < 0.05 were considered significant. Statistical analysis is based on published methods for similar assays [59].

The graphs describing the individual blood donors responses did not include error bars, as the count error (calculated as one over the square root of the number of observations) was less than one percent.

## 3.3. RESULTS

#### 3.3.1.1. Cell Death Kinetics

Thermal neutron- and gamma-irradiated cells were examined at 24, 28, 72, and 96 hours post-irradiation. Figure 38 details the percent of apoptotic, necrotic, live/damaged, and live cells at each time point. This was calculated by 100-fold absolute number of cells expressing the marker(s) of interest divided by the total number of cells collected per sample.

Following gamma radiation exposure, apoptosis was highest during the 48-72 hour period with approximately 5% apoptosis observed at 48 hours and approximately 10% apoptosis observed at 72 hours. Similarly, necrosis was also pronounced during the 48-72 hour period, with approximately 40% necrosis

occurring at 48 hours and approximately 48% necrosis occurring at 72 hours. Likewise, at 48 hours approximately 55% of all cells were alive, while at 72 hours approximately only 39% of cells were alive. The percentage of live-damaged cells was not significantly elevated at the 48-hour time point, however this increased to approximately 7% at 72 hours, and 30% at 96 hours post-irradiation.

In contrast, following thermal neutron irradiation, neither the apoptosis nor necrosis signals were significantly elevated at any of the sampling points. Similarly, the percentage of live and live-damaged cells was also unchanged throughout the sampling period.

#### 3.3.1.2. Cell Death Dose Response

Following both gamma and thermal neutron exposure, percentages of apoptosis, necrosis, live-damaged cells, and live cells were calculated for all four blood donors. The gamma data was pooled because 1) the doses were consistent across all donors, and 2) it was assumed that the behaviour of lymphocytes following irradiation was constant across donors. In contrast, as daily reactor power fluctuations made it difficult to ensure consistent dosing across all donors, the thermal neutron data could not be pooled.

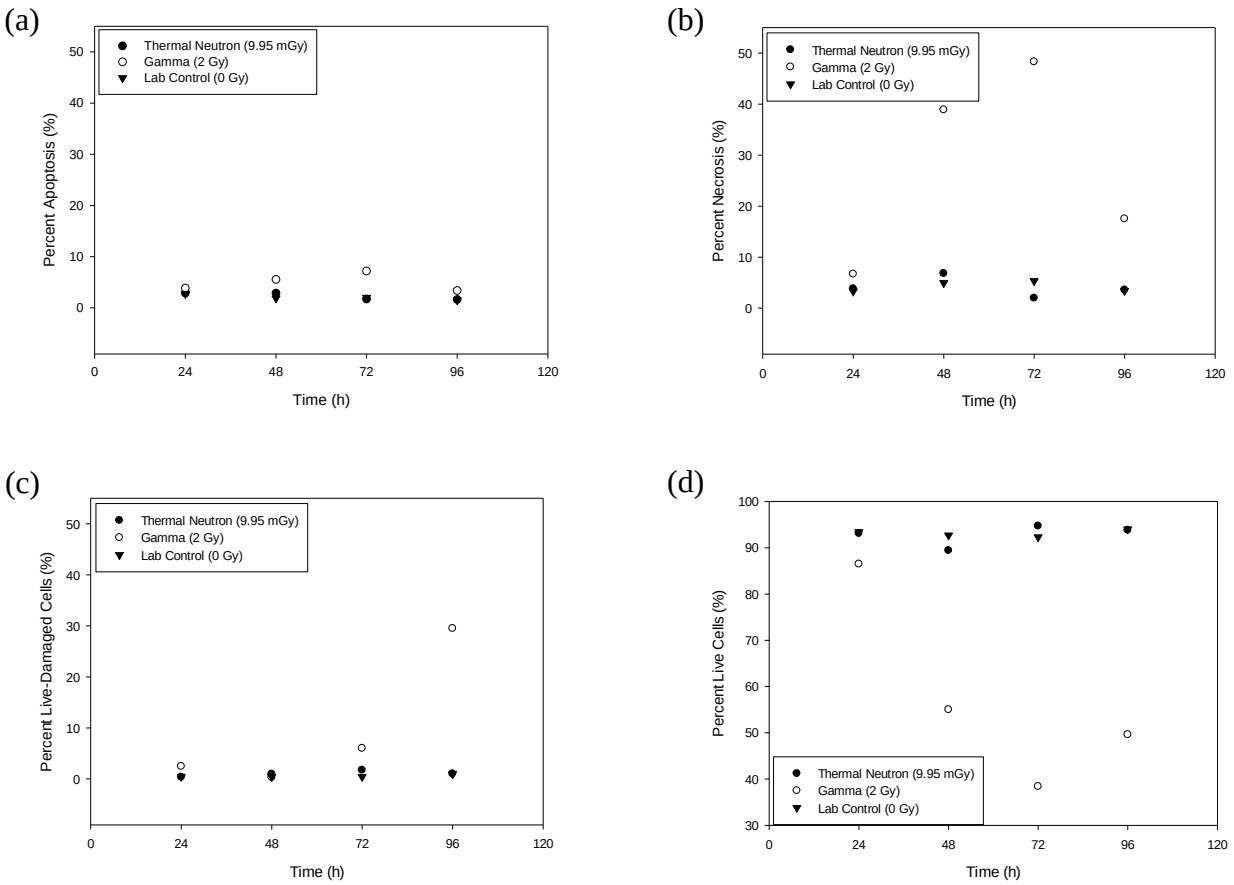


**Figure 38. Cell death kinetics for (a) apoptosis, (b) necrosis, (c) live cells, (d) live/damaged cells post-irradiation.**

### 3.3.1.2.1. Cell Death Following $^{60}$Co Gamma Exposure

The mean, standard deviation, and standard error of the pooled gamma data is reported below in Table 23.

**Table 23. Mean, standard deviation, and standard error for apoptosis, necrosis, live-damaged, and live cell populations following $^{60}$Co exposure.**

| | DOSE (Gy) | MEAN | STANDARD DEVIATION | STANDARD ERROR |
|---|---|---|---|---|
| APOPTOSIS | **0** | 0.06 | 0.03 | 0.01 |
| | **0.03** | 0.09 | 0.06 | 0.03 |
| | **0.06** | 0.10 | 0.02 | 0.01 |
| | **0.13** | 0.09 | 0.04 | 0.02 |
| | **0.19** | 0.09 | 0.04 | 0.02 |
| | **0.25** | 0.10 | 0.04 | 0.02 |
| | **0.63** | 0.11 | 0.02 | 0.01 |
| | **1.3** | 0.16 | 0.03 | 0.01 |
| | **1.9** | 0.15 | 0.04 | 0.02 |
| | **2.5** | 0.16 | 0.06 | 0.03 |
| | DOSE (Gy) | MEAN | STANDARD DEVIATION | STANDARD ERROR |
| NECROSIS | **0** | 0.06 | 0.02 | 0.01 |
| | **0.03** | 0.11 | 0.11 | 0.07 |
| | **0.06** | 0.10 | 0.04 | 0.02 |
| | **0.13** | 0.10 | 0.06 | 0.03 |
| | **0.19** | 0.14 | 0.06 | 0.03 |
| | **0.25** | 0.11 | 0.05 | 0.03 |
| | **0.63** | 0.26 | 0.14 | 0.07 |
| | **1.3** | 0.17 | 0.08 | 0.04 |
| | **1.9** | 0.28 | 0.09 | 0.04 |
| | **2.5** | 0.30 | 0.05 | 0.02 |
| | DOSE (Gy) | MEAN | STANDARD DEVIATION | STANDARD ERROR |
| LIVE-DAMAGED CELLS | **0** | 0.02 | 0.02 | 0.01 |
| | **0.03** | 0.03 | 0.01 | 0.01 |
| | **0.06** | 0.02 | 0.01 | 0.01 |
| | **0.13** | 0.02 | 0.01 | 0.01 |
| | **0.19** | 0.03 | 0.02 | 0.01 |
| | **0.25** | 0.03 | 0.02 | 0.01 |
| | **0.63** | 0.02 | 0.01 | 0.00 |
| | **1.3** | 0.04 | 0.03 | 0.01 |
| | **1.9** | 0.03 | 0.02 | 0.01 |
| | **2.5** | 0.02 | 0.01 | 0.01 |
| | DOSE (Gy) | MEAN | STANDARD DEVIATION | STANDARD ERROR |
| LIVE CELLS | **0** | 0.86 | 0.02 | 0.01 |
| | **0.03** | 0.77 | 0.15 | 0.09 |
| | **0.06** | 0.78 | 0.06 | 0.03 |
| | **0.13** | 0.79 | 0.11 | 0.06 |
| | **0.19** | 0.74 | 0.07 | 0.03 |
| | **0.25** | 0.76 | 0.08 | 0.04 |
| | **0.63** | 0.62 | 0.13 | 0.07 |
| | **1.3** | 0.63 | 0.05 | 0.02 |
| | **1.9** | 0.53 | 0.10 | 0.05 |
| | **2.5** | 0.53 | 0.04 | 0.02 |

Figure 39 and illustrates percent apoptosis as a function of absorbed dose for $^{60}$Co gamma ray exposure. A linear quadratic increase in apoptotic cell death with dose was observed. The $R^2$ value for the quadratic fit was 0.88. For comparison, if a linear fit was applied to the data, a lower $R^2$ value of 0.80 would result. All data points were tested to determine whether they were significantly elevated above background using the Student's *t*-test. Only the highest four doses of 0.63 Gy – 2.5 Gy showed a significant response.

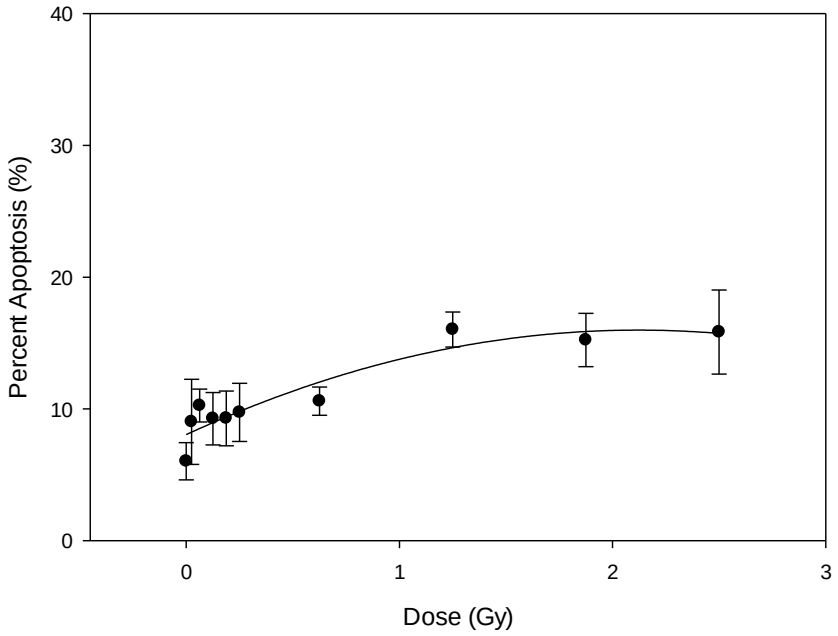


**Figure 39. Percent apoptosis versus dose for $^{60}$Co gamma rays. Error bars represent standard error of the mean**

Figure 40 illustrates percent necrosis as a function of absorbed dose. Following gamma exposure, a linear quadratic increase in necrotic cell death with dose was

observed ($R^2$ value of 0.79). As above, for comparison, if a linear trendline was added to this data set, the $R^2$ value would be slightly lower at 0.73. Using the Student's *t*-test, all doses points were tested to determine whether they were significantly elevated above background. As for apoptosis, only the highest four doses of 0.63 Gy - 2.5 Gy were found to be significantly different from the background level of necrosis.

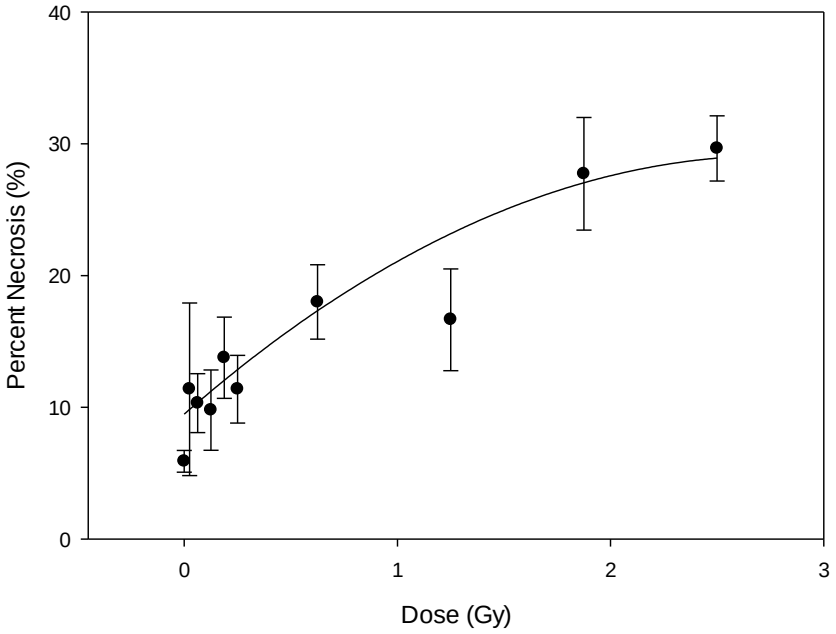


**Figure 40. Percent necrosis versus dose for $^{60}$Co gamma rays. Error bars represent standard error of the mean.**

Following $^{60}$Co gamma exposure, approximately 2-3% of all cells, at all dose points, were live-damaged as indicated in Figure 41. These cells were still

metabolically active at the time of anaylsis, but had cell membrane disruptions that allowed for 7AAD entry.

At 48-hours post exposure, the $^{60}$Co gamma-irradiated samples demonstrated a linear quadratic response with an $R^2$ value of 0.92, as depicted in Figure 42.

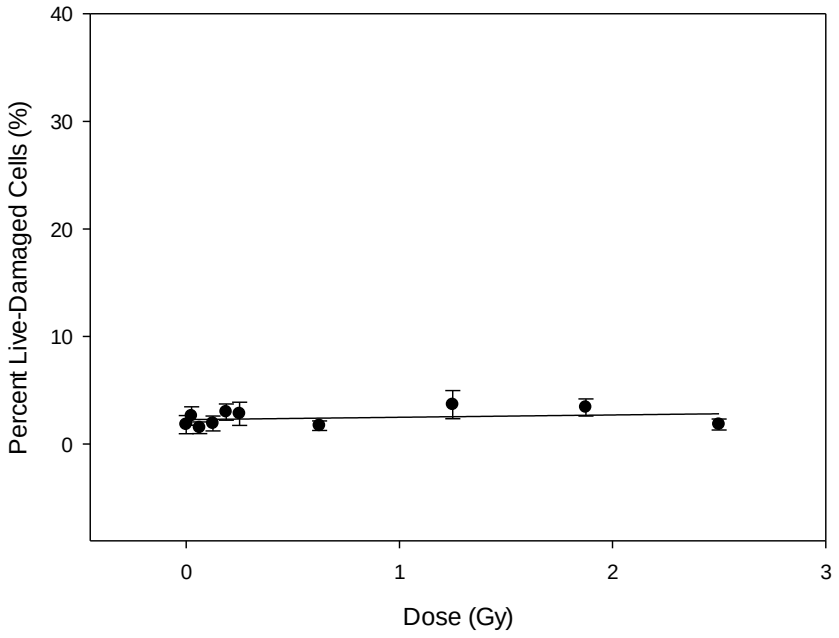


**Figure 41. Percent live-damaged cells versus dose for $^{60}$Co gamma rays. Error bars represent standard error of the mean.**

Following $^{60}$Co gamma exposure, the induction rates of apoptosis and necrosis were found to be disproportionate. As indicated in Figure 43, there is little difference between the percent of apoptosis and necrosis below 0.25 Gy, as confirmed by an equal variance Student's *t*-test (Table 24). However, at doses of 0.625 Gy, 1.875 Gy, and 2.5 Gy, there is a significantly more necrosis than

apoptosis following $^{60}$Co exposures as the Student's *t*-test P-values were found to be smaller than 0.05.

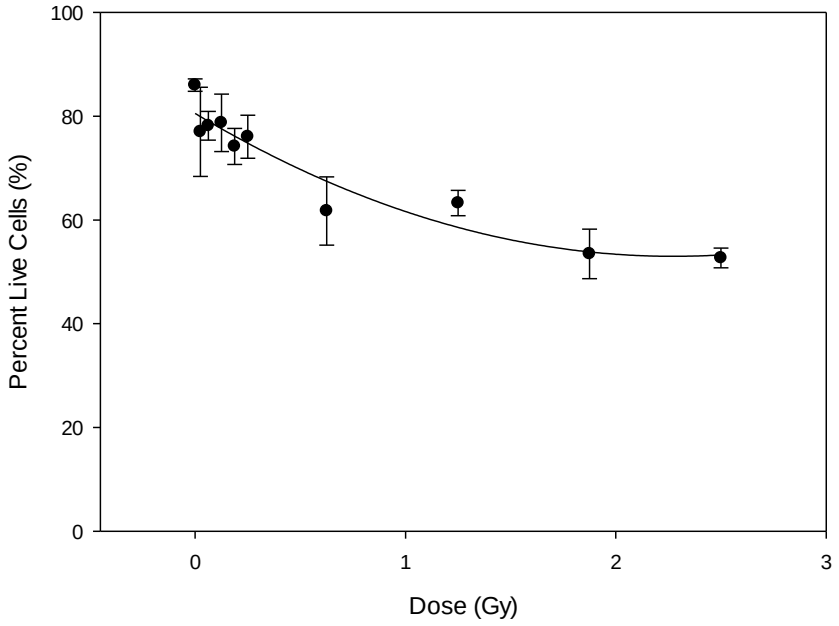


**Figure 42. Percent live cells versus dose for $^{60}$Co gamma rays. Error bars represent standard error of the mean.**

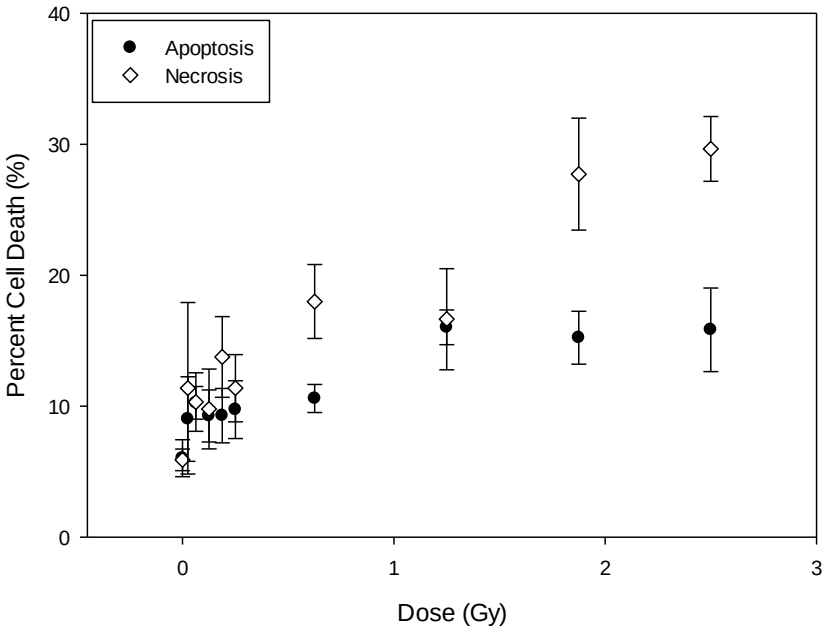


**Figure 43. Comparison of $^{60}$Co-induced apoptosis and necrosis.**

**Table 24. Assessing significance between cell death modalities using the Student's *t*-test.**

| GAMMA DOSE (Gy) | # SAMPLES PER GROUP | MEAN APOPTOSIS | MEAN NECROSIS | STUDENT'S t-TEST P-VALUE |
|---|---|---|---|---|
| 0 | 4 | 0.06 | 0.06 | 0.475 |
| 0.03 | 3 | 0.09 | 0.11 | 0.382 |
| 0.06 | 4 | 0.10 | 0.10 | 0.491 |
| 0.13 | 4 | 0.09 | 0.10 | 0.452 |
| 0.19 | 4 | 0.09 | 0.14 | 0.169 |
| 0.25 | 4 | 0.10 | 0.11 | 0.345 |
| 0.63 | 4 | 0.11 | 0.26 | 0.039 |
| 1.3 | 4 | 0.16 | 0.17 | 0.449 |
| 1.9 | 4 | 0.15 | 0.28 | 0.031 |
| 2.5 | 4 | 0.16 | 0.30 | 0.013 |

#### 3.3.1.2.2. Cell Death Following Low Dose Thermal Neutron Exposure

Following low-dose thermal neutron exposures, apoptosis levels remained fairly consistent at approximately 9%, despite increasing radiation doses, as shown in Figure 44. The $R^2$ value of the linear trend-line was found to be 0.0012.

Similarly, following thermal neutron exposure, there was no increase in necrosis with increasing dose ($R^2$ value of 0.0008), as demonstrated in Figure 44, nor was there any variation in the number of live-damaged cells ($R^2$ value of 0.016), as demonstrated in Figure 46. Likewise, the number of live cells also remained fairly constant at approximately 80% ($R^2$ value of 0.0002), as demonstrated in Figure 47.

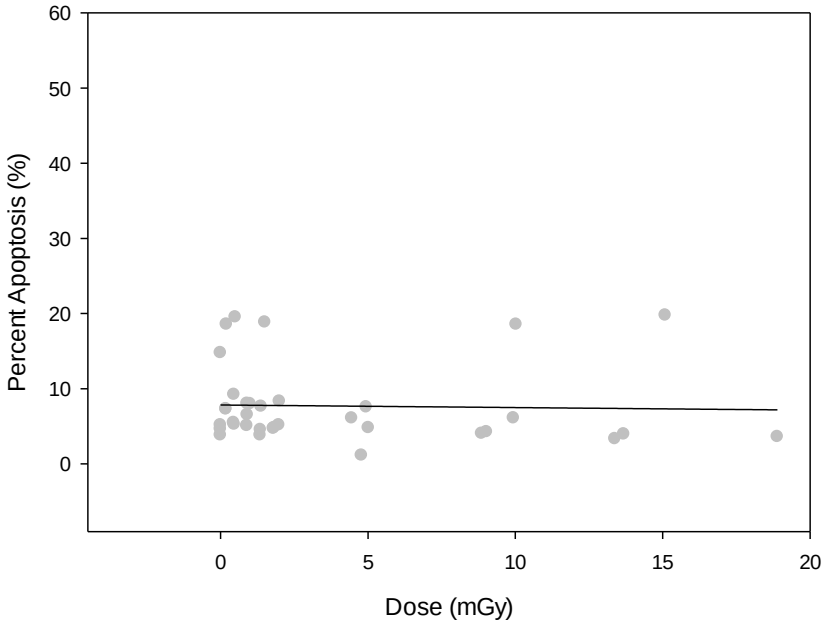


**Figure 44. Percent apoptosis versus dose following thermal neutron exposure.**

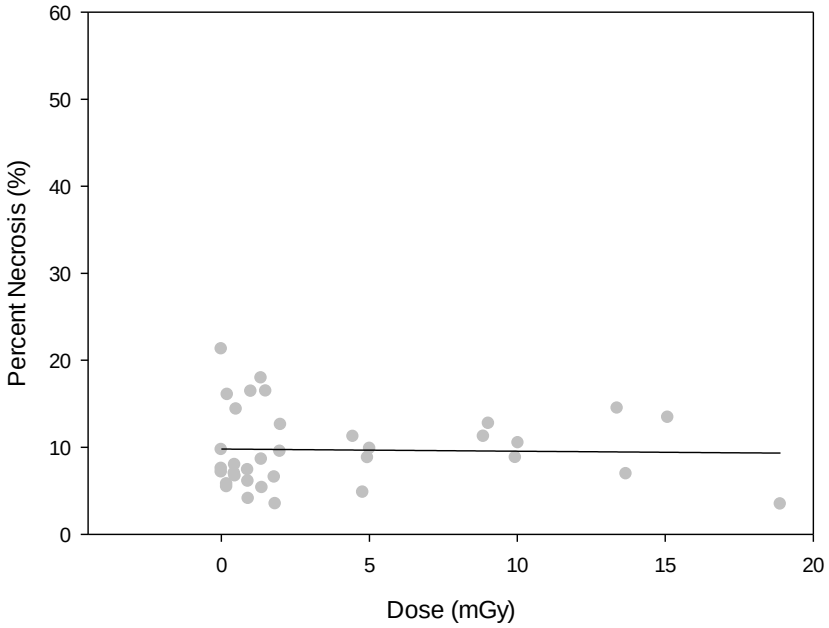


**Figure 45. Percent necrosis versus dose following thermal neutron exposure.**

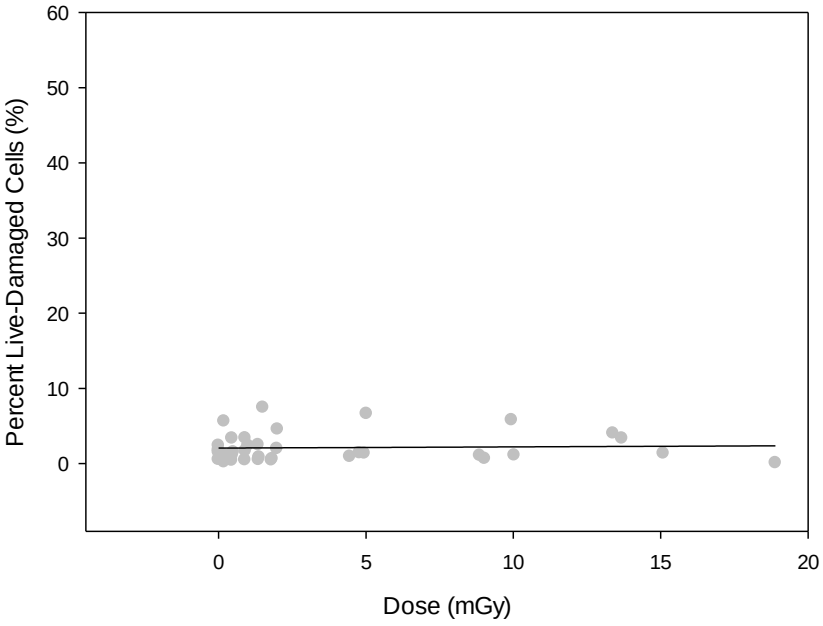


**Figure 46. Percent live-damaged cells versus dose following thermal neutron exposure.**

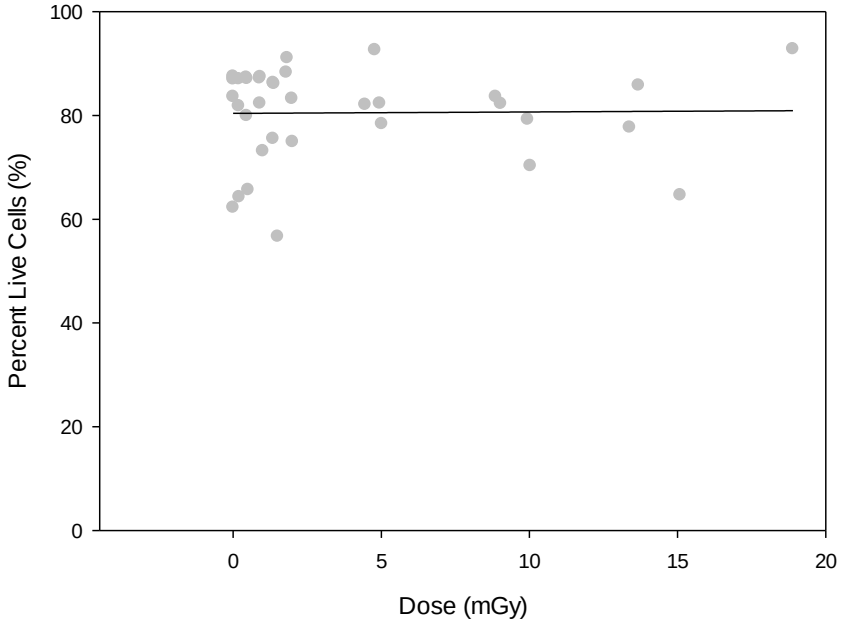


**Figure 47. Percent live cells versus dose following thermal neutron exposure.**

### 3.3.1.3. Individual Donor Variation

No one donor consistently demonstrated elevated or suppressed apoptosis or necrosis following either $^{60}$Co gamma radiation or low-dose thermal neutron radiation exposure, as described graphically in Figure 48 and Figure 49. Raw data is given in Table 25 and Table 26.

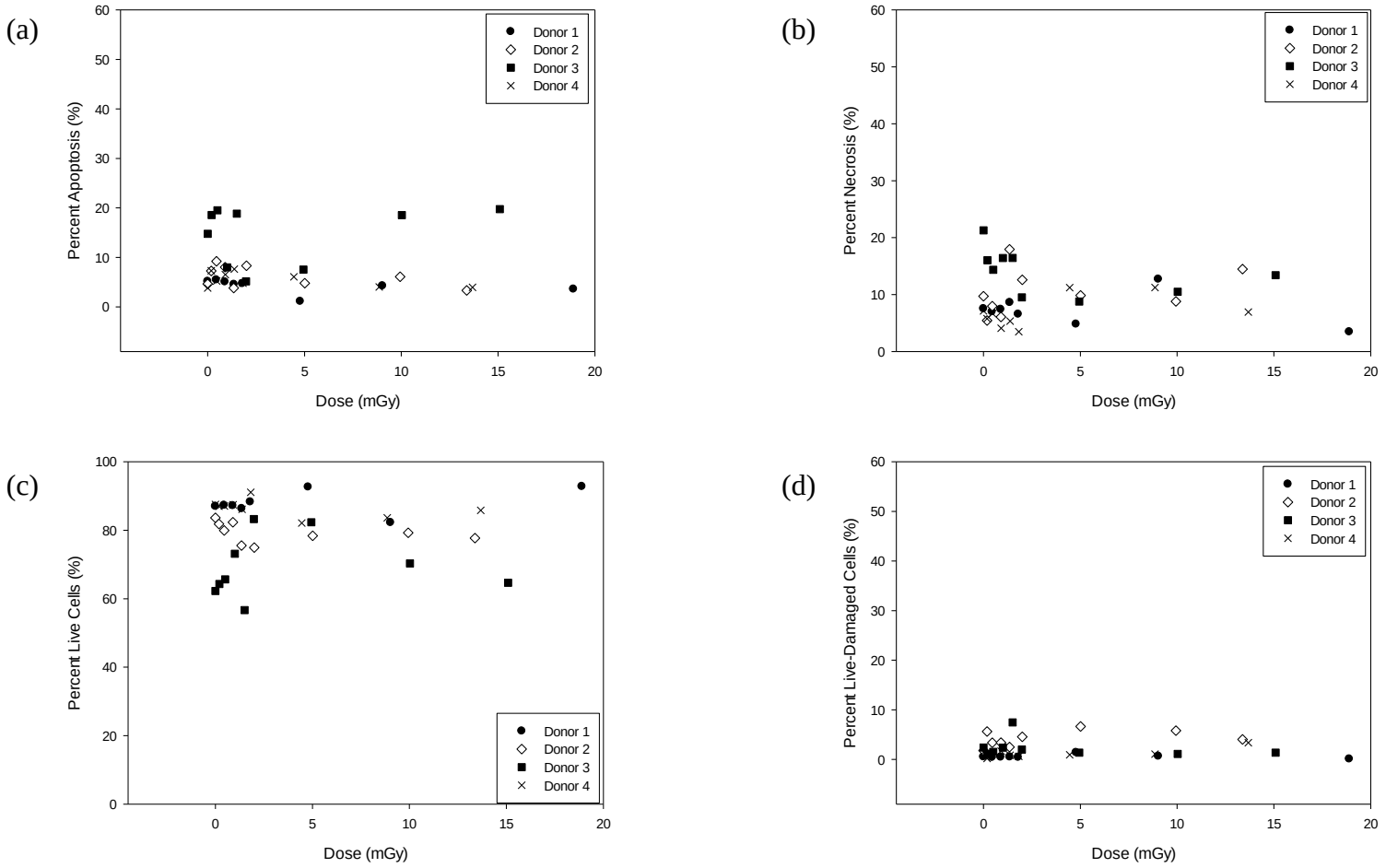


**Figure 48. Donor variation for (a) apoptosis, (b) necrosis, (c) live cells, and (d) live-damaged cells following low dose thermal neutron exposure.**

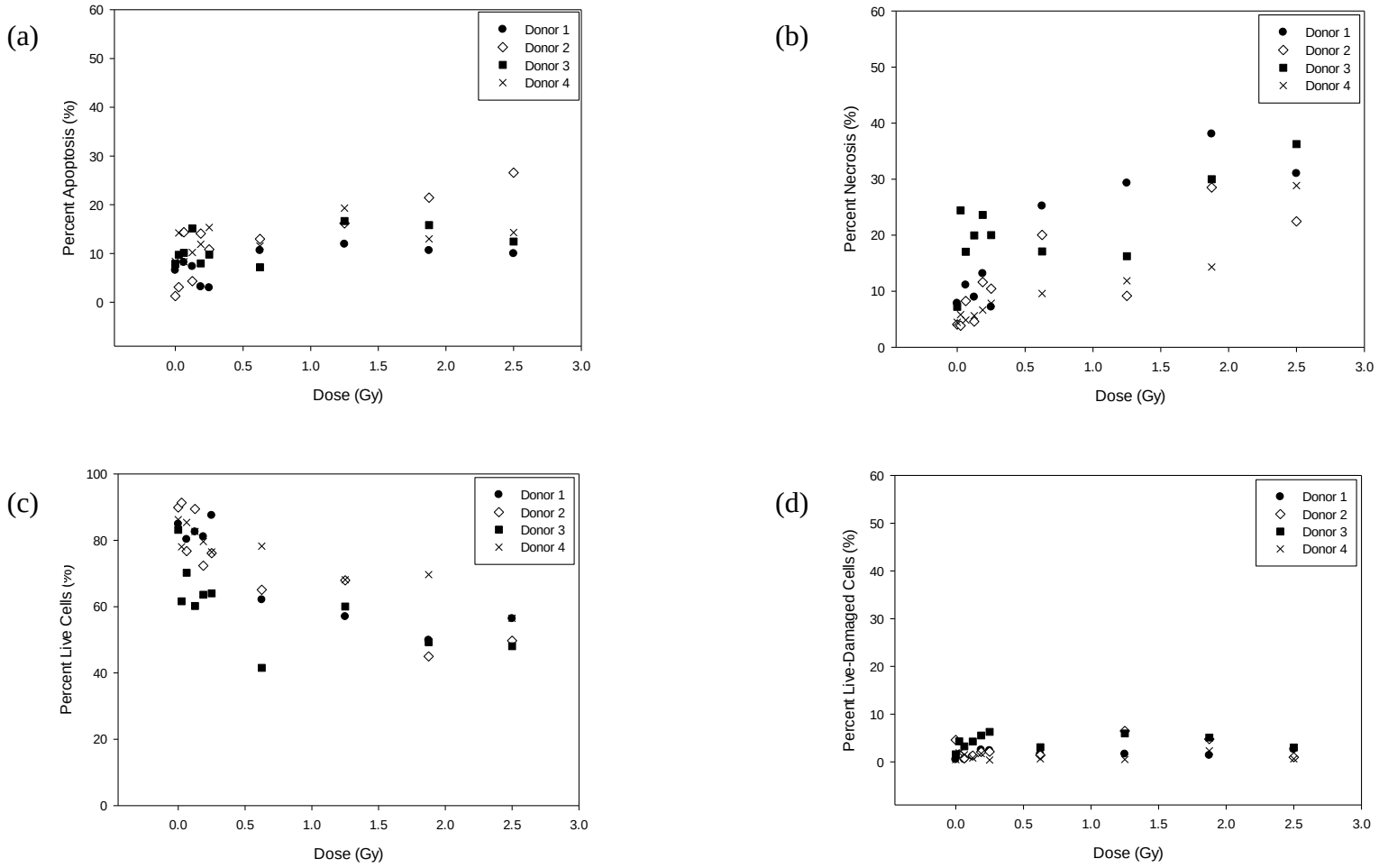


**Figure 49. Donor variation for (a) apoptosis, (b) necrosis, (c) live cells, and (d) live-damaged cells following $^{60}$Co gamma exposure.**

**Table 25. Individual donor variation for apoptosis and necrosis endpoints following $^{60}$Co gamma exposure.**

| | DOSE (Gy) | APOPTOSIS (%) | NECROSIS (%) | LIVE-DAMAGED (%) | LIVE CELLS (%) |
|---|---|---|---|---|---|
| DONOR 1 | 0 | 6.55 | 7.83 | 0.49 | 84.89 |
| | 0.06 | 8.18 | 11.10 | 0.51 | 80.30 |
| | 0.13 | 7.33 | 8.94 | 1.16 | 82.54 |
| | 0.19 | 3.17 | 13.14 | 2.52 | 81.12 |
| | 0.25 | 2.97 | 7.18 | 2.38 | 87.52 |
| | 0.63 | 10.63 | 25.21 | 1.64 | 62.09 |
| | 1.25 | 11.91 | 29.30 | 1.64 | 57.01 |
| | 1.88 | 10.61 | 38.06 | 1.38 | 49.89 |
| | 2.50 | 9.98 | 31.02 | 2.61 | 56.40 |
| DONOR 2 | DOSE (Gy) | APOPTOSIS (%) | NECROSIS (%) | LIVE-DAMAGED (%) | LIVE CELLS (%) |
| | 0 | 1.28 | 4.08 | 4.60 | 89.90 |
| | 0.03 | 3.11 | 3.85 | 1.60 | 91.34 |
| | 0.06 | 14.37 | 8.26 | 0.74 | 76.77 |
| | 0.13 | 4.33 | 4.59 | 1.33 | 89.47 |
| | 0.19 | 14.08 | 11.63 | 2.08 | 72.35 |
| | 0.25 | 10.84 | 10.45 | 2.16 | 76.13 |
| | 0.63 | 12.98 | 20.05 | 1.40 | 65.09 |
| | 1.25 | 16.20 | 9.16 | 6.49 | 67.94 |
| | 1.89 | 21.45 | 28.52 | 4.78 | 45.01 |
| | 2.50 | 26.59 | 22.47 | 0.97 | 49.76 |
| DONOR 3 | DOSE (Gy) | APOPTOSIS (%) | NECROSIS (%) | LIVE-DAMAGED (%) | LIVE CELLS (%) |
| | 0 | 7.90 | 7.23 | 1.60 | 83.20 |
| | 0.03 | 9.73 | 24.44 | 4.31 | 61.63 |
| | 0.06 | 10.13 | 17.05 | 3.26 | 70.23 |
| | 0.13 | 15.14 | 19.96 | 4.27 | 60.21 |
| | 0.19 | 7.96 | 23.61 | 5.53 | 63.62 |
| | 0.25 | 9.79 | 20.01 | 6.29 | 64.02 |
| | 0.63 | 7.17 | 17.10 | 3.08 | 41.53 |
| | 1.25 | 16.66 | 16.25 | 5.96 | 60.04 |
| | 1.89 | 15.83 | 30.00 | 5.12 | 49.28 |
| | 2.50 | 12.45 | 36.26 | 3.02 | 48.07 |
| DONOR 4 | DOSE (Gy) | APOPTOSIS (%) | NECROSIS (%) | LIVE-DAMAGED (%) | LIVE CELLS (%) |
| | 0 | 8.36 | 4.46 | 0.48 | 86.25 |
| | 0.03 | 14.21 | 5.82 | 1.90 | 78.05 |
| | 0.06 | 8.31 | 4.86 | 1.51 | 85.40 |
| | 0.13 | 10.20 | 5.64 | 0.83 | 82.69 |
| | 0.19 | 11.89 | 6.65 | 1.73 | 79.64 |
| | 0.25 | 15.33 | 7.84 | 0.39 | 76.51 |
| | 0.63 | 11.55 | 9.59 | 0.65 | 78.25 |
| | 1.25 | 19.30 | 11.86 | 0.52 | 68.13 |
| | 1.89 | 13.00 | 14.32 | 2.32 | 69.67 |
| | 2.50 | 14.31 | 28.87 | 0.65 | 56.53 |

**Table 26. Individual donor variation for apoptosis, necrosis, live-damaged, and live cell endpoints following thermal neutron exposure.**

| | DOSE (mGy) | APOPTOSIS (%) | NECROSIS (%) | LIVE-DAMAGED (%) | LIVE CELLS (%) |
|---|---|---|---|---|---|
| DONOR 1 | 0 | 5.2 | 7.5 | 0.53 | 87.0 |
| | 0.4 | 5.5 | 7.0 | 0.42 | 87.3 |
| | 0.9 | 5.0 | 7.4 | 0.47 | 87.2 |
| | 1.4 | 4.5 | 8.6 | 0.50 | 86.3 |
| | 1.8 | 4.7 | 6.6 | 0.45 | 88.3 |
| | 4.8 | 1.1 | 4.8 | 1.42 | 92.7 |
| | 9.0 | 4.3 | 12.7 | 0.66 | 82.3 |
| | 18.9 | 3.6 | 3.5 | 0.11 | 92.8 |
| | **DOSE (mGy)** | **APOPTOSIS (%)** | **NECROSIS (%)** | **LIVE-DAMAGED (%)** | **LIVE CELLS (%)** |
| DONOR 2 | 0 | 4.6 | 9.7 | 1.80 | 83.6 |
| | 0.2 | 7.3 | 5.4 | 5.63 | 81.9 |
| | 0.5 | 9.2 | 8.0 | 3.37 | 80.0 |
| | 0.9 | 8.0 | 6.1 | 3.40 | 82.4 |
| | 1.3 | 3.8 | 17.9 | 2.49 | 75.5 |
| | 2.0 | 8.3 | 12.6 | 4.57 | 74.9 |
| | 5.0 | 4.8 | 9.8 | 6.66 | 78.4 |
| | 9.9 | 6.1 | 8.8 | 5.80 | 79.3 |
| | 13.4 | 3.3 | 14.5 | 4.04 | 77.7 |
| | **DOSE (mGy)** | **APOPTOSIS (%)** | **NECROSIS (%)** | **LIVE-DAMAGED (%)** | **LIVE CELLS (%)** |
| DONOR 3 | 0 | 14.8 | 21.3 | 2.41 | 62.3 |
| | 0.2 | 18.6 | 16.0 | 1.14 | 64.3 |
| | 0.5 | 19.5 | 14.3 | 1.52 | 65.7 |
| | 1.0 | 8.0 | 16.4 | 2.38 | 73.1 |
| | 1.5 | 18.8 | 16.4 | 7.47 | 56.7 |
| | 2.0 | 5.2 | 9.5 | 2.00 | 83.3 |
| | 4.9 | 7.5 | 8.8 | 1.37 | 82.3 |
| | 10.0 | 18.5 | 10.5 | 1.13 | 70.3 |
| | 15.1 | 19.8 | 13.4 | 1.38 | 64.7 |
| | **DOSE (mGy)** | **APOPTOSIS (%)** | **NECROSIS (%)** | **LIVE-DAMAGED (%)** | **LIVE CELLS (%)** |
| DONOR 4 | 0 | 3.8 | 7.1 | 1.50 | 87.5 |
| | 0.2 | 7.3 | 5.8 | 0.21 | 87.0 |
| | 0.5 | 5.3 | 6.7 | 1.10 | 87.1 |
| | 0.9 | 6.5 | 4.1 | 1.69 | 87.5 |
| | 1.4 | 7.6 | 5.4 | 0.84 | 86.1 |
| | 1.8 | 4.8 | 3.5 | 0.64 | 91.1 |
| | 4.5 | 6.1 | 11.2 | 0.94 | 82.1 |
| | 8.9 | 4.0 | 11.2 | 1.07 | 83.6 |
| | 13.7 | 4.0 | 6.9 | 3.38 | 85.8 |

### 3.3.2. Control Samples

Figure 50 illustrates the mean percent cell death found in the three thermal neutron control samples (laboratory control, gamma field control, and NRU control), and the single $^{60}$Co gamma control sample. Background levels of apoptosis ranged between approximately 4-8 %, whereas the background levels of necrosis fell between 6-10%.

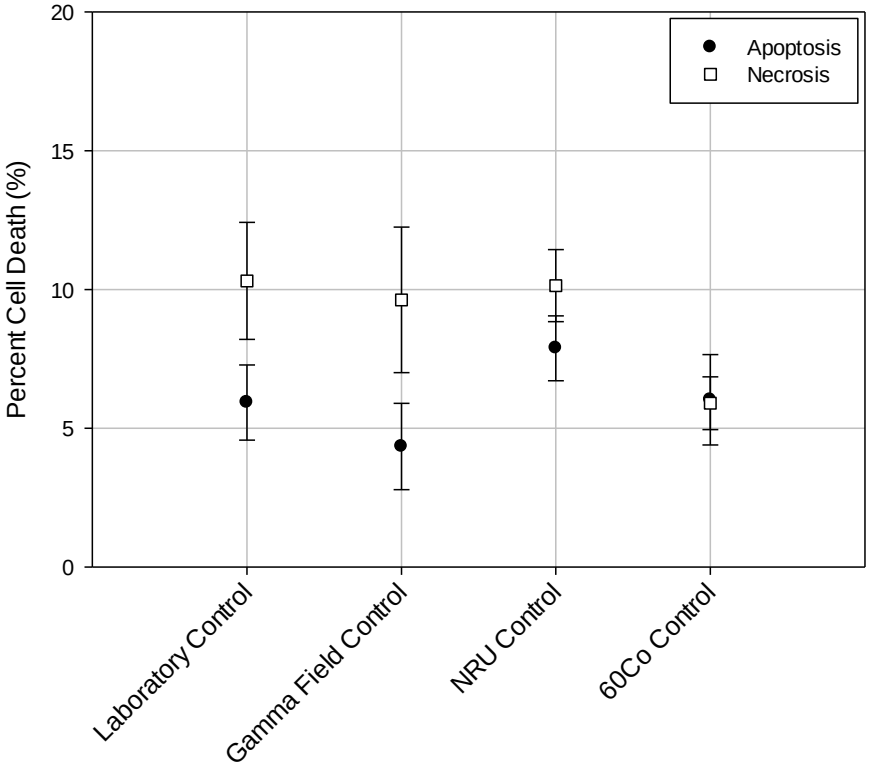


**Figure 50. Apoptosis and necrosis in control samples (0 Gy) at 48 hours post-irradiation. Error bars represent standard error.**

The standard error was calculated based on data from all four donors, except for the Gamma Field Control where data from only 3 donors exists. Using the Student's *t*-test, it was determined that apoptotic and necrotic induction was not statistically different within each control. Likewise, while the level of necrosis in the $^{60}$Co gamma control samples was statistically different from the level of necrosis in the NRU control samples ($p < 0.05$), the levels of apoptosis and necrosis in the remaining cell death control tubes were not statistically different than the comparable cell death response in the other control samples. Raw data is presented in Table 27.

**Table 27. Control sample mean, standard deviation, and standard error for all measured parameters**

| LABORATORY CONTROL | MEAN | STANDARD DEVIATION | STANDARD ERROR |
|---|---|---|---|
| % Live Cells | 0.822 | 0.077 | 0.038 |
| % Apoptosis | 0.059 | 0.027 | 0.014 |
| % Necrosis | 0.103 | 0.042 | 0.021 |
| % Live-Damaged Cells | 0.015 | 0.008 | 0.004 |
| | | | |
| **GAMMA FIELD CONTROL** | **MEAN** | **STD DEV** | **STD ERROR** |
| % Live Cells | 0.823 | 0.088 | 0.051 |
| % Apoptosis | 0.043 | 0.027 | 0.016 |
| % Necrosis | 0.096 | 0.045 | 0.026 |
| % Live-Damaged Cells | 0.038 | 0.025 | 0.014 |
| | | | |
| **NRU CONTROL** | **MEAN** | **STD DEV** | **STD ERROR** |
| % Live Cells | 0.795 | 0.038 | 0.019 |
| % Apoptosis | 0.079 | 0.023 | 0.012 |
| % Necrosis | 0.101 | 0.026 | 0.013 |
| % Live-Damaged Cells | 0.025 | 0.019 | 0.009 |
| | | | |
| **$^{60}$Co CONTROL** | **MEAN** | **STD DEV** | **STD ERROR** |
| % Live Cells | 0.860 | 0.029 | 0.014 |
| % Apoptosis | 0.060 | 0.033 | 0.016 |
| % Necrosis | 0.059 | 0.019 | 0.010 |
| % Live-Damaged Cells | 0.018 | 0.019 | 0.010 |

## 3.4. DISCUSSION

### 3.4.1. Apoptosis Following $^{60}$Co Gamma Exposure

There are currently only four published studies examining lymphocyte apoptosis following gamma radiation exposure, as described in Table 28. Both Ryan *et al*. [59] and Boreham et al. [121] examined the response following $^{60}$Co doses of approximately 0.25 Gy – 5 Gy, and 0.05 Gy -1 Gy, respectively. while both Torudd *et al*. [122] and Liegler *et al*. [123] examined the response following $^{137}$Cs exposure at higher doses of 1 Gy – 5 Gy, and 2.5 Gy – 45 Gy, respectively. In contrast, the dose range used for the current work was 0.03 – 2.5 Gy. The lowest dose of 0.03 Gy is nearly 10-fold lower than used in any published lymphocyte study, and the current results indicate that at doses below 0.63 Gy, the apoptotic and necrotic response are likely masked by the background rate of cell death. Thus, the five doses ranging from 0.03 Gy to 0.25 Gy did not show any significant elevation above background rate. Similarly, Boreham *et al*. [121] noted a significant response at 0.25 Gy and above using the TdT assay, with the lowest doses of 0.05 Gy and 0.1 Gy eliciting apoptotic responses similar to background levels. Furthermore, the study by Ryan *et al.* [59] noted a significant difference in apoptosis between 0 Gy and 0.25 Gy using the Annexin V assay, with approximately 12% apoptosis at 0 Gy and 24% apoptosis at 0.25 Gy. Taken together, it appears that while assay type likely affects the apoptotic resolution, doses below 0.63 Gy may not reliably produce an apoptotic response.

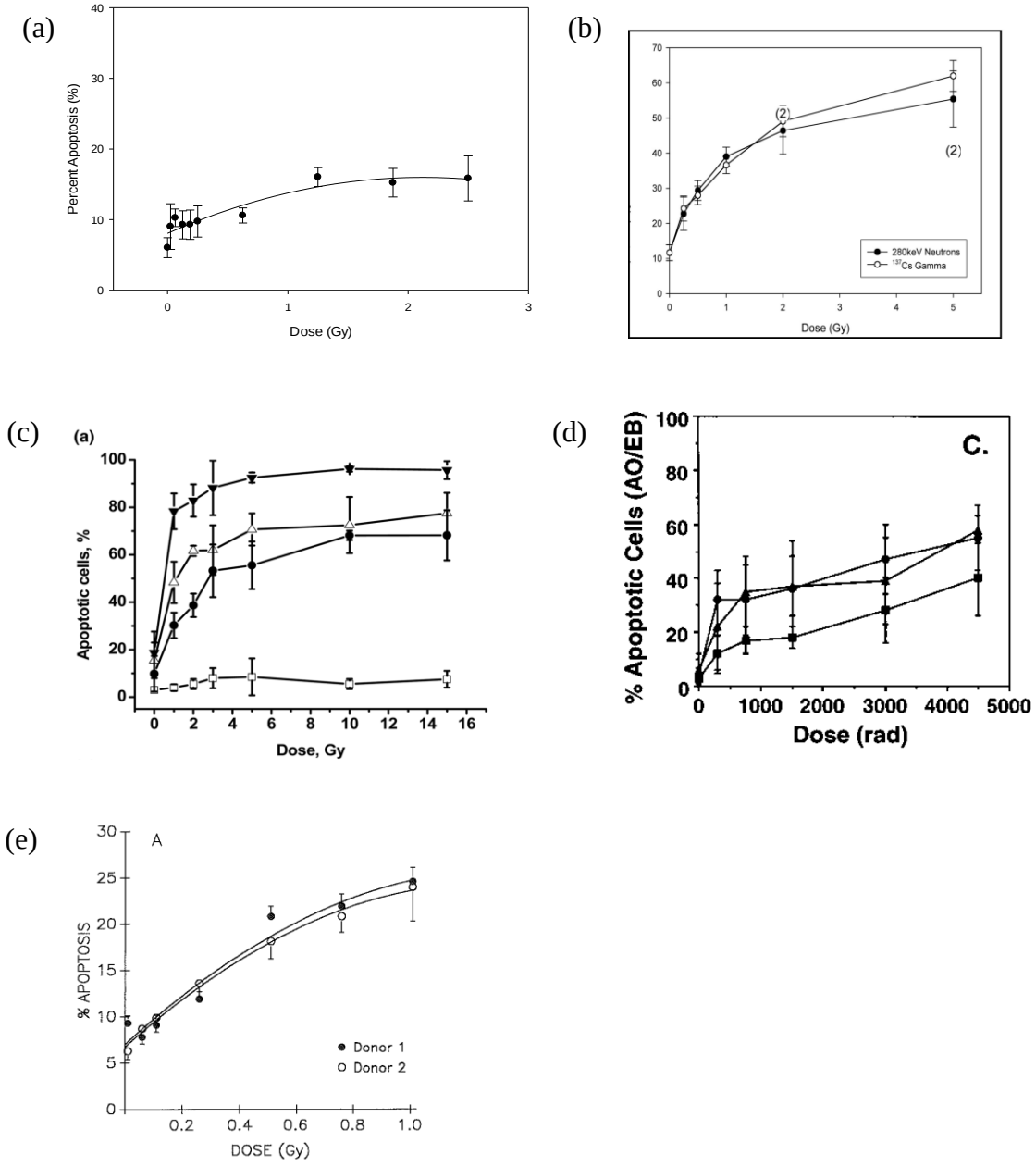


**Figure 51. Comparison of percent apoptosis induction following gamma radiation exposure. Graph (a) is the data presented in this thesis. Graph (b) is from Ryan *et al*. [59]. Graph (c) is from Torudd *et al*. [122] with the black circles representing the apoptotic response at 48-hours post-exposure. Graph (d) is from Liegler *et al*. [123], with the triangles representing the apoptotic response at 48-hours post- exposure. Graph (e) is from Boreham *et al*. [121].**

The four studies mentioned above all noted elevated apoptosis levels at the 48-hour time point, as compared to the 48-hour data presented in this thesis. For example, at 2.5 Gy, the current data generated at CNL indicates 16% apoptosis following a $^{60}$Co exposure. In contrast, Ryan *et al* [59]. noted nearly 50% apoptosis following a 2.5 Gy $^{137}$Cs gamma exposure, when apoptotic cells were examined using a flow cytometer following Annexin V staining. Interestingly, the same study noted that other markers of apoptosis including caspase-3 and the comet assay showed slightly lower levels of apoptotic induction of 30% and 35%, respectively, following a 2.5 Gy $^{137}$Cs gamma exposure [59]. Similarly, Torudd *et al*. [122] reported nearly 60% apoptosis following a 2.5 Gy $^{137}$Cs gamma exposure. In that study, cells were stained with acridine orange and propidium iodide and examined microscopically for morphological characteristics of apoptosis. Liegler *et al.* [123] noted approximately 20% apoptosis following a 2.5 Gy gamma exposure and analysed by flow cytometry using acridine orange and ethidium bromide staining. It should be noted that the characteristics of the gamma irradiation, including the source, dose rate, etc are unavailable. Lastly, Boreham *et al*. noted approximately 25% apoptosis following a 1 Gy $^{60}$Co gamma irradiation when cells were assessed via the TdT assay. The 16% apoptosis reported in this thesis is slightly lower than the published data, however in all cases, the shape of the apoptotic induction dose response curve is similar, as indicated in Figure 51. All the studies described above and the data published in this thesis note a steep increase in percent apoptosis between zero and

approximately 1-2 Gy, followed by a levelling off of the apoptotic response at higher doses [59, 121, 123, 124].

**Table 28. Comparison of studies that examined apoptosis in gamma-irradiated lymphocytes.**

| REFERENCE | GAMMA SOURCE | DOSE RATE | DOSE RANGE | IRRADIATED MATERIAL |
|---|---|---|---|---|
| This Thesis | $^{60}$Co | 0.076-0.079 Gy min$^{-1}$<br>3.57-3.7 Gy min$^{-1}$ | 0.03 Gy – 2.5 Gy | Whole blood |
| Ryan et al [59] | $^{137}$Cs | 0.33 Gy min$^{-1}$ | 0.25 Gy – 5 Gy | Whole blood |
| Torudd et al. [122] | $^{137}$Cs | 10.6 Gy min$^{-1}$ | 1 Gy – 15 Gy | Whole blood |
| Liegler et al. [123] | $^{137}$Cs | 3.5 Gy | 2.5 Gy – 45 Gy | Isolated lymphocytes at concentration of $10^7$ |
| Boreham et al. [121] | $^{60}$Co | 1.2 Gy min$^{-1}$ | 0.05 Gy – 1 Gy | Isolated lymphocytes at a concentration of $4.0 \times 10^5$ |

It is possible that the apoptosis induction value differences lie in choice of assay, culture conditions, and data analysis. The Annexin V-FITC/7AAD assay described in this thesis examined both apoptosis and necrosis in tandem. Late apoptotic cells that begin to break apart will allow 7AAD entry and thus express a necrotic signal where both the Annexin V-FITC probe and 7AAD dye is visible. As such, this population of cells was classified as necrotic as opposed to apoptotic. It is likely that the same phenomenon occurred in the Leigler *et al*. [123] study where two dyes were used in tandem to differentiate between apoptotic and necrotic cells. For this reason, it is unsurprising that the in-house apoptosis data is most similar to the 20% apoptosis noted by Leigler *et al*. [123]

### 3.4.2. Necrosis Following $^{60}$Co Gamma Exposure

(a) (b)

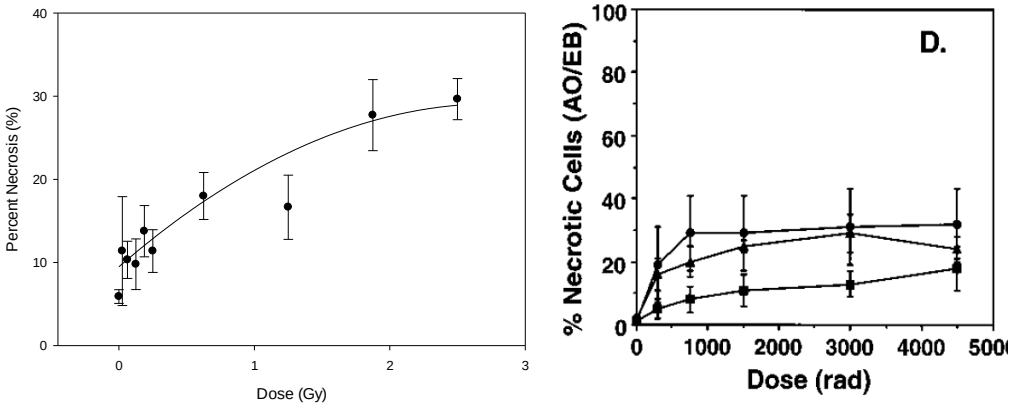


**Figure 52. Necrosis induction following gamma radiation exposure. Graph (a) represents the data presented in this thesis following $^{60}$Co exposure. Graph (b) was taken from Liegler et al. [123], with the triangles representing the necrotic response in lymphocytes at 48-hours post-$^{137}$Cs exposure.**

Only one published study has examined the effect of gamma radiation exposure on necrosis induction in human lymphocytes. Leigler e*t al.* [123] found that a dose of 2.5 Gy gamma induced approximately 18% necrosis when cells were stained with acridine orange and ethidium bromide and analysed by flow cytometry. This is slightly different than the results noted in this thesis, where approximately 30% necrosis was found following a 2.5 Gy $^{60}$Co gamma irradiation. As with the apoptosis dose response curves, the shape of the necrosis dose response curves described by Leigler *et al.* [123] and the necrosis dose response curve generated as part of the current study are similar and both show a

rapid increase in necrosis induction at lower doses - followed by a slowing of the dose response at doses above 2 Gy. It is possible that the slight differences in necrosis are a result of inter-laboratory variations including post-irradiation cell culture handling.

### 3.4.3. Comparison of Apoptosis and Necrosis Induction Following $^{60}$Co Exposure

As described in Figure 43 and Table 24, there is no significant difference between the induction rate of apoptosis or necrosis at doses up to 0.25 Gy. However, at 0.63 Gy, 1.9 Gy and 2.5 Gy, necrosis is induced at significantly higher rates than apoptosis. Only Leigler *et al.* [123] examined both apoptosis and necrosis in lymphocytes following gamma exposure and found similar levels of apoptosis and necrosis at 2.5 Gy.

### 3.4.4. Apoptosis and Necrosis Following Thermal Neutron Exposure

A dose-response was not observed for either apoptosis or necrosis following thermal neutron exposures between 0.18 mGy and 18.9 mGy (0.45 mSv to 47.2 mSv, $w_R$ = 2.5). This is the first study to examine low-dose neutron-induced cell death.

To date, fast neutron studies cell death studies have focused on significantly higher doses of radiation. In these studies, the dose at which an apoptotic response was first detected was significantly higher than any of the doses in this thesis. For example, Ryan *et al*. [59] began to see an increase of apoptosis at

approximately 0.25 Gy (4.1 Sv) following 280 keV neutron exposure and Vral *et al*. [62] first noted an increase in apoptosis between 0.25 Gy (2.9 Sv) and 0.50 Gy (5.8 Sv) following 5.5 MeV fast neutron exposure. Similarly, Cornelissen *et al.* [125] observed an apoptotic dose response in lymphocytes following 5.5 MeV neutron exposure at 5 Gy (57 Sv). Interestingly, the same study failed to find any elevated necrotic response at doses up to 20 Gy.

### 3.4.5. Cell Death Kinetics Following Thermal Neutron Exposure

In an attempt to determine whether the thermal neutron response peaked at a time point other than 48 hours, a kinetics experiment was performed. However, it was found that thermal neutrons did not induce either an apoptotic or necrotic response that was discernible above background at any of the sampling points. The 48 hour post-irradiation analysis time-point was initially chosen because 1) chromosome aberrations are traditionally assessed 48 hours post-stimulation [29]; 2) current literature indicates cell death analysis at 48 hours post-irradiation is an acceptable time-point to examine lymphocyte apoptosis following both fast neutron and heavy-ion (high-LET) radiation exposures [59-61, 124]; and 3) at sampling points beyond 48 hours, un-irradiated cells undergo apoptotic cell death as a result of the culture conditions [124].

In contrast to the low-dose thermal neutron results, following $^{60}$Co gamma exposure, both apoptosis and necrosis were found to peak at 72 hours (Figure 38). This agrees with published results [121, 124, 126] and is an indicator that the assay is working correctly. Neither the apoptosis nor necrosis signals were

discernible above background at the 24 hour sampling point (Figure 38), and at the 96 hour time-point, both the apoptosis and necrosis signals were diminished, compared to the 48-72 hour period signals. It is likely that by 96 hours, a large fraction of cells had already broken apart and were no longer exhibiting the cell death signals.

### 3.4.6. Control Samples

The background level of both apoptosis and necrosis did not significantly differ in any of the control samples examined, with the exception of the level of necrosis induction between the $^{60}$Co gamma control and the NRU environmental control sample. As such, it is unlikely that extraneous factors related to radiation field exposure and sample handling significantly increased or decreased the likelihood of cell death.

### 3.4.7. Individual Variation

Blood from four donors, ranging in age from 25-65, was used throughout the duration of this project. At the time of sampling, one donor was between the age of 26 and 30, two donors were between the ages of 31 and 35, and one donor was older than 60. Previous studies have demonstrated that peripheral blood mononuclear cells (PBMC) of younger males exhibit higher levels of apoptosis than PBMC's of older males following a 5 Gy $^{137}$Cs irradiation and a subsequent 24-hour incubation [127]. However, in the present work, no significant age-related effects were noted for either apoptotic or necrotic induction following

either $^{60}$Co gamma or thermal neutron exposure. It should be noted, there were a number of differing parameters between the work published in this thesis and the aforementioned study which may have affected the perceived age-related differences, including health status, radiation type/energy, dose, dose rate, incubation time, and cell population.

### 3.4.8. Possible Sources of Error

#### 3.4.8.1. Nonspecific Staining

Nonspecific staining refers to the staining of an unintended target, possibly skewing the resulting data. While the 7AAD stain has low rates of nonspecific staining [128], the Annexin V antibody has been known to nonspecifically bind to unintended ligands under certain conditions. To ensure conditions were consistent, an Annexin V-FITC/7AAD kit (Beckman Coulter) was used for this work, and particular attention was paid to cell culture and staining conditions to minimize the effect of nonspecific staining. Furthermore, the un-irradiated controls showed levels of apoptosis that are consistent with published data. For example, Ryan *et al.* [59] noted a background rate of approximately 10% apoptosis in peripheral blood lymphocytes, which is similar to the background level of apoptosis published in this thesis. Taking this into consideration, it is unlikely that non-specific staining by Annexin V-FITC, affected the experimental outcome of the current work.

#### 3.4.8.2. Primary and Secondary Necrosis

Secondary necrosis is a result of late-stage apoptotic cell death *in vitro* – this process is not normally observed *in vivo* where phagocytic cells take up apoptotic cells prior to self-degradation (which results in plasma membrane breakdown, and provides a mechanism for 7AAD entry) [112]. As such, the necrotic population likely includes a significant portion of late apoptotic/secondary necrotic cells that enhance the necrotic cell count.

### 3.4.9. Other Notes

#### 3.4.9.1. CD45 Marker

The CD45 leukocyte marker was added to all cell death cultures for the purpose of confirming that cells were being analyzed as opposed to debris. However, during data analysis it was noted that debris tended to express CD45 and gating on the presence of CD45 resulted in significantly lower numbers of 7AAD+ cells available for analysis. For this reason, while CD45 was initially added for the purpose of gating leukocytes, it was not utilized for population confirmation during data analysis.

### 3.4.10. Future Work

Only apoptotic and necrotic cell death were examined in this study. Alternative cell death modalities, including mitotic catastrophe and autophagocytosis, or indeed senescence, were not examined. It is possible that thermal neutrons

predominately cause cell death via an alternative pathway. In tumor cells, mitotic catastrophe has been identified as an important cell death pathway following radiation exposure [129] however, the un-stimulated lymphocytes used in this study were not able to undergo mitotic catastrophe as they exist predominantly in resting $G_0$ phase.

### 3.4.11. Summary

High doses of gamma radiation elicited cell death responses in-line with published data. However, very low doses of thermal neutron radiation did not elicit an apoptotic or a necrotic response.

For the gamma-irradiated samples, the background rate of apoptosis was found to be approximately 6% for the Annexin V-FITC/7AAD assay, whereas the background rate of necrosis was slightly higher at nearly 10%. In addition, no specific age-related cell death responses were noted across the four donors that participated in the study.

As a result of the neutron/gamma dosing mis-match created by a last-minute fluence and dose rate recalculation, it is not possible to conclude whether apoptosis and/or necrosis, as detected by the Annexin V-FITC/7AAD imaging flow cytometry assay, is a viable marker of radiation quality. Additional thermal neutron irradiations at a higher fluence rate are necessary to draw any concrete biomarker conclusions. However, the absence of elevated levels of markers at the similar highest neutron doses and lowest gamma doses employed suggests that an

RBE of 20+, such as that found using DCA, is unlikely to be present. This needs to be confirmed using higher neutron doses.

# 4. CHAPTER 4 – DISCUSSION AND CONCLUSIONS

## 4.1. Summary of Thesis Findings

This thesis examined chromosome aberrations following fast and thermal neutron exposures and apoptosis and necrosis following thermal neutron and $^{60}$Co gamma exposures. The main findings are as follows:

(1) Lymphocytes exposed to low doses of thermal neutron radiation between 1.2 mGy and 13.4 mGy demonstrated a linear dose-dependent increase in dicentric chromosome induction.

(2) Lymphocytes exposed to low doses between 10 mGy and 108 mGy of $^{252}$Cf radiation demonstrated a linear dose-dependent increase in dicentric chromosome induction.

(3) The calculated $RBE_M$ for dicentric chromosome induction in lymphocytes following low-dose thermal neutron exposure was 26.1 ± 7.0 (±SE).

(4) The calculated $RBE_M$ for dicentric chromosome induction in lymphocytes following low-dose $^{252}$Cf radiation exposure was 20 ± 3.0 (± SE).

(5) No significant chromosome aberration clustering was noted following thermal and fast neutron exposure.

(6) Thermal neutron radiation did not induce significant apoptosis or necrosis in lymphocytes at low doses between 0.2 mGy and 18.9 mGy.

(7) Lymphocytes exposed to $^{60}$Co gamma radiation demonstrated a quadratic dose-dependent increase for both apoptosis and necrosis.

(8) No donor age-related differences were noted for either apoptosis or necrosis induction following $^{60}$Co exposure.

This is the first time that low doses of thermal neutron radiation, ranging between 1.2 mGy to 13.4 mGy, have been shown to induce dicentric chromosomes. Similarly, this is the first time that a dicentric chromosome dose response has been demonstrated following low doses of $^{252}$Cf radiation (10 mGy – 108 mGy). Both the low-dose thermal neutron and $^{252}$Cf dicentric induction experiments demonstrated RBE values in-line with those produced by higher radiation doses. It was also found that aberration clustering is nearly absent at low doses of thermal neutron and $^{252}$Cf radiation, as indicated by the *u* value and the resulting lack of overdispersion.

As noted in Section 2.3.2, the highest thermal neutron dose of 13.4 mGy resulted in 0.029 aberrations per cell, meaning that a dicentric or ring chromosome was found in approximately 2.9% of all cells examined. As lymphocytes containing dicentric chromosomes are preferentially eliminated *via* apoptosis [58], it is likely

that the apoptotic response was masked by the background level of apoptosis (~6%). For this reason, it is unsurprising that low doses of thermal neutrons did not induce a cell death response.

## 4.2. Assumptions and Constraints

### 4.2.1. Neutron Sources

At the beginning if this research project, it was expected that $^{252}$Cf fast neutrons would be used as a second radiation source for both the chromosome aberration and cell death studies. Unfortunately, due to source availability, low activity, and the short half-life of $^{252}$Cf, it was difficult to conduct a multi-year study that would examine the effects of fast neutrons. As such, both the $^{252}$Cf source and the thermal neutron beam were used for the chromosome aberration work (Chapter 2), however only the thermal neutron beam was used for the cell death study (Chapter 3). The thermal neutron beam has a number of advantages over the $^{252}$Cf source as it does not decay and has a higher fluence rate.

### 4.2.2. Modelling Discrepancies

Based on the recommendations of ICRP 23, it was assumed that the nitrogen content of the blood was 2.9% [7]. This value was incorporated into MCNP 5 to obtain the dose conversion coefficient of 0.231pGy cm$^2$. However, more recent ICRP guidelines indicate that the nitrogen content of blood may be closer to 3.3% [130]. Additionally, the sodium citrate anticoagulant comprised approximately

10% of the final blood volume and therefore, the nitrogen concentration in the irradiated blood samples would have been slightly less than the modelled value due to blood dilution by the anticoagulant. This small reduction in nitrogen concentration would have slightly reduced the doses delivered and this may have had an impact on the level of cell death seen. Lastly, blood was modelled as a homogenous mixture in MCNP 5 according to the guidelines given in ICRP 23, however approximately half of the blood nitrogen is located inside leukocytes, with the remaining portion found mostly in erythrocytes and a small portion in blood plasma [7]. As the range of the proton from the $^{14}N(n,p)^{14}C$ reaction is approximately 11 μm [7], it is highly unlikely that $^{14}N(n,p)^{14}C$ reactions occurring in erythrocytes would be unable to cause damage in lymphocytes. It would be beneficial to experimentally verify the blood nitrogen, both with and without the erythrocytes to better refine the fluence to kerma conversion coefficient, and thus the resulting doses.

### 4.2.3. Errors on Doses

#### 4.2.3.1. $^{60}$Co Gamma Dose

Two different GammaCell irradiators were used to complete the gamma irradiations. The dose error includes: (1) measurement error of the Keithly Therapy Dosimeter used to characterize the radiation environment, (2) error on the GammaCell timer, (3) errors resulting from inhomogenous radiation

environments (due to scatter and decay of the volume source), and (4) potential error stemming from variations in sample positioning during irradiations.

#### 4.2.3.2. $^{252}$Cf Fast Neutron Dose

Likewise, the error on the $^{252}$Cf doses includes: (1) the error of the REM500 detector used to measure the doses during irradiation as well as (2) dose inconsistencies due to fast neutron scatter and (3) possible slight changes in position of blood tubes during sample removal and/or daily variations in apparatus set-up. Furthermore, the $^{252}$Cf dosimetry was performed using the REM500 which only detects neutrons. Gamma rays account for approximately 33% of the radiation released by $^{252}$Cf, so it is likely the dose was underestimated.

#### 4.2.3.3. Thermal Neutron Dose

The error on the calculation of the thermal neutron doses would be related to (1) the errors on the instruments previously used to quantify fluence rate, and (2) reactor power at the time of measurement. Additional errors can be introduced as a result of (3) inadvertent apparatus set-up differences, (4) neutron scatter, and (5) timer error. The CNBC thermal neutron beam lines are normally used for neutron scattering experiments, and the work outlined in this thesis is the first set of experiments where the CNBC spectrometers have been used for radiobiology purposes. As such, the error on the doses is not currently available.

The CNBC thermal neutron beam is contaminated with an unknown amount of low-LET radiation, however experimental controls placed inside the gamma field, but outside the thermal neutron beam, showed no increase in chromosome aberrations or cell death compared to background. This is in agreement with the findings of Schmid *et al*. who had high levels of low-LET radiation contamination (24% of the total dose), but did not see an increase in chromosome aberrations [28]. Thus, any biological effects stemming from the current thermal neutron irradiation exposures can be confidently attributed to the thermal neutron capture reactions, and not the result of the unknown gamma field.

### 4.2.4. Influence of Anticoagulant

Most of the literature detailing fast and thermal neutron blood irradiations describe using heparin as an anticoagulant, or fail to disclose the use of any anticoagulant (Table 5) despite significantly long whole blood irradiation times which would necessitate an anti-clotting agent. Common anticoagulants, such as sodium and lithium heparin, contain nitrogen and have the potential to affect thermal neutron dose via the $^{14}N(n,p)^{14}C$ reaction. Furthermore, following fast neutron exposure, lithium may undergo an $(n,\alpha)$ reaction, also influencing sample dosing. It is not possible to easily account for the additional nitrogen or lithium molecules added to the system, as heparin is qualified by the measurement of activity, not a measurement of how many heparin molecules are in solution (ie. a large amount of low grade heparin, or a small amount of high grade heparin

would produce the same anticoagulant effect) [131]. To avoid this potential complication, sodium citrate was used as an anticoagulant for all the thermal neutron exposures, and sodium heparin was used for all the fast neutron exposures.

### 4.2.5. Lymphocyte Stimulation

To obtain metaphase chromosome spreads, lymphocytes were stimulated with PHA to encourage cell cycle entry. However, for lymphocyte-based cell death assays, it is common practice to not stimulate cells, even when making comparisons to PHA-stimulated DCA data [59, 61, 62, 64]. It is possible that PHA stimulation prior to cell death analysis could have yielded different results.

### 4.2.6. Effect of Temperature Variations on Cell Death Response

Previous studies have shown little effect of temperature on dicentric induction at temperatures between 20°C and 37°C [76, 132]. As such, it is not expected that irradiating and transporting the cells at room temperature would significantly alter the cellular response.

## 4.3. Future Work

### 4.3.1. Dicentric Chromosome Assay

The CNL biodosimetry group is currently planning to create a proper calibration curve for thermal neutron exposures. This will involve multiple scorers and at

least two separate blood donors. In addition, as mentioned in Chapter 2, it is also important that the CNL biodosimetry group consider the utility of creating a reference $^{60}$Co calibration curve, as it is currently the published standard.

### 4.3.2. Alternate Cell Death Pathway

It is possible that lymphocytes preferentially undergo cell death via a pathway not considered in this thesis. As described above, the cells analyzed for apoptosis and necrosis were not stimulated with PHA. As such, it would be advantageous to investigate whether PHA stimulation resulted in higher levels of mitotic catastrophe, a special type of apoptosis that occurs during mitosis [133].

### 4.3.3. Understanding Cell Hits

To better understand the results detailed in this thesis, information about the proportion of cells damaged by the $^{14}N(n,p)^{14}C$ reaction would be valuable. This can be achieved through the γH2AX assay where cells with a large number of DNA repair foci would be indicative of high-LET proton exposure.

### 4.3.4. Thermal Neutron Beam Modifications

The CNBC is currently testing beam-line modifications to achieve a higher fluence rate, and thereby a higher dose rate. This will allow for future thermal neutron irradiations at higher doses.

## REFERENCES


[1] ICRP, *The 2007 Recommendations of the International Commission on Radiological Protection. ICRP Publication 103* vol. 37 (2-4), 2007.

[2] E. B. Podgorsak, *Radiation Physics for Medical Physicists*. Berlin: Springer, 2010.

[3] D. T. Goodhead, "The initial physical damage produced by ionizing radiations," *Int J Radiat Biol,* vol. 56, pp. 623-34, Nov 1989.

[4] D. T. Goodhead, "Mechanisms for the biological effectiveness of high-LET radiations," *J Radiat Res,* vol. 40 Suppl, pp. 1-13, Dec 1999.

[5] E. J. Hall and A. J. Giaccia, *Radiobiology for the Radiologist*, 6th Edition ed. Philadelphia Lippincott Williams & Wilkins, 2006.

[6] R. W. Howell, V. R. Narra, K. S. Sastry, and D. V. Rao, "On the equivalent dose for Auger electron emitters," *Radiat Res,* vol. 134, pp. 71-8, Apr 1993.

[7] ICRP, *Report on the Task Group on Reference Man. ICRP Publication 23* vol. 23, 1975.

[8] Z. Yamani, Z. Tun, and D. H. Ryan, "Neutron scattering study of the classical antiferromagnet MnF2: a perfect hands-on neutron scattering teaching course," *Canadian Journal of Physics,* vol. 88, pp. 771-797, Oct 2010.

[9] M. W. Swanepoel, "The role of the 14N(n,p)14C reaction in neutron irradiation of soft tissues," *Radiation Measurements,* vol. 45, pp. 1458-1461, 2010.

[10] ICRU-63, "Nuclear Data for Neutron and Proton Radiotherapy and for Radiation Proetction. Technical Report 63," Bethesda, USA2000.

[11] R. C. Martin, J. B. Knauer, and P. A. Balo, "Production, Distribution, and Applications of Californium-252 Neutron Sources," presented at the IRRMA 4th Topical Meeting on Industrial Radiation and Radioisotope Measurement Applications, Raleigh, North Carolina, 1999.

[12] K. Tanaka, N. Gajendiran, and N. Kamada, "Relative biological effectiveness (RBE) and dose rate dependent ratio of translocation to dicentric chromosome yield in 252Cf neutrons," *Indian Journal of Science and Technology,* vol. 2, pp. 1-11, 2009.

[13] B. E. Watt, "Energy Spectrum of Neutrons from Thermal Fission of U235," *Phys. Rev.,* vol. 87, pp. 1037-1041, 1952.

[14] E. M. Manders, A. E. Visser, A. Koppen, W. C. de Leeuw, R. van Liere, G. J. Brakenhoff*, et al.*, "Four-dimensional imaging of chromatin dynamics during the assembly of the interphase nucleus," *Chromosome Res,* vol. 11, pp. 537-47, 2003.

[15] B. Alberts, A. Johnson, J. Lewis, M. Raff, K. Roberts, and P. Walter, *Molecular Biology of the Cell*, 4th ed. New York: Garland, 2002.

[16] A. Mozumder and J. L. Magee, "Model of tracks of ionizing radiations for radical reaction mechanisms," *Radiat Res,* vol. 28, pp. 203-14, Jun 1966.

[17] J. F. Ward, "DNA damage produced by ionizing radiation in mammalian cells: identities, mechanisms of formation, and reparability," *Prog Nucleic Acid Res Mol Biol,* vol. 35, pp. 95-125, 1988.

[18] M. M. Vilenchik and A. G. Knudson, "Endogenous DNA double-strand breaks: production, fidelity of repair, and induction of cancer," *Proc Natl Acad Sci U S A,* vol. 100, pp. 12871-6, Oct 28 2003.

[19] K. Rothkamm and S. Horn, "gamma-H2AX as protein biomarker for radaition exposure," *Annali dell'Istituto Superiore di Sanità,* vol. 45, pp. 265-271, 2009.

[20] K. Rothkamm and M. Lobrich, "Mis-repair of radiation-induced DNA double-strand breaks and its relevance for tumorigenesis and cancer treatment (Review)," *International Journal of Oncology,* vol. 21, pp. 433-440, 2002.

[21] D. C. van Gent, J. H. Hoeijmakers, and R. Kanaar, "Chromosomal stability and the DNA double-stranded break connection," *Nat Rev Genet,* vol. 2, pp. 196-206, Mar 2001.

[22] A. Gandarillas, "Epidermal differentiation, apoptosis, and senescence: common pathways?," *Exp Gerontol,* vol. 35, pp. 53-62, Feb 2000.

[23] K. Rothkamm, I. Kruger, L. H. Thompson, and M. Lobrich, "Pathways of DNA double-strand break repair during the mammalian cell cycle," *Mol Cell Biol,* vol. 23, pp. 5706-15, Aug 2003.

[24] A. Pastink, J. C. Eeken, and P. H. Lohman, "Genomic integrity and the repair of double-strand DNA breaks," *Mutat Res,* vol. 480-481, pp. 37-50, Sep 1 2001.

[25] P. Pfeiffer, W. Goedecke, S. Kuhfittig-Kulle, and G. Obe, "Pathways of DNA double-strand break repair and their impact on the prevention and formation of chromosomal aberrations," *Cytogenet Genome Res,* vol. 104, pp. 7-13, 2004.

[26] M. N. Cornforth, "Analyzing radiation-induced complex chromosome rearrangements by combinatorial painting," *Radiation Research,* vol. 155, pp. 643-659, May 2001.

[27] J. R. Savage and P. J. Simpson, "FISH "painting" patterns resulting from complex exchanges," *Mutat Res,* vol. 312, pp. 51-60, Feb 1994.

[28] E. Schmid, F. M. Wagner, L. Canella, H. Romm, and T. E. Schmid, "RBE of thermal neutrons for induction of chromosome aberrations in human lymphocytes," *Radiat Environ Biophys,* vol. 52, pp. 113-21, Mar 2013.

[29] IAEA, *Cytogenetic Dosimetry: Applications in Preparedness for and Response to Radiation Emergencies*. Vienna: IAEA, 2011.

[30] L. Manuelidis, "Individual interphase chromosome domains revealed by in situ hybridization," *Hum Genet,* vol. 71, pp. 288-93, 1985.

[31] T. Cremer and C. Cremer, "Chromosome territories, nuclear architecture and gene regulation in mammalian cells," *Nat Rev Genet,* vol. 2, pp. 292-301, Apr 2001.

[32] J. J. Boei, J. Fomina, F. Darroudi, N. J. Nagelkerke, and L. H. Mullenders, "Interphase chromosome positioning affects the spectrum of radiation-induced chromosomal aberrations," *Radiat Res,* vol. 166, pp. 319-26, Aug 2006.

[33] M. Durante, D. Pignalosa, J. A. Jansen, X. F. Walboomers, and S. Ritter, "Influence of nuclear geometry on the formation of genetic rearrangements in human cells," *Radiat Res,* vol. 174, pp. 20-6, Jul 2010.

[34] R. K. Sachs, A. M. Chen, and D. J. Brenner, "Review: proximity effects in the production of chromosome aberrations by ionizing radiation," *Int J Radiat Biol,* vol. 71, pp. 1-19, Jan 1997.

[35] J. J. Boei, S. Vermeulen, L. H. Mullenders, and A. T. Natarajan, "Impact of radiation quality on the spectrum of induced chromosome exchange aberrations," *Int J Radiat Biol,* vol. 77, pp. 847-57, Aug 2001.

[36] F. Darroudi, V. Bezrookove, J. Fomina, W. E. Mesker, J. C. A. G. Wiegant, A. K. Raap*, et al.*, "Insights into the sites of X ray and neutron induced chromosomal aberrations in human lymphocytes using COBRA-MFISH," *Radiation Protection Dosimetry,* vol. 99, pp. 189-192, 2002.

[37] I. Testard, B. Dutrillaux, and L. Sabatier, "Chromosomal aberrations induced in human lymphocytes by high-LET irradiation," *Int J Radiat Biol,* vol. 72, pp. 423-33, Oct 1997.

[38] B. D. Loucas and M. N. Cornforth, "Complex chromosome exchanges induced by gamma rays in human lymphocytes: an mFISH study," *Radiat Res,* vol. 155, pp. 660-71, May 2001.

[39] D. L. Spector, "Macromolecular domains within the cell nucleus," *Annu Rev Cell Biol,* vol. 9, pp. 265-315, 1993.

[40] B. K. Singleton, C. S. Griffin, and J. Thacker, "Clustered DNA damage leads to complex genetic changes in irradiated human cells," *Cancer Res,* vol. 62, pp. 6263-9, Nov 1 2002.

[41] H. Nikjoo, S. Uehara, I. G. Khvostunov, F. A. Cucinotta, W. E. Wilson, and D. T. Goodhead, "Monte Carlo track structure for radiation biology and space applications," presented at the 1st International Workshop on Space Radiation Research and 11th Annual NASA Space Radiation Health Investigators' Workshop, Arona, Italy, 2000.

[42] D. T. Goodhead, "Initial events in the cellular effects of ionizing radiations: clustered damage in DNA," *Int J Radiat Biol,* vol. 65, pp. 7-17, Jan 1994.

[43] A. Chatterjee and R. Holley, "Energy deposition mechanisms and biochemical aspects of DNA strand breaks by ionizing radiation," *International Journal of Quantum Chemistry,* vol. 39, pp. 709-727, 1991.

[44] M. Hada, F. A. Cucinotta, S. R. Gonda, and H. Wu, "mBAND analysis of chromosomal aberrations in human epithelial cells exposed to low- and high-LET radiation," *Radiat Res,* vol. 168, pp. 98-105, Jul 2007.

[45] R. M. Anderson, S. J. Marsden, S. J. Paice, A. E. Bristow, M. A. Kadhim, C. S. Griffin*, et al.*, "Transmissible and nontransmissible complex chromosome aberrations characterized by three-color and mFISH define a biomarker of exposure to high-LET alpha particles," *Radiat Res,* vol. 159, pp. 40-8, Jan 2003.

[46] R. M. Anderson, D. L. Stevens, and D. T. Goodhead, "M-FISH analysis shows that complex chromosome aberrations induced by alpha-particle tracks are cumulative products of localized rearrangements," *Proceedings of the National Academy of Sciences of the United States of America,* vol. 99, pp. 12167-12172, Sep 17 2002.

[47] M. Durante, K. George, H. Wu, and F. A. Cucinotta, "Karyotypes of human lymphocytes exposed to high-energy iron ions," *Radiat Res,* vol. 158, pp. 581-90, Nov 2002.

[48] S. V. Costes, I. Chiolo, J. M. Pluth, M. H. Barcellos-Hoff, and B. Jakob, "Spatiotemporal characterization of ionizing radiation induced DNA damage foci

and their relation to chromatin organization," *Mutation Research-Reviews in Mutation Research,* vol. 704, pp. 78-87, Apr-Jun 2010.

[49] A. Asaithamby, B. Hu, and D. J. Chen, "Unrepaired clustered DNA lesions induce chromosome breakage in human cells," *Proc Natl Acad Sci U S A,* vol. 108, pp. 8293-8, May 17 2011.

[50] B. P. Kysela, J. E. Arrand, and B. D. Michael, "Relative Contributions of Levels of Initial Damage and Repair of Double-strand Breaks to the Ionizing Radiation-sensitive Phenotype of the Chinese Hamster Cell Mutant, XR-V15B. Part II. Neutrons," *International Journal of Radiation Biology,* vol. 64, pp. 531-538, 1993.

[51] D. Eriksson and T. Stigbrand, "Radiation-induced cell death mechanisms," *Tumor Biol,* vol. 31, pp. 363-372, 2010.

[52] E. Cohen–Jonathan, E. J. Bernhard, and W. G. McKenna, "How does radiation kill cells?," *Current Opinion in Chemical Biology,* vol. 3, pp. 77-83, 1999.

[53] L. Galluzzi, M. C. Maiuri, I. Vitale, H. Zischka, M. Castedo, L. Zitvogel*, et al.*, "Cell death modalities: classification and pathophysiological implications," *Cell Death Differ,* vol. 14, pp. 1237-43, Jul 2007.

[54] S. Goldstein, "Replicative senescence: the human fibroblast comes of age," *Science,* vol. 249, pp. 1129-33, Sep 7 1990.

[55] N. Shinomiya, "New concepts in radiation-induced apoptosis: 'premitotic apoptosis' and 'postmitotic apoptosis'," *Journal of Cellular and Molecular Medicine,* vol. 5, pp. 240-253, Jul-Sep 2001.

[56] M. Verheij and H. Bartelink, "Radiation-induced apoptosis," *Cell Tissue Res,* vol. 301, pp. 133-42, Jul 2000.

[57] C. M. Payne, C. G. Bjore, Jr., and D. A. Schultz, "Change in the frequency of apoptosis after low- and high-dose X-irradiation of human lymphocytes," *J Leukoc Biol,* vol. 52, pp. 433-40, Oct 1992.

[58] P. Belloni, R. Meschini, D. Lewinska, and F. Palitti, "Apoptosis preferentially eliminates irradiated g0 human lymphocytes bearing dicentric chromosomes," *Radiat Res,* vol. 169, pp. 181-7, Feb 2008.

[59] L. A. Ryan, R. C. Wilkins, N. M. McFarlane, M. M. Sung, J. P. McNamee, and D. R. Boreham, "Relative biological effectiveness of 280 keV neutrons for apoptosis in human lymphocytes," *Health Phys,* vol. 91, pp. 68-75, Jul 2006.

[60] D. Coelho, B. Fischer, V. Holl, G. M. Jung, P. Dufour, J. P. Bergerat*, et al.*, "Involvement of TP53 in apoptosis induced in human lymphoblastoid cells by fast neutrons," *Radiat Res,* vol. 157, pp. 446-52, Apr 2002.

[61] A. E. Meijer, U. S. Kronqvist, R. Lewensohn, and M. Harms-Ringdahl, "RBE for the induction of apoptosis in human peripheral lymphocytes exposed in vitro to high-LET radiation generated by accelerated nitrogen ions," *Int J Radiat Biol,* vol. 73, pp. 169-77, Feb 1998.

[62] A. Vral, M. Cornelissen, H. Thierens, H. Louagie, J. Philippe, K. Strijckmans*, et al.*, "Apoptosis induced by fast neutrons versus 60Co gamma-rays in human peripheral blood lymphocytes," *Int J Radiat Biol,* vol. 73, pp. 289-95, Mar 1998.

[63] H. M. Warenius and J. D. Down, "RBE of fast neutrons for apoptosis in mouse thymocytes," *Int J Radiat Biol,* vol. 68, pp. 625-9, Dec 1995.

[64] T. E. Schmid, L. Canella, P. Kudejova, F. M. Wagner, A. Rohrmoser, and E. Schmid, "The effectiveness of the high-LET radiations from the boron neutron capture [(10)B(n,alpha) (7)Li] reaction determined for induction of chromosome aberrations and apoptosis in lymphocytes of human blood samples," *Radiat Environ Biophys,* vol. 54, pp. 91-102, Mar 2015.

[65] E. B. Golden, I. Pellicciotta, S. Demaria, M. H. Barcellos-Hoff, and S. C. Formenti, "The convergence of radiation and immunogenic cell death signaling pathways," *Front Oncol,* vol. 2, p. 88, 2012.

[66] J. I. Hitomi, D. E. Christofferson, A. Ng, J. H. Yao, A. Degterev, R. J. Xavier*, et al.*, "Identification of a Molecular Signaling Network that Regulates a Cellular Necrotic Cell Death Pathway," *Cell,* vol. 135, pp. 1311-1323, Dec 26 2008.

[67] D. Hanahan and R. A. Weinberg, "Hallmarks of Cancer: The Next Generation," *Cell,* vol. 144, pp. 646-674, Mar 4 2011.

[68] ICRP, *Relative Biological Effectiveness, Radiation Weighting and Quality Factor. ICRP Publication 92* vol. 33(4), 2003.

[69] E. Schmid, D. Schlegel, S. Guldbakke, R. P. Kapsch, and D. Regulla, "RBE of nearly monoenergetic neutrons at energies of 36 keV-14.6 MeV for induction of dicentrics in human lymphocytes," *Radiation and Environmental Biophysics,* vol. 42, pp. 87-94, Jul 2003.

[70] E. J. Hall and T. K. Hei, "Genomic instability and bystander effects induced by high-LET radiation," *Oncogene,* vol. 22, pp. 7034-42, Oct 13 2003.

[71] A. A. Edwards, "Neutron RBE values and their relationship to judgements in radiological protection," *J Radiol Prot,* vol. 19, pp. 93-105, Jun 1999.

[72] M. S. Sasaki, S. Ende, Y. Ejima, I. Saito, K. Okamura, Y. Oka*, et al.*, "Effective dose equivalent of A-bomb radiation in Hiroshima and Nagasaki as assessed by chromosomal effectiveness of spectrum energy photons and neutrons," *Radiat Environ Biophys,* vol. 45, pp. 79-91, 2006.

[73] A. V. Sevan'kaev, E. A. Zherbin, N. V. Luchnik, G. M. Obaturov, V. M. Kozlov, E. G. Tyatte*, et al.*, "Cytogenetic effects induced by neutrons in human peripheral blood lymphocytes in vitro," *Genetika,* vol. 15, pp. 1046-1060, 1979.

[74] A. V. Sevan'kaev, E. A. Zherbin, N. V. Luchnik, G. M. Obaturov, V. M. Kozlov, E. G. Tyatte*, et al.*, "Neutron-induced cytogenetic effects in lymphocytes of human peripheral blood in vitro.," *Genetika,* vol. 15, pp. 1046-1060, 1979.

[75] D. C. Lloyd, R. J. Purrott, E. J. Reeder, A. A. Edwards, and G. W. Dolphin, "Chromosome aberrations induced in human lymphocytes by radiation from 252Cf," *Int J Radiat Biol Relat Stud Phys Chem Med,* vol. 34, pp. 177-86, Aug 1978.

[76] E. Schmid, D. Regulla, S. Guldbakke, D. Schlegel, and M. Roos, "Relative biological effectiveness of 144 keV neutrons in producing dicentric chromosomes in human lymphocytes compared with 60Co gamma rays under head-to-head conditions," *Radiat Res,* vol. 157, pp. 453-60, Apr 2002.

[77] E. Schmid, D. Regulla, S. Guldbakke, D. Schlegel, and M. Bauchinger, "The effectiveness of monoenergetic neutrons at 565 keV in producing dicentric chromosomes in human lymphocytes at low doses," *Radiation Research,* vol. 154, pp. 307-312, Sep 2000.

[78] D. C. Lloyd, R. J. Purrott, G. W. Dolphin, and A. A. Edwards, "Chromosome aberrations induced in human lymphocytes by neutron irradiation," *Int J Radiat Biol Relat Stud Phys Chem Med,* vol. 29, pp. 169-82, Feb 1976.

[79] E. Schmid, H. Schraube, and M. Bauchinger, "Chromosome aberration frequencies in human lymphocytes irradiated in a phantom by a mixed beam of fission neutrons and g-rays," *Radiation Biology,* vol. 73, pp. 263-267, 1998.

[80] M. Bauchinger, L. Koester, E. Schmid, J. Dresp, and S. Streng, "Chromosome aberrations in human lymphocytes induced by fission neutrons," *Int J Radiat Biol Relat Stud Phys Chem Med,* vol. 45, pp. 449-57, May 1984.

[81] L. Fabry, A. Leonard, and A. Wambersie, "Induction of chromosome aberrations in G0 human lymphocytes by low doses of ionizing radiations of different quality," *Radiat Res,* vol. 103, pp. 122-34, Jul 1985.

[82] D. C. Lloyd, A. A. Edwards, J. S. Prosser, D. Bolton, and A. G. Sherwin, "Chromosome aberrations induced in human lymphocytes by D-T neutrons," *Radiat Res,* vol. 98, pp. 561-73, Jun 1984.

[83] M. Bauchinger, E. Schmid, G. Rimpl, and H. Kuhn, "Chromosome aberrations in human lymphocytes after irradiation with 15.0-MeV neutrons in vitro. I. Dose-response relation and RBE," *Mutat Res,* vol. 27, pp. 103-9, Jan 1975.

[84] R. Nolte, K. H. Muhlbradt, J. P. Meulders, G. Stephan, M. Haney, and E. Schmid, "RBE of quasi-monoenergetic 60 MeV neutron radiation for induction of dicentric chromosomes in human lymphocytes," *Radiat Environ Biophys,* vol. 44, pp. 201-9, Dec 2005.

[85] A. R. McLean and C. A. Michie, "In vivo estimates of division and death rates of human T lymphocytes," *Proc Natl Acad Sci U S A,* vol. 92, pp. 3707-11, Apr 25 1995.

[86] H. Romm, U. Oestreicher, and U. Kulka, "Cytogenetic damage analysed by the dicentric assay," *Ann Ist Super Sanita,* vol. 45, pp. 251-9, 2009.

[87] M. A. Bender and P. C. Gooch, "Types and rates of X-ray induced chromosome aberrations in human blood irradiated in vitro," *Proceedings of the National Academy of Sciences of the United States of America,* vol. 48, pp. 522-532, 1962.

[88] F. N. Flegal, Y. Devantier, L. Marro, and R. C. Wilkins, "Validation of QuickScan dicentric chromosome analysis for high throughput radiation biological dosimetry," *Health Phys,* vol. 102, pp. 143-53, Feb 2012.

[89] D. J. Brenner and R. K. Sachs, "Chromosomal "fingerprints" of prior exposure to densely ionizing radiation," *Radiat Res,* vol. 140, pp. 134-42, Oct 1994.

[90] R. M. Anderson, S. J. Marsden, E. G. Wright, M. A. Kadhim, D. T. Goodhead, and C. S. Griffin, "Complex chromosome aberrations in peripheral blood lymphocytes as a potential biomarker of exposure to high-LET alpha-particles," *Int J Radiat Biol,* vol. 76, pp. 31-42, Jan 2000.

[91] M. Bauchinger and E. Schmid, "Is there reliable experimental evidence for a chromosomal "fingerprint" of exposure to densely ionizing radiation?," *Radiat Res,* vol. 147, pp. 506-510, 1997.

[92] N. Nakamura, J. D. Tucker, M. Bauchinger, L. G. Littlefield, D. C. Lloyd, R. J. Preston*, et al.*, "F Values as Cytogenetic Fingerprints of Prior Exposure to

Different Radiation Qualities: Prediction, Reality and Future " *Radiat Res,* vol. 150, pp. 492-494, 1998.

[93] R. K. Sachs, D. J. Brenner, A. M. Chen, P. Hahnfeldt, and L. R. Hlatky, "Intra-arm and inter-arm chromosome intrachanges: Tools for probing the geometry and dynamics of chromatin," *Radiat Res,* vol. 148, pp. 330-340, 1997.

[94] J. N. Lucas, "Cytogenetic signature for ionizing radiation," *Int J Radiat Biol,* vol. 73, pp. 15-20, Jan 1998.

[95] W. Deng, D. P. Morrison, K. L. Gale, and J. N. Lucas, "A comparative study on potential cytogenetic fingerprints for radiation LET in human lymphocytes," *International Journal of Radiation Biology,* vol. 76, pp. 1589-1598, Dec 2000.

[96] M. P. Hande, T. V. Azizova, L. E. Burak, V. F. Khokhryakov, C. R. Geard, and D. J. Brenner, "Complex chromosome aberrations persist in individuals many years after occupational exposure to densely ionizing radiation: an mFISH study," *Genes Chromosomes Cancer,* vol. 44, pp. 1-9, Sep 2005.

[97] E. J. Tawn, C. A. Whitehouse, D. Holdsworth, K. De Ruyck, K. Vandenbulcke, and H. Thierens, "mBAND analysis of chromosome aberrations in lymphocytes exposed in vitro to alpha-particles and gamma-rays," *Int J Radiat Biol,* vol. 84, pp. 447-53, Jun 2008.

[98] J. Atanackovic, A. Yonkeu, J. Dubeau, S. H. Witharana, and N. Priest, "Characterization of neutron fields from bare and heavy water moderated (252)Cf spontaneous fission source using Bonner Sphere Spectrometer," *Appl Radiat Isot,* vol. 99, pp. 122-32, May 2015.

[99] F. Ali, "Design and Characterization of Next-Generation Tissue Equivalent Proportional Counters for use in Low Energy Neutron Fields," Doctor of Philosophy in Nuclear Engineering, Faculty of Energy Systems and Nuclear Science, University of Ontario Institute of Technology, Oshawa, ON, 2014.

[100] MCNP, "MCNP - A General Monte Carlo N-Particle Transport Code, Version 5," Los Alamos National Laboratory, Los Alamos2008.

[101] W. G. Cross and H. Ing, "Conversion and Quality Factors Relating Neutron Fluence and Dosimetric Quantities," *Radiation Protection Dosimetry,* vol. 10, pp. 29-42, 1985.

[102] M. Szluinska, A. A. Edwards, and D. C. Lloyd, "Statistical Methods for Biological Dosimetry," HPA Radiation Protection Division, Chilton, Didcot, Oxfordshire2005.

[103] E. A. Ainsbury and D. C. Lloyd, "Dose estimation software for radiation biodosimetry," *Health Phys,* vol. 98, pp. 290-5, Feb 2010.

[104] M. M. P. Lemos-Pinto, M. Cadena, N. Santos, T. S. Fernandes, E. Borges, and A. Amaral, "A dose-response curve for biodosimetry from a 6 MV electron linear accelerator," *Brazilian Journal of Medical and Biological Research,* vol. 48, pp. 908-914, Oct 2015.

[105] R. P. Virsik and D. Harder, "Statistical interpretation of the overdispersed distribution of radiation-induced dicentric chromosome aberrations at high LET," *Radiat Res,* vol. 85, pp. 13-23, Jan 1981.

[106] M. S. Sasaki, K. Kobayashi, K. Hieda, T. Yamada, Y. Ejima, H. Maezawa*, et al.*, "Induction of chromosome aberrations in human lymphocytes by

monochromatic X-rays of quantum energy between 4.8 and 14.6 keV," *Int J Radiat Biol,* vol. 56, pp. 975-88, Dec 1989.

[107] D. C. Lloyd and A. A. Edwards, *Chromosome aberrations in human lymphocytes: effect of radiation quality, dose, and dose rate.* New York: AR Liss, 1983.

[108] UNSCEAR, "Sources and Effects of Ionizing Radiation," United Nations1993.

[109] J. F. Kerr, A. H. Wyllie, and A. R. Currie, "Apoptosis: a basic biological phenomenon with wide-ranging implications in tissue kinetics," *Br J Cancer,* vol. 26, pp. 239-57, Aug 1972.

[110] A. G. Renehan, C. Booth, and C. S. Potten, "What is apoptosis, and why is it important?," *British Medical Journal,* vol. 322, pp. 1536-1538, Jun 23 2001.

[111] V. A. Fadok, D. R. Voelker, P. A. Campbell, J. J. Cohen, D. L. Bratton, and P. M. Henson, "Exposure of phosphatidylserine on the surface of apoptotic lymphocytes triggers specific recognition and removal by macrophages," *J Immunol,* vol. 148, pp. 2207-16, Apr 1 1992.

[112] K. Kurosaka, M. Takahashi, N. Watanabe, and Y. Kobayashi, "Silent cleanup of very early apoptotic cells by macrophages," *Journal of Immunology,* vol. 171, pp. 4672-4679, Nov 1 2003.

[113] E. Hallan, H. K. Blomhoff, E. B. Smeland, and J. Lomo, "Involvement of ICE (Caspase) family in gamma-radiation-induced apoptosis of normal B lymphocytes," *Scand J Immunol,* vol. 46, pp. 601-8, Dec 1997.

[114] Y. Yu and J. B. Little, "p53 is involved in but not required for ionizing radiation-induced caspase-3 activation and apoptosis in human," *Cancer Research,* vol. 58, pp. 4277-4281, 1998.

[115] S. Elmore, "Apoptosis: a review of programmed cell death," *Toxicol Pathol,* vol. 35, pp. 495-516, Jun 2007.

[116] X. Saelens, N. Festjens, L. Vande Walle, M. van Gurp, G. van Loo, and P. Vandenabeele, "Toxic proteins released from mitochondria in cell death," *Oncogene,* vol. 23, pp. 2861-74, Apr 12 2004.

[117] Z. Darzynkiewicz, G. Juan, X. Li, W. Gorczyca, T. Murakami, and F. Traganos, "Cytometry in cell necrobiology: analysis of apoptosis and accidental cell death (necrosis)," *Cytometry,* vol. 27, pp. 1-20, Jan 1 1997.

[118] M. T. Silva, "Secondary necrosis: the natural outcome of the complete apoptotic program," *FEBS Lett,* vol. 584, pp. 4491-9, Nov 19 2010.

[119] Amnis, "Ideas, Image Stream Analysis Software User's Manual," ed, 2014.

[120] D. Basiji, W. Ortyn, C. Zimmerman, R. Bauer, D. Perry, R. Esposito*, et al.*, "Image Data Exploration and Analysis Software," Amnis Corporation

[121] D. R. Boreham, K. L. Gale, S. R. Maves, J. A. Walker, and D. P. Morrison, "Radiation-induced apoptosis in human lymphocytes: potential as a biological dosimeter," *Health Phys,* vol. 71, pp. 685-91, Nov 1996.

[122] J. Torudd, M. Protopopova, R. Sarimov, J. Nygren, S. Eriksson, E. Markova*, et al.*, "Dose-response for radiation-induced apoptosis, residual 53BP1 foci and DNA-loop relaxation in human lymphocytes," *Int J Radiat Biol,* vol. 81, pp. 125-38, Feb 2005.

[123] T. J. Liegler, W. Hyun, T. S. Yen, and D. P. Stites, "Detection and quantification of live, apoptotic, and necrotic human peripheral lymphocytes by single-laser flow cytometry," *Clin Diagn Lab Immunol,* vol. 2, pp. 369-76, May 1995.

[124] R. C. Wilkins, B. C. Kutzner, M. Truong, J. Sanchez-Dardon, and J. R. N. McLean, "Analysis of radiation-induced apoptosis in human lymphocytes: Flow cytometry using Annexin V and propidium iodide versus the neutral comet assay," *Cytometry,* vol. 48, pp. 14-19, May 1 2002.

[125] M. Cornelissen, H. Thierens, and L. De Ridder, "Interphase death in human peripheral blood lymphocytes after moderate and high doses of low and high LET radiation: an electron microscopic approach," *Anticancer Res,* vol. 22, pp. 241-5, Jan-Feb 2002.

[126] K. Hertveldt, J. Philippe, H. Thierens, M. Cornelissen, A. Vral, and L. De Ridder, "Flow cytometry as a quantitative and sensitive method to evaluate low dose radiation induced apoptosis in vitro in human peripheral blood lymphocytes," *Int J Radiat Biol,* vol. 71, pp. 429-33, Apr 1997.

[127] M. A. Applebaum, A. D. Skol, E. E. Bond, M. Overholtzer, G. L. Bond, and K. Onel, "Radiation-induced apoptosis varies among individuals and is modified by sex and age," *Int J Radiat Biol,* vol. 90, pp. 903-8, Oct 2014.

[128] M. C. O'Brien and W. E. Bolton, "Comparison of cell viability probes compatible with fixation and permeabilization for combined surface and intracellular staining in flow cytometry," *Cytometry,* vol. 19, pp. 243-55, Mar 1 1995.

[129] D. Eriksson and T. Stigbrand, "Radiation-induced cell death mechanisms," *Tumour Biol,* vol. 31, pp. 363-72, Aug 2010.

[130] ICRP, *Basic Anatomical and Physiological Data for Use in Radiological Protection Reference Values. ICRP Publication 89* vol. 32 (3-4), 2002.

[131] J. Beirne, H. Truchan, and L. Rao, "Development and qualification of a size exclusion chromatography coupled with multiangle light scattering method for molecular weight determination of unfractionated heparin," *Anal Bioanal Chem,* vol. 399, pp. 717-25, Jan 2011.

[132] K. Gumrich, R. P. Virsik-Peuckert, and D. Harder, "Temperature and the formation of radiation-induced chromosome aberrations. I. The effect of irradiation temperature," *Int J Radiat Biol Relat Stud Phys Chem Med,* vol. 49, pp. 665-72, Apr 1986.

[133] M. Castedo, J. L. Perfettini, T. Roumier, A. Valent, H. Raslova, K. Yakushijin*, et al.*, "Mitotic catastrophe constitutes a special case of apoptosis whose suppression entails aneuploidy," *Oncogene,* vol. 23, pp. 4362-70, May 27 2004.

# APPENDIX A – RISK ASSESSMENT

## Table A1. Risk assessment for the DCA and the Annexin V-FITC/7AAD assay

| Activity / Step | Hazard | Risk | Maximum Severity | Avoidance / Mitigation |
|---|---|---|---|---|
| Preparation of Workpackage documentation, data analysis, scoring slides using a microscope and final report writing. | Musculoskeletal damage caused by bad posture, wrongly configured computer. | A common hazard. Probability of occurrence is high. | Medium (Back pain, repetitive strain injury) | Will use correct adjustment of chair. Will ensure correct positioning of computer. Will limit time sitting down without break to 10 minutes. |
| Repetitive laboratory work, processing of multiple samples | Repetitive strain injuries | Probability medium | Medium (carpal tunnel syndrome, blisters, muscle strains and sprains, etc) | Ergonomic adjustments in laboratory |
| Everyday workplace interactions | Stress arising from conflicting priorities, priority changes, sudden requests to respond to new issues, deadlines, concerns about availability of resources | A common hazard. Probability of occurrence is high | Medium (Physiological effects) | Organization of time and resources |
| Handling human blood. | Blood-borne disease such as Hepatitis A or B. | Probability low. | Medium (chronic liver disease) | Vaccination, where possible, to blood-borne diseases (Hepatitis A and B). Proper PPE&C when handling blood: e.g. gloves and safety glasses. |
| Processing blood samples for flow cytometery. | Blood-borne disease (see above) and chemical hazards (e.g. ethanol, p16 antibody, PBS, PHA, RPMI, FBS) | Probability low. | Low | Proper PPE&C when handling blood and chemicals: e.g. gloves, lab coat and safety glasses. Staff shall be familiar with the MSDS for chemicals that they use. |
| Travel between floors in B513. | Trip, slips and falls. See blood, chemical and slide risk above for confounding factors. | Probability low. | High (Death) | Wear appropriate footwear and use caution while walking up/down stairwells. |
| Sample irradiations (Gamma cells, NRU, etc) | Investigators exposed to radiation fields | Probability low | High (full-body irradiation) | Irradiations will be performed by experienced staff. Detection instruments will be available. |

| | | | | |
|---|---|---|---|---|
| Adverse environmental conditions (high/low buildingtemperatures) | Headaches and other illness resulting from dehydration. Heat stroke. Hypothermia. Trouble concentrating or performing work properly (more apt to make mistakes) | Probability moderate | High | Take breaks in warm/cool areas whenever possible. Drink fluids. Dress appropriately for environmental conditions |
| Handling hazardous reagents that are possibly carcinogenic, teratogenic, caustic, and poisonous | Severe health problems including cancer, birth defects | Probability low | High | Handle reagents according to OSH guidelines in approved areas only. Use small volumes to limit exposure concerns |